Dedicated to my father
who is a constant source of
inspiration in my educational life

BANDWIDTH BROADENING AND POLARIZATION DIVERSITY IN SMALL MICROSTRIP SLOT ANTENNAS FOR WIRELESS APPLICATIONS

By

Saeed Iftakhar Reza Latif

A thesis

Submitted to the Faculty of Graduate Studies

in partial fulfillment of the requirements for the degree of

MASTER OF SCIENCE

Department of Electrical and Computer Engineering

The University of Manitoba

THE UNIVERSITY OF MANITOBA

FACULTY OF GRADUATE STUDIES

*****

COPYRIGHT PERMISSION

BANDWIDTH BROADENING AND POLARIZATION DIVERSITY IN SMALL MICROSTRIP SLOT ANTENNAS FOR WIRELESS APPLICATIONS

BY

Saeed Iftakhar Reza Latif

A Thesis/Practicum submitted to the Faculty of Graduate Studies of The University of Manitoba in partial fulfillment of the requirement of the degree

Of

MASTER OF SCIENCE

Table of Contents

ACKNOWLEDGEMENTS

I would like to express my heartiest thanks and gratitude to my supervisor Professor L. Shafai for his wise advice, valuable guidance, enthusiasm, patience and continuous encouragement. I have no doubt to declare that, because of his constant educational, moral and financial support, my first ever endeavor in a university abroad has come to a success.

I would like to thank Dr. S. Noghanian and Dr. M. S. Mathur to serve on my committee. I also thank Dr. Satish K. Sharma and Dr. G. Rafi for helping me in different stages of this research work.

Special thanks to Mr. B. Tabachnick for his patient cooperation while performing experimental measurements. Extended thanks to Ms. S. Girardin for her kind help when it was required. I would like to thank Mr. Mehran Fallah-Rad also for various suggestions he provided during my M.Sc. study at this university.

Finally, I wish to express my deep indebtness to my parents, brothers, only sister, my friends, and above all, my beloved wife, for their kind support, generous love and moral encouragement.

ABSTRACT

Microstrip line-fed monopole slot antenna is studied in this thesis. This antenna is very compact in size and designed for very wide band operation, which will find applications in mobile handsets, PC cards for laptop computers etc. A monopole slot is cut on the center of a finite ground plane edge and fed by a microstrip line. This antenna has numerous parameters, which have effects on the operating frequency and impedance bandwidth of the antenna. The effects of these parameters are studied thoroughly. A bandwidth in excess of 50% can be achieved, if a proper stub tuning is done. This antenna has bi-directional radiation in one of the principal planes and omni-directional radiation pattern in the other. The space available in the ground plane, after the slot is etched, can be used by the electronic circuitry as electrical ground.

To reduce the antenna size, an L-shaped monopole slot is introduced, which shows an ultra wide impedance bandwidth. The radiation patterns are almost similar to those of the straight monopole slot. With the L-shaped slot, more space is now available for electronic circuitry in the ground plane.

For further investigation, an inverted T-shaped slot antenna is also studied, which is a symmetric configuration, and shows wide impedance bandwidths. In another study, the inverted T-shaped slot antenna is splitted into two parts to form two L-shaped slots. These slots are placed side-by-side, with certain separation, and excited individually using two bent feed lines. The radiation patterns of this antenna are investigated to achieve polarization diversity, as well as, wide impedance bandwidths. Experimental investigations are conducted to confirm the simulated results.

List of Figures

List of Tables

CHAPTER ONE

Introduction

The strive for the development of effective communication system has a long history, which in the last one hundred year is dominated by the radio. A key component of such a modern system is the antenna, needed in order to transmit information signal as electromagnetic wave. Among many antenna candidates, microstrip antennas have become one of the most attractive antennas in the past three decades. This is due to their compact size, lightweight, low-cost, simplicity in fabrication, conformability to any surface and many other such advantages. Consequently, microstrip antennas have been receiving increasing attention from academic and industrial researchers since 1953 till today.

1.1 Purpose of the Thesis

This thesis deals with lightweight and miniaturized, but wideband microstrip antennas, which may be suitable for mobile communications in handsets, laptop computers or PCS applications. The material for this goal and its challenges are provided below.

Miniaturized, lightweight and low profile antennas are in great demand due to advances in telecommunications and reduction in the physical size of electronic components. Earlier antennas were considered as bulky devices, compared to other components in communication systems. With the advent of microstrip antennas, the need for small and low profile antennas were met, making them useful for mobile and

satellite communications and in applications such as aircraft, missiles and telemetry antennas [1]. But in certain applications such as mobile handset terminals, laptop computer cards or various remote-sensing devices, even the small size of microstrip antennas is still too large for use. Saving space for electronic circuitry in these mobile units is a key issue at the present time.

The size of microstrip patch antennas is specified in terms of the wavelength, λ. In order to transmit electromagnetic waves efficiently, the patch should be of the order of half a wavelength or larger. It may be considered as a small antenna (i.e. electrically small) if its size becomes smaller than $\lambda/2$. Microstrip antennas can be made smaller using different techniques, such as loading with dielectric material, using short circuits or modifying the antenna geometry. All such techniques, unfortunately, lead to the reduction in their impedance bandwidth, gain and efficiency. [2], some of which also disturb the polarization purity.

Microstrip patch antennas are inherently very narrowband and reducing their size make their bandwidth even narrower. It is, therefore, very difficult to achieve both miniaturization and broad bandwidth properties simultaneously for small microstrip antennas. On the other hand, it was found that the transition of a microstrtip feed line and a transverse slot of optimum lengths in its ground plane radiates effectively and shows a wide band property [3]. This transition can be used as an antenna if fabricated on a low permittivity substrate. This type of slot antennas can be very useful in some wireless communications, where omni-directional radiation pattern, low gain and good impedance matching may be required. Since slot is cut in the ground plane, the microstrip line-fed slot antenna offers lightweight and small size. Moreover, space

available in the ground plane, after the slot is cut, can be used as the electrical ground of the electronic circuitry, required for signal processing and other purposes, which can be integrated in the same substrate.

Conventional microstrip line-fed slot antennas have a rectangular slot cut in the ground plane. Slots cut at one corner of the ground plane edge and fed by a microstrip line was studied in [4,5]. In [5], an array of two slots, separated spatially, was introduced in the ground plane, which enabled polarization diversity.

In this thesis, monopole slots, cut at one edge of a finite ground plane, and fed by a microstrip line is studied. Initially, a quarter-wavelength rectangular slot, cut at one edge of the ground plane and fed by microstirp transmission line is considered. This antenna is parametrically studied. The important parameters, which have significant effects on the antenna performance, are the slot width, feed line length, feed line position, stub length, ground plane length and width and the substrate permittivity and height. Then, the monopole slot is bent into an "L" shape in order to reduce its size and provide more space for the electronic circuitry. This L-shaped slot in the ground plane is fed using straight, inclined and bent microstrip feed lines and studied by numerical simulation for the effects due to the slot width and the stub length variation. Next, an inverted T-shaped slot on the ground plane fed by a straight feed line, which is symmetric in configuration, is studied to generate wider impedance bandwidth. The inverted T-shaped slot is divided into two parts to form two L-shaped slots, placed side by side, and fed separately using two bent microstrip feed lines, to achieve polarization diversity. Three antennas with different slot geometries, fed by a microstrip line, were fabricated and tested. The experimental results are compared with the simulated results.

1.2 Organization of the Thesis

The thesis is divided into six chapters. Chapter one gives an introduction and the objective of the thesis. The second chapter presents a background of the research work. In this chapter, miniaturization of microstrip antennas is explained, highlighting the limitations of different techniques. Broadbanding methods of small microstrip antennas are also addressed. Chapter three provides a detail study of the microstrip monopole slot antenna. Each parameter affecting the antenna performance is studied individually. Chapters four and five cover the study of the L-shape and inverted T-shape slot antennas, respectively. In chapter four, different feed line geometries to feed the L-shape slot antenna are presented. The effects of varying the width of the L-slot are studied. Chapter five deals with the inverted T-shaped slot antenna, fed by a microstrip line, and studied for the wide bandwidth. The inverted T-shaped slot is then divided into two parts resulting two L-shape slots, fed separately, and discussed for polarization diversity application. The thesis ends with concluding remarks and a note for the future research scope.

CHAPTER TWO

Microstrip Antenna and its Miniaturization

2.1 Introduction

Since the size of electronic components was reduced greatly in recent years, the need for miniaturized and low profile antennas have increased in communication systems. Miniaturization of antennas is a challenging task, as it leads to reduced impedance bandwidth and gain. Consequently, in recent past, there has been extensive research on miniaturization of microstrip antennas. In this chapter, the antenna miniaturization and their effects on the antenna performance are reviewed which provides the motivation for this research work.

2.2 Design Parameters of Microstrip Antennas

A microstrip patch antenna consists of a microstrip patch and a ground plane, separated by a dielectric substrate. The radiating patch may be rectangular, circular, square, triangular, ring or any other shape. The patch can be excited by a transmission line, a coaxial probe or an aperture coupling. A simple configuration of a probe-fed rectangular microstrip patch antenna is shown in Fig. 2.1:

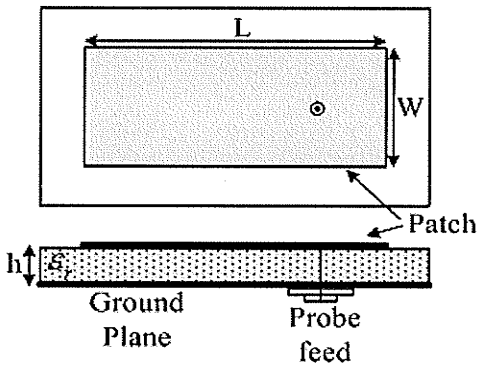

Fig. 2.1: Microstrip patch antenna fed by coaxial probe

At the resonant frequency, the patch length is equal to one half of the effective wavelength or wavelength in the dielectric, λ_d. The effective wavelength is defined as:

$$\lambda_d = \frac{\lambda_0}{\varepsilon_{eff}} \tag{2.1}$$

where λ_0 is the free space wavelength and ε_{eff} is the effective dielectric constant. The electric fields at the patch edges undergo fringing as shown in Fig. 2.2 [1]. Most of the electric field lines reside in the substrate and a portion of those exists in the air. For this reason, it is necessary to introduce the term, effective dielectric constant, ε_{eff} to account for the fringing and traveling of the wave in the patch in the presence of dielectric. The expression for ε_{eff} is:

$$\varepsilon_{eff} = \frac{\varepsilon_r + 1}{2} + \frac{\varepsilon_r - 1}{2}\left(1 + \frac{10h}{L}\right)^{-\frac{1}{2}} \tag{2.2}$$

where ε_r is the relative dielectric constant of the substrate.

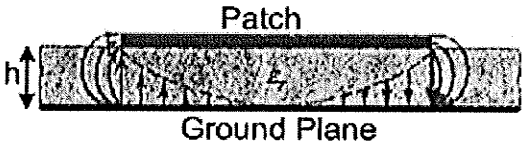

Fig. 2.2: Fringing affect at open ends of the microstrip patch

Since for small h, fringing of the fields occurs at the open ends, the patch of a microstrip antenna appears greater than its physical dimensions. The size extension is small and can be determined by adding equivalent lengths ΔL at both patch ends. ΔL can be expressed by the following equation [6]:

$$\Delta L = 0.412h\frac{\left(\varepsilon_{eff}+0.3\right)\left(\frac{L}{h}+0.264\right)}{\left(\varepsilon_{eff}-0.258\right)\left(\frac{L}{h}+0.8\right)} \tag{2.3}$$

Hence, the effective length of the patch is $L_{eff} = L + 2\Delta L$. Based on these, the expression for the resonant frequency is given by:

$$f_r = \frac{C}{\lambda_d\sqrt{\varepsilon_{eff}}} = \frac{C}{2(L+2\Delta L)\sqrt{\varepsilon_{eff}}} \tag{2.4}$$

The bandwidth is an important parameter for the antennas. In general form, it can be defined as a certain frequency range within which the antenna performance conforms to a set of specified standards [1]. For micrsotrip antennas, impedance or VSWR bandwidths are usually specified. The voltage standing wave ratio or VSWR is defined as the ratio of the maximum to minimum voltage of the standing wave, present at the input of the antenna due to mismatch. Thus, the bandwidth (BW) can be defined by the following expression in terms of its VSWR and total quality factor [7]:

$$BW = \frac{VSWR-1}{Q_t\sqrt{VSWR}} \tag{2.5}$$

where Q_t is the total quality factor which is a measure of the losses in microstrip antennas and given by:

$$\frac{1}{Q_t} = \frac{1}{Q_{rad}} + \frac{1}{Q_{cu}} + \frac{1}{Q_{di}} + \frac{1}{Q_{sw}} \tag{2.6}$$

Q_{rad} is the quality factor due to radiation loss

Q_{cu} is the quality factor due to conductor loss

Q_{sw} is the quality factor due to surface wave excitation

Q_{di} is the quality factor due to dielectric loss

Using the cavity model, the far field equations for a rectangular microstrip antenna are given by [8]:

$$E_\theta = \left[\frac{jkWV_0}{\pi}\frac{e^{-jkr}}{r}e^{j(X+Y+Z)}\right]\left[\cos X\frac{\sin Y}{Y}\right]\cos\phi \tag{2.7}$$

$$E_\phi = \left[-\frac{jkWV_0}{\pi}\frac{e^{-jkr}}{r}e^{j(X+Y+Z)}\right]\left[\cos X\frac{\sin Y}{Y}\right]\cos\theta\sin\phi \tag{2.8}$$

$$Y = \frac{kW}{2}\sin\theta\sin\phi$$

$$X = \frac{kL_{eff}}{2}\sin\theta\cos\phi$$

$$Z = \frac{kh}{2}\cos\theta$$

V_o is the applied voltage at the feed

E_θ, E_ϕ are the electric fields in the two planes in spherical co-ordinate

θ, ϕ are elevation and azimuth angles, respectively, in spherical co-ordinate system

k is the wave number in the free space

h is the height of the substrate

L, W are the length and width of the rectangular patch, respectively (see Fig. 2.1)

L_{eff} is the effective length of the rectangular patch

Approximate expressions for the directivity (D) and gain (G) of a rectangular patch are given by the following equations: [25]

$$D = \frac{\frac{1}{2}\mathrm{Re}\left(E_\theta H_\phi^* - E_\phi H_\theta^*\right)_{\theta=0}}{\frac{P_r}{4\pi r^2}} = \frac{\frac{r^2}{2\eta_0}\left(\left|E_\theta\right|^2 + \left|E_\phi\right|^2\right)_{\theta=0}}{\frac{P_r}{4\pi}} \tag{2.9}$$

$$D \cong \frac{4(kW)^2}{\pi \eta_o G_r} \tag{2.10}$$

$$G = e_r D \tag{2.11}$$

H_θ^*, H_ϕ^* are the conjugate of magnetic fields in the two planes in spherical co-ordinate

P_r is the radiated power

G_r is the radiation conductance

e_r is the radiation efficiency

η_o is the free space impedance

2.3 Antenna Miniaturization

The length of a microstrip patch, also applicable to other antenna types, should be normally half a wavelength or larger to ensure efficient transmission of electromagnetic waves. For certain applications, half-wavelength antennas are considered to be large. So in the last 40 years, there has been increasing research to miniaturize the antennas. Antennas smaller than half a wavelength can be considered as small antennas. The definition of small antenna as given in [9] is: "A miniaturized

antenna can be defined as one which, for a given frequency, has its linear dimension smaller compared to a similar type of conventional antenna operating at the same frequency". Several techniques to miniaturize antennas are available in the literature. These can be categorized in the following way:

2.3.1 Loading the Antenna with Lumped Elements:

The simplest method to make antennas smaller than a resonant size, still keeping resonant behaviors, is loading them (putting some materials on or around the antenna). If an antenna is smaller than $\lambda/2$, it will have strong reactive input impedance. This can be compensated for by loading with resistive (R) or reactive (L or C) components, or by adding conductive parts as shown in Fig. 2.3. If the element added has losses, the efficiency of the antenna will decrease. Again, if the loss is less, the quality factor will increase resulting in a reduction in the bandwidth [2].

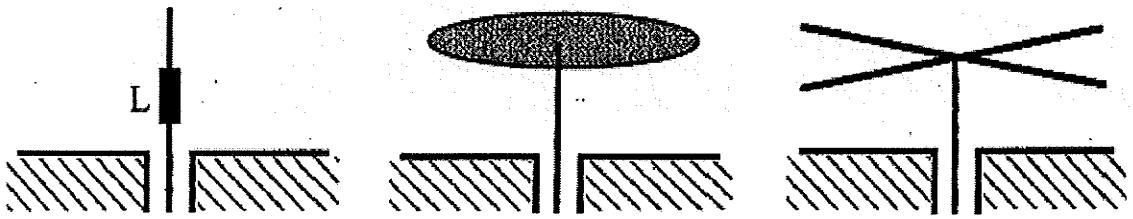

Fig. 2.3: Loading techniques: (a) Inductive, (b) Capacitive (c) Conductor

2.3.2 Loading the Antennas with Dielectric Material

Loading with a dielectric material was the method used, in order to reduce the antenna size. Previously, this use was limited by the availability of appropriate substrates and their cost [10]. In this method, the size reduction depends on the

dielectric constant of the substrate. Since, the wavelength is smaller in a high permittivity substrate, the antenna size reduces, when loaded with such substrates [2]. Thus for size reduction, the use of high permittivity substrates is proposed.

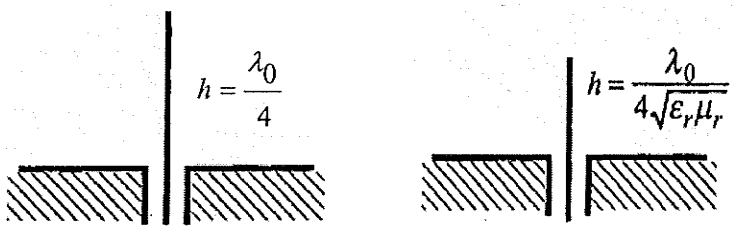

Fig. 2.4: (a) Monopole: $h=\lambda_o/4$ & (b) Dielectric loaded monopole: $h=\lambda_o/4\sqrt{(\varepsilon_r\mu_r)}$. h is the height of the monopole, λ_o is the free space wavelength, ε_r and μ_r are relative permittivity and permeability of the dielectric, respectively

However, in high permittivity material, the electric fields are trapped inside the substrate making radiation more difficult. The quality factor is enhanced and the bandwidth goes down. Also, due to the radiation loss and higher dielectric losses in high permittivity material, the gain decreases, in using such substrate loadings. The gain can be recovered by using a high permittivity superstrate loading, again at the cost of reduced bandwidth [11].

2.3.3 Using Short Circuits

This is the most popular technique for miniaturization of the antennas. The principle can be explained with the example of a dipole. When the length of the dipole is one-half wavelength, it is resonant. The length can be halved by replacing one dipole arm by a ground plane, which acts like a mirror and creates an image of the half-dipole arm [2]. So the antenna remains resonant at the same frequency, but its size reduces in

half. In the case of microstrip antennas, miniaturization can be obtained by adding short circuits to the ground plane as shown Fig. 2.5.

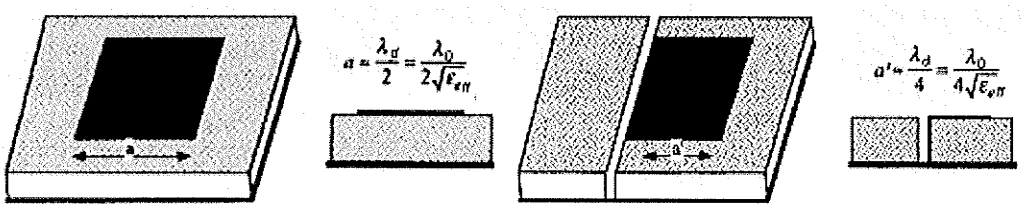

(a) *(b)*

Fig. 2.5: (a) A microstrip patch antenna, (b) A shorted microstrip patch antenna. λ_o is the free space wavelength, λ_d is the wavelength in dielectric and ε_{eff} is the effective dielectric constant

To be resonant at the fundamental TM_{10} mode, the length of the patch should be about half a wavelength. The electric field of the TM_{10} mode is zero at its center and a short circuit may be placed there without affecting its resonant frequency. Thus, at a given operating frequency, the patch dimensions can be significantly reduced. The reduction in the patch size is limited by the distance between the null-voltage point in the patch and the patch edge. The shorted part acts as an electric wall and the patch edge becomes the magnetic wall. The radiation occurs mainly from the magnetic walls. Appendix A provides the theoretical design method for a quarter-wave patch.

The shorted quarter-wave patch has lower gain and efficiency, as the radiating element is smaller in size. It has a high input impedance at its radiating edge, and as such, is difficult to feed via a microstrip line. Also, it has a narrower impedance bandwidth. As the substrate is cut to place the short circuit plate, this antenna becomes mechanically weak.

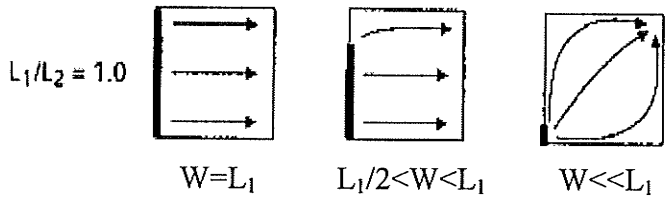

Fig. 2.6: Variation of surface current flow due to the short circuit plate width (W) variation. L_1 and L_2 are two sides of the shorted patch, as mentioned in Fig. 2.7(a)

By short-circuiting only a portion of the zero potential plane, not the entire width, further reduction of the patch can be done [9, 12]. When the width of the short circuit plate is set narrower than that of the planar element, the effective length of the current flow on the short-circuit plate and planar element becomes longer as can be seen in Fig. 2.6. Consequently, the resonant frequency becomes lower than that of the conventional short circuit microstrip antenna having the same sized planar element. In Fig. 2.7(b), the variation of resonant frequency with the width of the short circuit plate is shown. It is evident that the frequency lowers as the width *W* gets narrower, as such the length of the short circuited microstrip antenna can be further reduced.

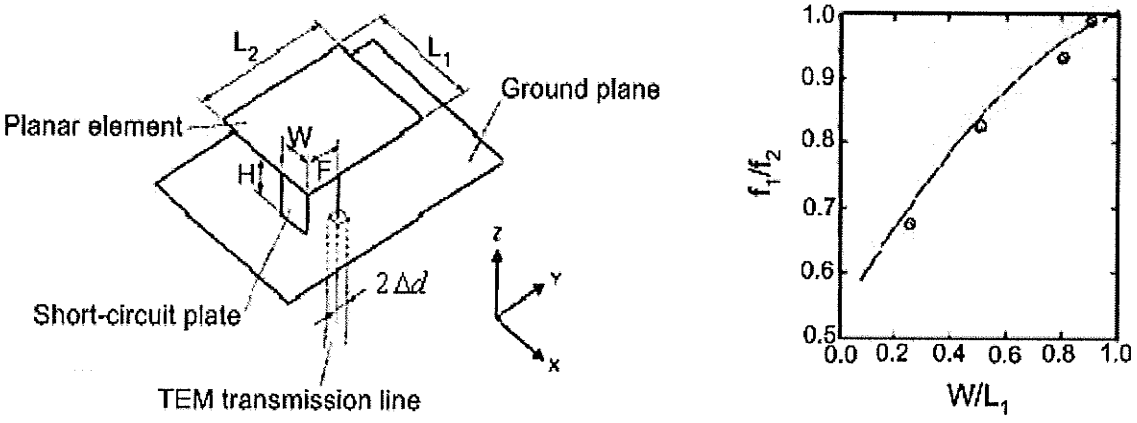

(a) *(b)*

Fig. 2.7: (a) Shorted patch with narrower short-circuit plate width (W), (b) Variation of resonance frequency with W

In practice, it was found that, it is convenient to realize the short circuit at one end of the patch by using conducting pins rather than using a short circuit plate, as shown in the Fig. 2.8 [13]. These pins produce residual inductance at the patch edge rather than realizing perfect short circuit, so that the patch will need to be shortened slightly. The important features of using shorting pins are well documented in the references [14-16]. It is reported that the use of a very small number of shoring pins, instead of a complete short circuit, reduces the size of the quarter-wavelength antenna considerably, without affecting its performance. In fact, the maximum reduction in physical size can be achieved if only a single shoring post is used. From manufacturing point of view, construction of shorting posts is much easier than that of shorting plate.

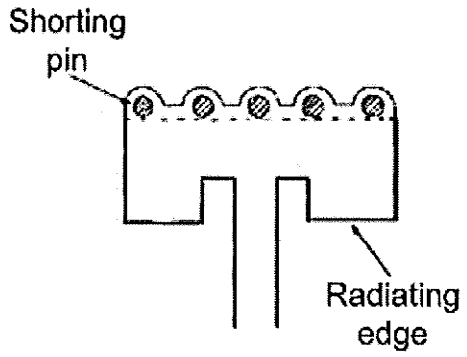

Fig. 2.8: Shorting pins instead of shorting plate

The closer the shoring posts to the edge, the smaller the overall size of the patch. At a fixed frequency, modified patch size can be increased or decreased depending on the distance of the shorting pin from the feed. But there is a strong dependence of the input impedance on the close positioning of the shoring post with respect to the feed and once again the narrow impedance bandwidth. Fabrication, in this case, is also difficult. By increasing the number of pins, this distance can be increased

easing the fabrication, but enlarging the patch. The radii of the pins also play an important role in the overall size of the patch conductor, as well as the shorting pin distance from the feed. The larger the radii of the shoring pins, the greater this distance. So it can be said that, there is a trade-off between the number of pins, radius of the pins and the distance between the shorting pin and feed, depending on whether the overall size of the antenna is more important or ease of its fabrication.

2.3.4 Modifying Antenna Geometry

By modifying the antenna geometry and shape, smaller antennas can be found. The idea here is to meander the surface current, so that the effective length of the current flow path becomes longer. As a result, the resonant frequency goes down which represents a reduction in the antenna size. A good example of antenna geometry modification is the inverted-L antenna, which was derived from the monopole by bending it. When a short circuit is added to the inverted-L antenna, the inverted-F antenna is found [2]. This derivation is shown below in Fig. 2.9(a-c):

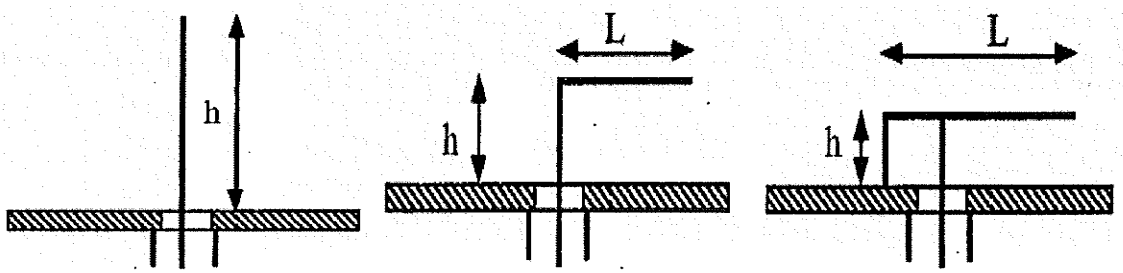

Fig. 2.9: (a) The monopole antenna, length: $h \approx \lambda_o/4$, (b) the inverted-L antenna, length: $h+L \approx \lambda_o/4$ (c) the inverted-F antenna. λ_o is the free space wavelength

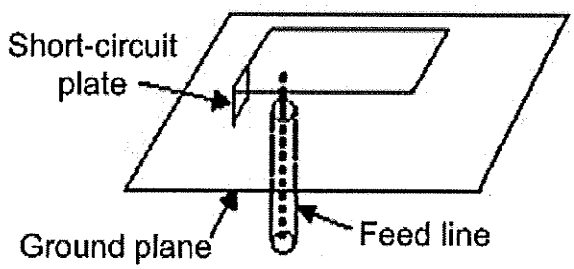

Fig. 2.10: Planar Inverted-F antenna (PIFA)

By replacing a wire antenna by a planar element (microstrip antenna), the very popular planar inverted-F antenna (PIFA) is found which is a good example of a miniaturized antenna, shown in Fig. 2.10. This idea is extended to the microstrip antenna to reduce the antenna size. Here, slots are inserted into the microstrip patch to force the surface currents (J_s) to meander, thus the effective length of the current path gets longer, and the antenna size is reduced. One example is given below:

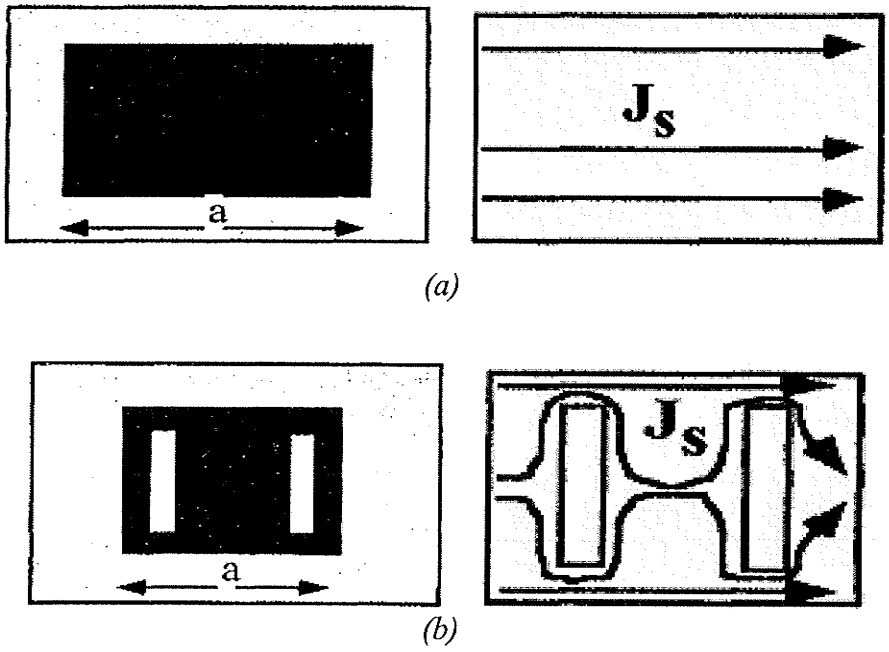

Fig. 2.11: The effect of slots in a microstrip patch antenna (a) The microstrip antenna, $a=\lambda_d/2$, (b) the microstrip antenna with slots, $a<\lambda_d/2$. λ_d is the wavelength in dielectric

Embedded slots in the finite ground planes are also investigated to miniaturize microstrip antennas, based on the same concept of increasing the length of current flow path [17].

2.4 Limitations on Miniaturization of Antennas

The problems associated with different miniaturization techniques are stated here while discussing each of them individually. Reducing the antenna size has effects on radiation pattern, gain and impedance. Here, the main disadvantages of small antennas are summarized:

Effect on Gain: A simple formula, which gives a practical upper limit for the gain of a small antenna, while still having a reasonable bandwidth, is [2]:

$$G = (ka)^2 + 2ka \tag{2.1}$$

Here, k is the wave number and a is the radius of the smallest sphere enclosing the antenna. So a very small antenna is not practical if an appreciable gain is needed.

Effect on Efficiency: A miniaturized antenna will show a higher concentration of surface currents toward one point. Thus, ohmic losses will be enhanced, as such, miniaturization decreases the efficiency of the antenna.

Effect on Bandwidth: The quality factor Q of a small antenna can be represented as

$$Q \cong \frac{1}{(ka)^3} + \frac{1}{ka} \tag{2.2}$$

Now Fractional bandwidth is

$$FBW = \frac{\Delta f}{f_0} = \frac{1}{Q} \tag{2.3}$$

Different techniques of miniaturization increase the quality factor of the antenna, so the bandwidth is affected due to miniaturization [2].

Effect on polarization purity: In many cases, miniaturization of an antenna affects the polarization purity. As mentioned earlier, in small antennas the concentration of the surface current is higher toward one point, which leads to cross-polarization radiation.

Feed problem: The last limitation in antenna miniaturization is the difficulty in correctly feeding small antennas. From manufacturing point of view, small antennas are complicated to feed properly.

2.5 Broadbanding Of Small Microstrip Antennas

Since miniaturization of microstrip antennas experiences very narrow impedance bandwidth problem, several attempts have been made to enhance their bandwidth. One popular technique is to lower the quality factor of the antenna, which means an increase in the impedance bandwidth. This is achieved by increasing the substrate height or by chip-resistor loading or by using meandered or a slotted ground plane [18]. When a high substrate material is used, in case of a probe feed microstrip antenna, a long probe pin is required, which means a large reactance for the small microstrip antennas, thereby causing an impedance mismatch. In chip-resistor loading technique, due to the presence of the resistor, the losses increase representing lowering of the quality factor. For the slits in the ground plane, the surface currents are forced to meander. This results in lengthening of the equivalent surface current path. The

fundamental resonant frequency is thus decreased. The slits also lower the quality factor of the antenna and increase the impedance bandwidth.

Embedding suitable slots in the microstrip patch is also a good technique to increase the bandwidth of the miniaturized microstrip antennas. But less than two times impedance bandwidth of a conventional microstrip antenna is achieved [18]. Another popular technique is to use stacked shorted patches. This technique is based on the fact that two or more resonant modes of similar radiation characteristics are excited at adjacent frequencies using slightly different size stacked patches and these frequencies are combined to form a wide operating bandwidth [18]. But this technique causes the increase in volume or size of the antenna.

2.6 Conclusion

In this chapter, the important design parameters of a simple rectangular micrsotrip antenna were presented. It showed that the patch length of a rectangular micrsotrip antenna is usually half a wavelength. To make antennas smaller, common antenna miniaturization techniques were described and, the problems of each technique were addressed. As small microstrip antennas suffer from narrow impedance bandwidth, broadbanding techniques, available so far, were also discussed. However, for small microstrip antennas, the enhancement in percentage impedance bandwidth greater than 10% is very difficult to obtain using the techniques mentioned above. A promising alternative was proposed by Sharma et. al. in [4,5] using a microstrip monopole slot antenna, which provides a wide impedance bandwidth. Because of its small size and potential for wide bandwidths, it is selected as the candidate for further study in this thesis. The next three chapters will present the detail of this study.

CHAPTER THREE

Wideband Microstrip Monopole Slot Antenna

3.1 Introduction

In order to transmit voice, data and video information in wireless communication system, wideband antennas are essential. The compactness and lightweight in antenna size are other key issues. Small microstrip antennas are narrow band but several techniques are reported in the literature to enhance the impedance of microstrip antennas. Some common broadbanding techniques are the use of multimode resonators, use of parasitic elements with main radiating patch and the use of stacked patches [19]. In this chapter, a wideband microstrip monopole slot antenna fed by a microstrip line is investigated which has all these properties. At first the microstrip slot antenna theory is discussed briefly, after that the proposed antenna is parametrically studied. Experimental results are also presented.

3.2 Microstrip Slot Antennas

Slot line, as an alternative to microstrip line, was first proposed by Cohn [20]. The simplest form of a slot line is a narrow slot in the conductive metal layer of a dielectric substrate. The other surface is directly exposed to air. The configuration is shown in Fig. 3.1. Slot lines can be easily used in microwave integrated circuits (MICs). To use slot lines as transmission lines, the radiation from the slots should be minimized. This can be achieved by etching the slots on high permittivity substrates. As a result, the slot-mode wavelength will be much smaller compared to free-space wavelength. Hence, the slot fields will be closely bound to the slot with an insignificant radiation loss.

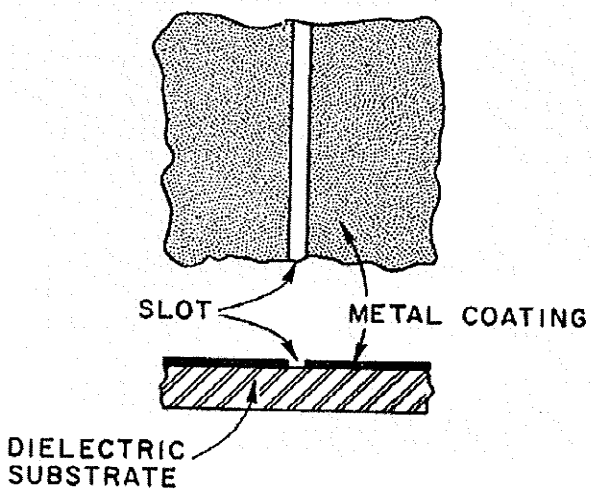

Fig. 3.1: Slot line on high-permittivity dielectric substrate

The slot line mode is non-TEM in nature; so the basic electrical parameters of the slot line, such as, characteristic impedance and phase velocity, are not constant, rather they vary with frequency. It also has no cut-off frequency; therefore, propagation of wave occurs at all frequencies, even at zero [21].

Resonant slots are used as radiating elements. If a very thin rectangular slot is assumed in an infinitely large metallic ground plane, the radiation characteristics of this type of slot are exactly identical to those of a fictitious magnetic dipole. The radiated fields from the slot are due to the magnetic current distribution M, which is numerically equal to the distribution of electric voltage V across the slot [22]. Hence, the slot can be considered as a magnetic dipole filling the slot.

The electric and magnetic field configurations in a slot line on a dielectric substrate are shown in Fig. 3.2. There exists a voltage difference between the two edges of the slot. Therefore, the electric field is present across the slot traveling from one edge to the other. From Fig. 3.2(a), it is evident that the magnetic fields are in a plane perpendicular to the slot plane [3]. The surface current paths on the metal surface are

shown in Fig. 3.2(b). The current density is highest at the edges of the slot and decreases rapidly with the distance from the slot. At every half-wavelength interval, the magnetic current direction changes.

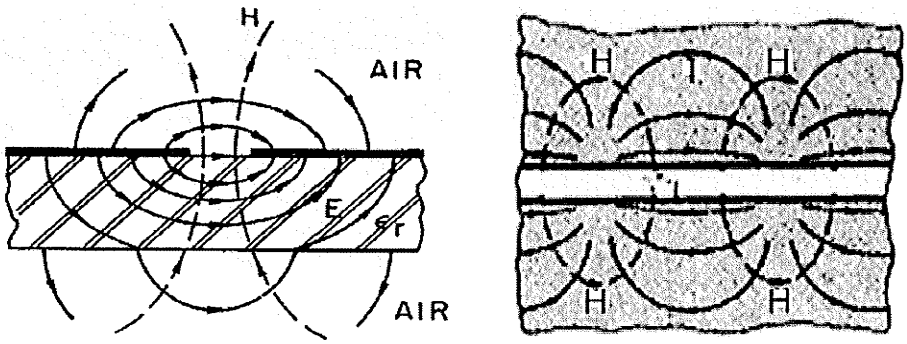

Fig. 3.2: (a) Field distribution in cross-section and (b) current distribution on metal surface of a slot line etched on a dielectric substrate

In microwave integrated circuits, crossing of the slot line and micrsotrip line is very frequent. A promising wide band property was found when the slot line on one side of a substrate and microstirp line on the other side cross each other at the right angle [3]. When the slot line and micrsotrip line are far apart, the coupling between them is not strong, but when they are close to each other, the coupling is very tight. This coupling can be utilized intentionally to radiate electromagnetic energy when fabricated on a low permittivity substrate material.

If a rectangular slot is etched on the ground plane of a microstrip line, with a low permittivity substrate, placed perpendicular to each other as shown in the Fig. 3.3, the transition between the slot and microstrip lines radiates effectively with a large bandwidth. When the lengths of both the slot and microstrip lines are optimized properly, a good impedance match can be found with a fairly large impedance bandwidth.

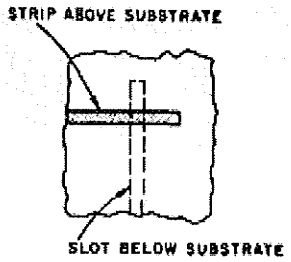

Fig. 3.3: Microstrip line and slot line transition

The operating frequency of the microstrip-line fed slot antenna is primarily dependent on the electrical length of the slot. But practically, it is also dependent on the stub length and the coupling between the slot and microstrip line [23]. Some higher order modes are excited in slot-microstrip line transition [24], which can be combined to get a wider bandwidth, by adjusting different parameters of the microstrip slot antenna, such as microstrip feed line length, its position over the slot line, stub length etc. Another important property of the microstrip slot antenna is its bi-directional radiation pattern. If this bi-directional radiation is not desired, a metal reflector can be used on one side to force the radiation to the other side [24].

For a good impedance match, the impedance of the slot seen by the microstrip line should be matched with the characteristic impedance of the microstrip line. Typically a microstrip line with 50Ω characteristic impedance is used to excite the slot line. Hence, the microstrip line should be placed in a position over the slot in the ground plane such that the slot impedance matches with the impedance of the feed line to give effective radiation and wide impedance bandwidth.

When microstrip line crosses the center of the slot, cut on the ground plane, the slot offers high radiation resistance compared to the characteristic impedance of the microstrip line. For a given slot size, the radiation resistance can be reduced by three

possible techniques. Yoshimura showed that if the feed line is slightly displaced from the center of the slot, the radiation resistance of the slot is less compared to that when placed at the center [25].

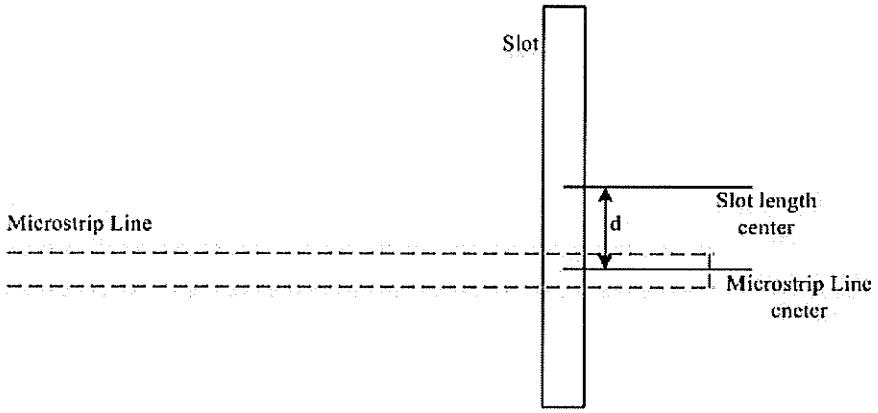

Fig. 3.4: Offset microstrip feed to excite the slot

The configuration of the offset microstrip feed line to excite the slot on its ground plane is shown in Fig. 3.4. Here *d* is the offset distance of the feed line from the slot center. As *d* increases, the resonant frequency of the antenna decreases toward the self-resonant frequency of the antenna [26]. The frequency independent conductance data of the offset-fed slot in the ground plane of a microstrip line are presented in [27]. The theoretical and measured impedance of the center-fed and offset-fed slots can be found in [28,29]. In the theoretical expression of the impedance of the slot, the authors used complex radiated power from the radiation resistance representing the slot. The discontinuity in the modal voltage in the microstrip line, induced due to the slot cut on the ground plane, was also employed.

The second technique is the use of a stub tuning, where an open circuit stub is connected to the microstrip feed line after the slot-microstrip line transition as shown in the Fig. 3.5.

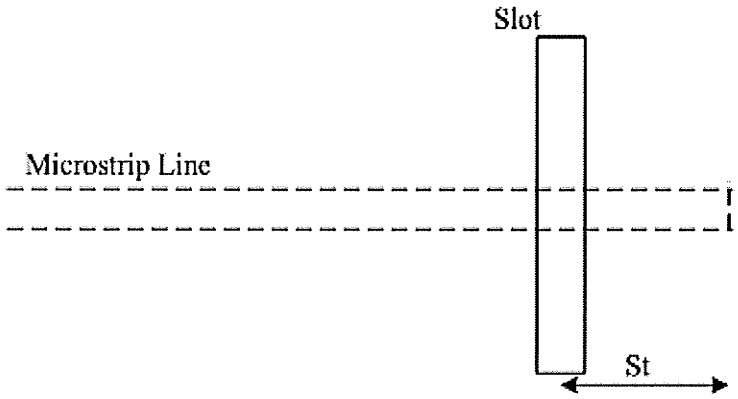

Fig. 3.5: Stub tuned microstrip line-fed slot

The stub length is chosen such that the reactance at the resonant frequency of the slot antenna is cancelled by the open-circuited tuning stub [30]. By varying the stub length, the resonant frequency can be changed and at the new frequency, the slot impedance matches well with the characteristic impedance of the feed line.

Another technique to reduce the radiation resistance of the slot is feeding the slot at the center but inclining the feed line, as shown in the Fig. 3.6. Here, the microstrip line is no longer perpendicular to the slot line. The inclination angle between the slot axis and the microstrip line axis is an important parameter for this type of feeding scheme.

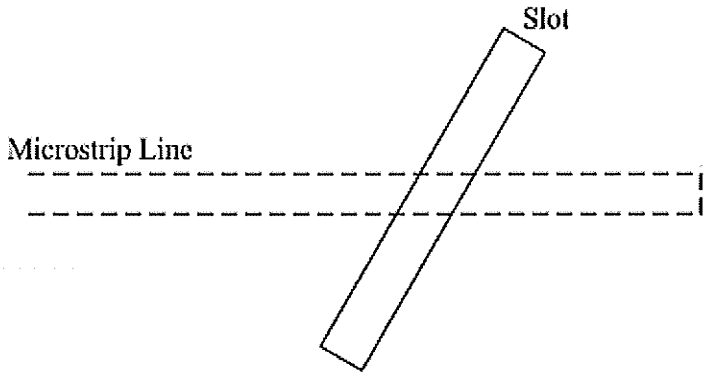

Fig. 3.6: Inclined microstrip line-fed Slot

The full wave analysis for the inclined feeding technique to excite the slot was carried out by Bhattcharyya et. al. [31]. An improved two-port network model to analyze the inclined microstrip-fed slot antenna was presented in [26]. Here, the effects of slot inclination angle on the impedance seen by the feed line have been studied. It was found that as this angle increases, the resonant frequency of the antenna also decreases.

Microstrip slot antennas are analyzed by many researchers to design the antenna efficiently. From microwave integrated circuit point of view, both slot line and microstrip line are present in two-level circuit design and their transition is common in such circuits [24]. Knorr represented this transition (Fig. 3.3) as a transformer to transform energy from the microstrip line to the slot line as shown in Fig. 3.7 [32]. He also calculated the turn ratio of the transformer, which is an important parameter for the equivalent circuit of microstrip-slot transition.

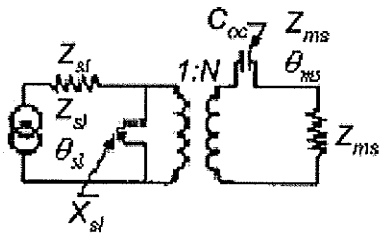

Fig. 3.7: Equivalent Circuit of microstrip-slot transition

Here, Z_{Sl} is slot impedance

θ_{Sl} is electrical length of slot stub

X_{Sl} is equivalent reactance of shorted slot

Z_{ms} is micrsotrip impedance

θ_{ms} is electrical length of micrsotrip stub

C_{OC} is equivalent capacitance of open microstrip

In most of the analysis available in the literature, the researchers used this transformer model to analyze microstrip-slot transition and microstrip slot antennas.

3.3 Proposed Micrsotrip Monopole Slot Antenna

Wide radiating slots in the ground plane of a micrsotrip line is analyzed in [33]. The analysis is different from the narrow slot analysis discussed in the previous section because in the case of a wide slot, both components of the electric fields in the slot have been considered. The analysis is based on the method of moments (MoM). If the slot width increases, the radiation resistance of the slot increases which leads to a reduction in the impedance bandwidth [34]. Efforts were made to increase the impedance bandwidth of a microstrip line-fed slot antenna by a T-shaped and fork-like tuning stubs, located within the slot [34, 35]. In [5], a monopole slot cut at one corner of the ground plane edge, fed by a microstrip line of 50Ω characteristic impedance, was presented with simulated and experimental results. This antenna shows a wide band property. In this research work, a monopole slot at the center of one of the edges of the ground plane of a 50Ω microstrip transmission line is parametrically studied. Its radiation characteristics are also investigated.

The antenna geometry with the co-ordinate system is shown in Fig. 3.8. A monopole slot is cut at the edge of the ground plane of a microstrip line. The slot is at the center of the ground plane of width, G_W. Its length L_S = 30 mm is a quarter wavelength in free space at 2.50 GHz. The slot is electromagnetically fed by a 50Ω

microstrip transmission line. A 50Ω SMA probe is connected to the feed line, to excite the slot as shown in the Fig. 3.8. After several simulations, initial design parameters were chosen as tabulated in table 3.1. A low-cost substrate material FR-4 was used for simulation. The stub length, *St* and feed line length, *fl* are two important parameters of this antenna. The feed length is measured from the probe position to the slot center and the open-end stub is also considered from the slot center to the opposite side, as indicated in Fig. 3.8. The feed line position along the slot line with respect to the rim of the ground plane is L_f.

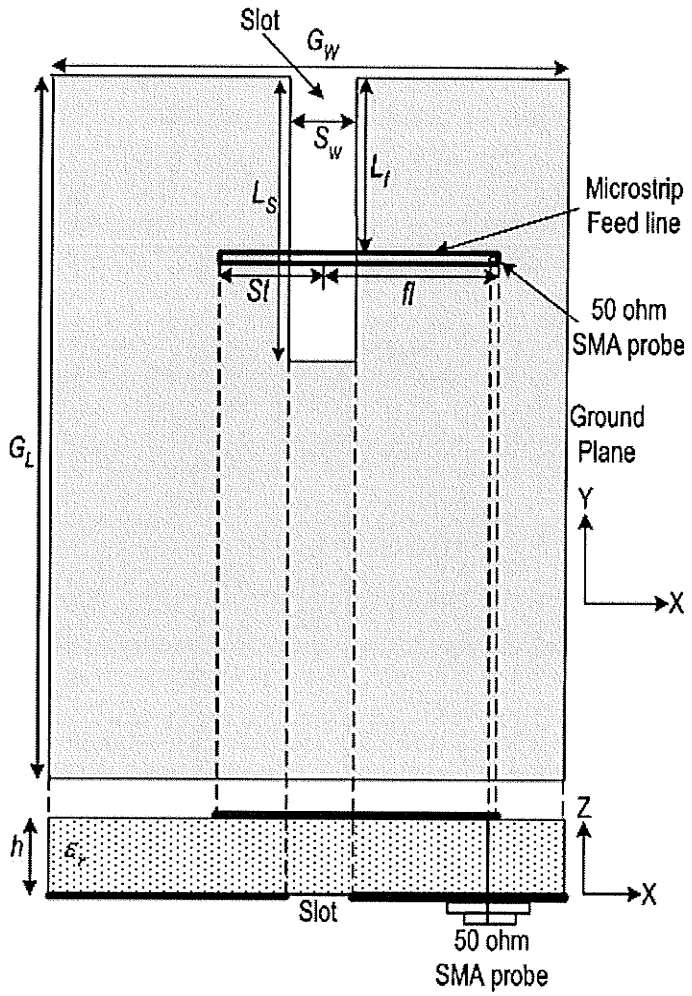

Fig. 3.8: The geometry of the microstrip monopole slot antenna on the ground plane of a microstrip line along with the co-ordinate system

Table 3.1: Initial design parameters of the antenna in Fig. 3.8

Ground Plane Width, G_W	50 mm
Ground Plane Length, G_L	80 mm
Slot Length, L_S	30 mm
Slot Width, S_w	7 mm
Feed Line Position, L_f	15.2 mm
Microstrip Line Characteristic Impedance	50Ω
Microstrip Line Width	1.528 mm
Substrate Dielectric Constant, ε_r	4.5
Substrate Height, h	0.8128 mm
Loss Tangent, $tan\delta$	0.02

3.3.1 Parametric Study

As it is evident from the above discussion, this antenna has numerous parameters such as *St*, *fl*, L_f, S_W, G_W, G_L, ε_r and h, each of which having significant effect on its impedance bandwidth and operating frequency. In this section, these effects are studied individually. In order to understand the behavior of each of the parameters appropriately, only one of the parameters is varied at a time, keeping the rest fixed. Here, –10 dB return loss bandwidth is considered. The simulation work is carried out for impedance bandwidths (S_{11} = -10 dB), using a Method of Moments (MoM) software Ensemble 8.0 [36]. The radiation patterns are investigated using HFSS 8.0 which is another software based on the Finite Element Method (FEM) [37]. The simulation results are confirmed by experimental verifications at the end.

3.3.1.1 Effect of Stub Length

The stub length is an important parameter in microstrip line-fed slot antenna. In this study, the microstrip line is terminated by an open-end stub. To study the effect of

the open-end stub, its length is varied for a fixed length of the microstrip feed line (18.5 mm). Other parameters are kept constant as in table 3.1. It was mentioned previously that, the slot length is primarily responsible for the resonant frequency. Also the stub length plays a role in determining the operating frequency of the antenna. It can be stated from Fig. 3.9 and table 3.2 that, the stub length has effect on both the operating frequency and impedance bandwidth of the antenna. As the stub length increases, the frequency for the minimum S_{11} decreases which indicates that the operating frequency decreases with the increase in the stub length. As the stub length increases from 4 to 6 mm, the impedance bandwidth increases from 29.9% (3.41 to 4.61 GHz) to 51.2% (2.54 to 4.29 GHz). If it is increased further, the bandwidth decreases. But it is significant to note that, the lower end frequency limit continues to decrease. A decrease in the operating frequency indicates a relative reduction in the antenna size.

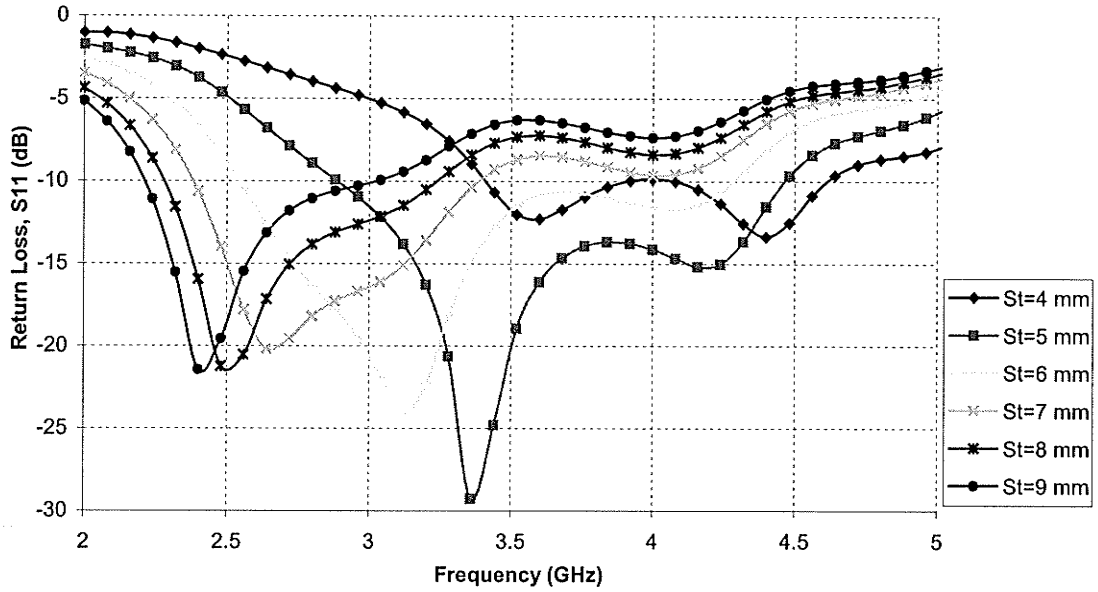

Fig. 3.9: The effect of varying stub length (St) of the slot antenna in Fig. 3.8 on its return loss. Other parameters are kept the same as in Table 3.1.

Table 3.2: The effect of varying the stub length (St) on the impedance bandwidth and operating frequency of the antenna in Fig. 3.8

St (*mm*)	Frequency Limits (*GHz*)	Center Frequency (*GHz*)	Frequency for min. S_{11} (*GHz*)	BW (%)
4	3.41 – 4.61	4.01	4.4	29.9%
5	2.89 – 4.47	3.68	3.4	42.9%
6	2.54 – 4.29	3.415	3.12	51.2%
7	2.38 – 3.39	2.895	2.64	34.9%
8	2.28 – 3.24	2.76	2.52	34.8%
9	2.21 – 3.03	2.62	2.44	31.3%

3.3.1.2 Effect of Feed Line Length

The microstrip feed line, on a dielectric substrate, is used here to excite the slot in its ground plane. The characteristic impedance is chosen to be 50Ω. The variation of S_{11} for different feed line lengths, *fl*, with a fixed value of *St* = 6 mm, is shown in Fig. 3.10. It is evident that when *fl* is increased from 15 mm to 19 mm, the impedance bandwidth increases from 29.40% (2.55 to 3.43 GHz) to 51.60% (2.53 to 4.28 GHz). If it is increased further, the bandwidth reduces. The frequency for minimum S_{11} increases with the increase in the feed line length. It should be noted here that, the increase in the feed line length has an effect on the upper end frequency limit. As the stub length is fixed at 6 mm, the lower end frequency remaining constant with the increase of feed line length, but the upper end frequency increases, increasing the bandwidth. But for the selected small ground plane, this increase in *fl* has a practical physical limit. An increase in the bandwidth is also strongly dependent on the stub length and slot size.

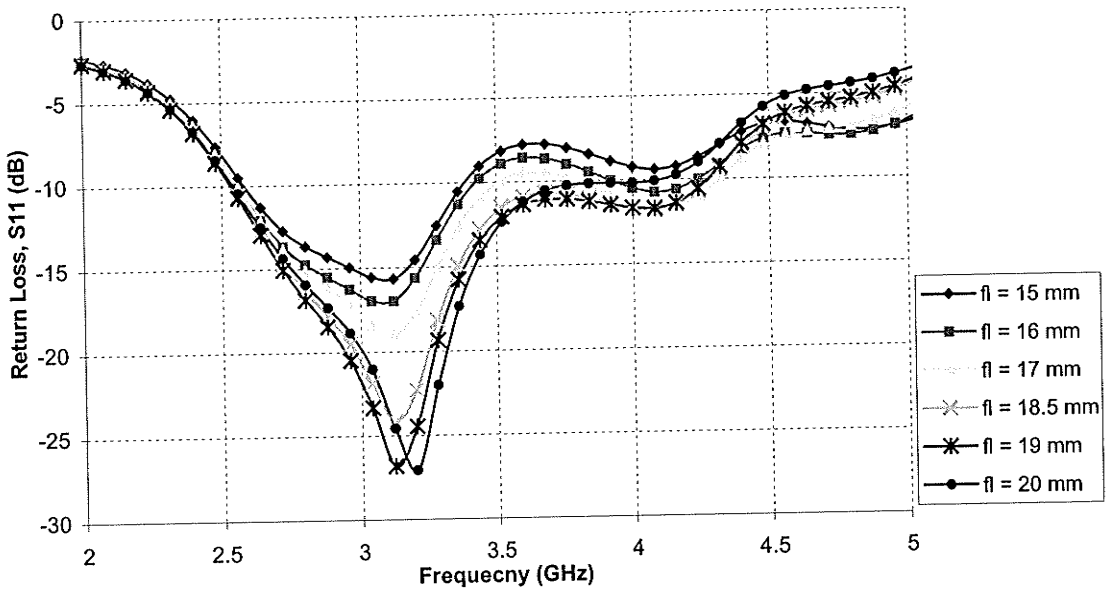

Fig. 3.10: The effect of varying the feed line length (fl) of the slot antenna in Fig. 3.8 on its return loss. Other parameters are kept the same as in Table 3.1.

Table 3.3: The effect of varying feed line length (fl) on the impedance bandwidth and operating frequency of the antenna in Fig. 3.8

fl (*mm*)	Frequency Limits (*GHz*)	Center Frequency (*GHz*)	Minimum S_{11} (*dB*)	Frequency for minimum S_{11} (*GHz*)	BW (%)
15	2.6 – 3.39	2.995	-15.7	3.12	26.4%
16	2.55 – 3.43	2.99	-17.0	3.12	29.4%
17	2.55 – 3.51	3.03	-19.0	3.08	31.7%
18.5	2.54 – 4.29	3.415	-24.2	3.12	51.2%
19	2.53 – 4.28	3.39	-26.8	3.12	51.6%
20	2.54 – 4.1	3.32	-27.1	3.2	47%

3.3.1.3 Effect of Feed Line Position

The feed line position (L_f) plays an important role on the radiation resistance of the slot, consequently on the impedance bandwidth. The effect of varying L_f is shown in Fig. 3.11 for St = 6 mm and fl = 18.5 mm. It has significant effect on impedance bandwidth and on the frequency for minimum S_{11}. As we can see from Fig. 3.13, increase in L_f from 11.2 mm to 13.2 mm gives an increase in bandwidth from 24.6% (3 to 3.84 GHz) to 52.8% (2.62 to 4.5 GHz). Further increase in L_f reduces the bandwidth and at L_f= 18.2, the bandwidth reduces to 27.5% (2.48 to 3.27 GHz). In the range L_f = 13.2 to 16.2 mm, more than 50% bandwidth can be achieved. Frequency for minimum S_{11} goes down from 3.4 to 2.8 GHz as $L_f$increases from 11.2 to 18.2 mm. It is necessary to mention at this point that when the slot is fed at its center point (L_f= 15.2 mm), the bandwidth is 51.2% (2.54 to 4.29 GHz). The position of the feed line also changes the operating frequency of the antenna.

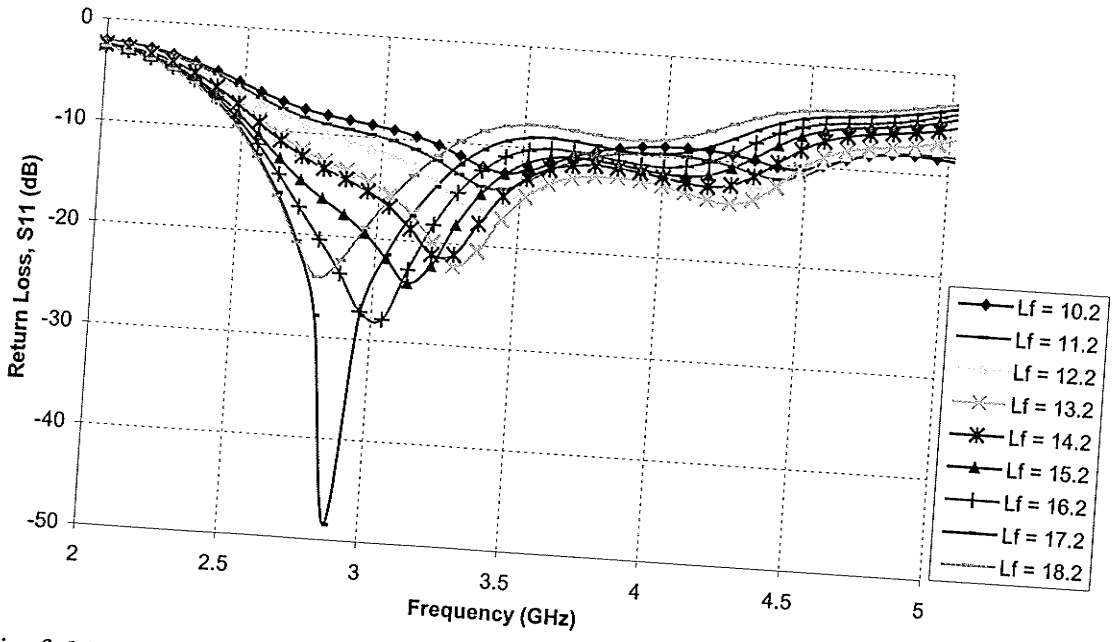

Fig. 3.11: The effect of varying the feed line position (L_f) of the slot antenna in Fig. 3.8 on its return loss. Other parameters are kept the same as in Table 3.1.

Table 3.4: The effect of varying feed line position (L_f) on the impedance bandwidth and operating frequency of the antenna in Fig. 3.8

L_f (*mm*)	Frequency Limits (*GHz*)	Center Frequency (*GHz*)	Frequency for min. S_{11} (*GHz*)	BW (%)
10.2	3.16 - 3.75	3.455	3.44	17%
11.2	3.0 - 3.84	3.42	3.4	24.6%
12.2	2.8 - 4.54	3.67	3.36	47.4%
13.2	2.62 - 4.5	3.56	3.28	52.8%
14.2	2.59 - 4.41	3.5	3.24	52%
15.2	2.54 - 4.29	3.415	3.12	51.2%
16.2	2.51 - 4.2	3.355	3.0	51.4%
17.2	2.5 - 3.4	2.95	2.88	30.5%
18.2	2.48 - 3.27	2.875	2.8	27.5%

3.3.1.4 Effect of Slot Width

As the width of the slot changes, the radiation resistance of the slot also changes. Fig. 3.12 shows the effect of varying the slot width, while the feed line length (*fl*) is kept fixed at 18.5 mm and the stub length (*St*) at 6 mm, on its impedance bandwidth. It reveals that, bandwidth increases from 24% (2.75 to 3.5 GHz) to 52.4% (2.56 to 4.38 GHz) as S_W decreases from 11 mm to 5 mm (Table 3.5). But, if it is further decreased, the bandwidth decreases. Between S_W = 3 mm to 7 mm, a bandwidth in excess of 48% is achieved. The reduction in the bandwidth due to the decrease in slot width can be attributed to reduction in the radiation resistance, hence the impedance bandwidth of the antenna increases.

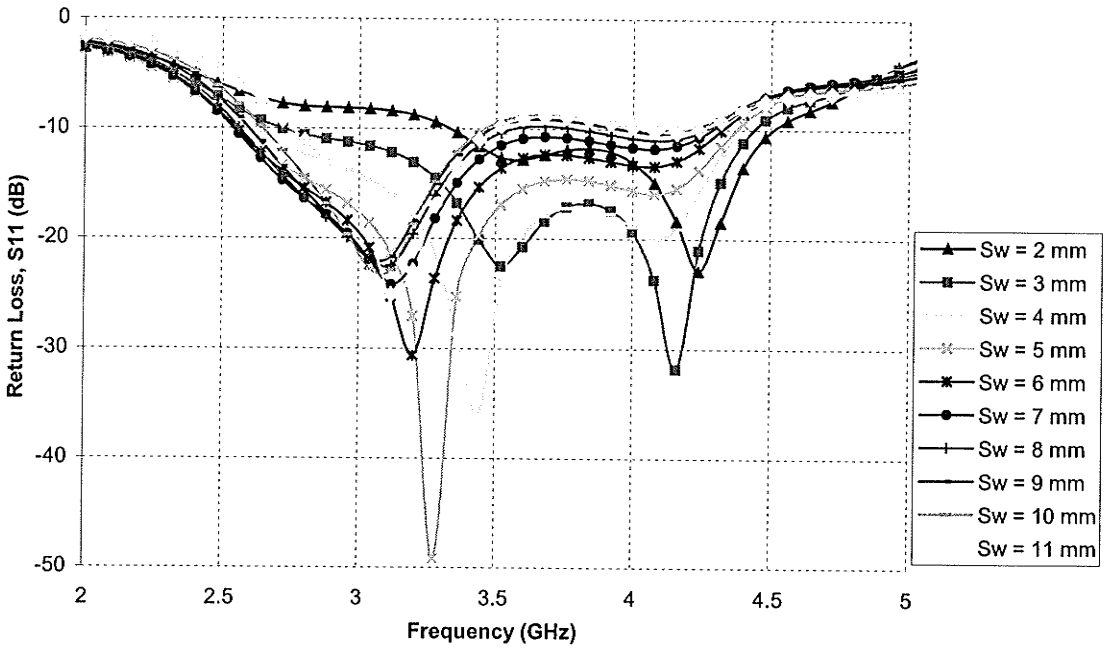

Fig. 3.12: The effect of varying slot width (S_W) of the slot antenna in Fig. 3.8 on its return loss. Other parameters are kept the same as in Table 3.1.

Table 3.5: The effect of varying slot width (S_W) on the impedance bandwidth and operating frequency of the antenna in Fig. 3.8

S_W *(mm)*	Frequency Limits *(GHz)*	Center Frequency *(GHz)*	Frequency for min. S_{11} *(GHz)*	BW (%)
2	3.33 - 4.5	3.915	4.24	29%
3	2.71 - 4.44	3.575	4.16	48.4%
4	2.61 - 4.4	3.505	3.4	51.1%
5	2.56 - 4.38	3.47	3.28	52.4%
6	2.55 - 4.32	3.435	3.2	51.5%
7	2.54 - 4.29	3.415	3.12	51.2%
8	2.56 - 3.56	3.06	3.08	29.2%
9	2.6 - 3.49	3.045	3.08	26.5%
10	2.65 - 3.46	3.055	3.08	26.5%
11	2.75 - 3.5	3.125	3.16	24%

3.3.1.5 Effect of Ground Plane Width

A change in the ground plane width or length means a change in the overall antenna size. As mentioned earlier, the space available in the ground plane, after the slot, can be utilized for the electronic circuitry, the ground plane size is an important factor. Moreover, the ground plane size has an effect on the radiation pattern of the antenna. For this reason, the effects of varying the ground plane width and length are studied next. Fig. 3.13 shows the effect of varying ground plane width, G_W while keeping St = 6 mm and fl = 18.5 mm. When G_W is increased from 40 mm to 60 mm, the –10 *dB* return loss bandwidth enhances from 25.8% (2.74 to 3.55 GHz) to 55.2% (2.44 to 4.3 GHz). If it is increased further, the bandwidth goes down. In the range G_W = 50 mm to 60 mm, bandwidth in excess of 51% can be achieved but at the expense of increasing the frequency (from 3.12 to 3.96 GHz) for minimum S_{11}. It should be mentioned here that the lower end frequency limit of the antenna goes down from 2.54 GHz to 2.44 GHz in the above-mentioned range.

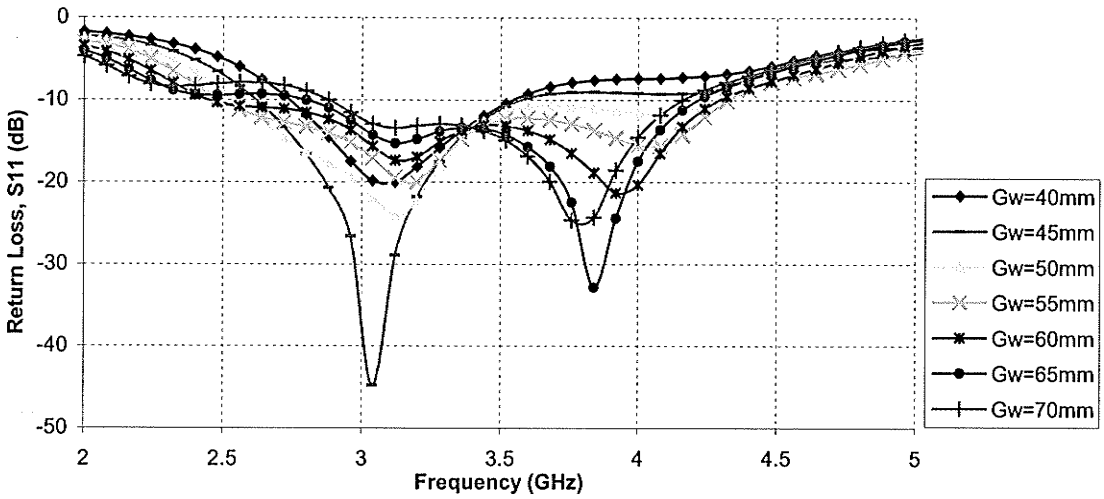

Fig. 3.13: The effect of varying ground plane width (G_W) of the slot antenna in Fig. 3.8 on its return loss. Other parameters are kept the same as in Table 3.1.

Table 3.6: The effect of varying ground plane width (G_W) on the impedance bandwidth and operating frequency of the antenna in Fig. 3.8

G_W (*mm*)	Frequency Limits (*GHz*)	Center Frequency (*GHz*)	Frequency for min. S_{11} (*GHz*)	BW (%)
40	2.74 - 3.55	3.145	3.08	25.8%
45	2.62 - 3.58	3.1	3.04	31%
50	2.54 - 4.29	3.415	3.12	51.2%
55	2.49 - 4.33	3.41	3.16	54%
60	2.44 - 4.3	3.37	3.96	55.2%
65	2.8 - 4.22	3.51	3.84	40%
70	2.88 - 4.16	3.52	3.8	36.3%
75	2.94 - 4.07	3.505	3.72	32%

3.3.1.6 Effect of Ground Plane Length

The influence of varying ground plane length (G_L) is shown in Fig. 3.14 with St = 6 mm and fl = 18.5 mm. It shows that from G_L = 50 mm to 90 mm, the impedance bandwidth is always greater than 40%, indicating less effect of varying the ground plane length on the bandwidth.

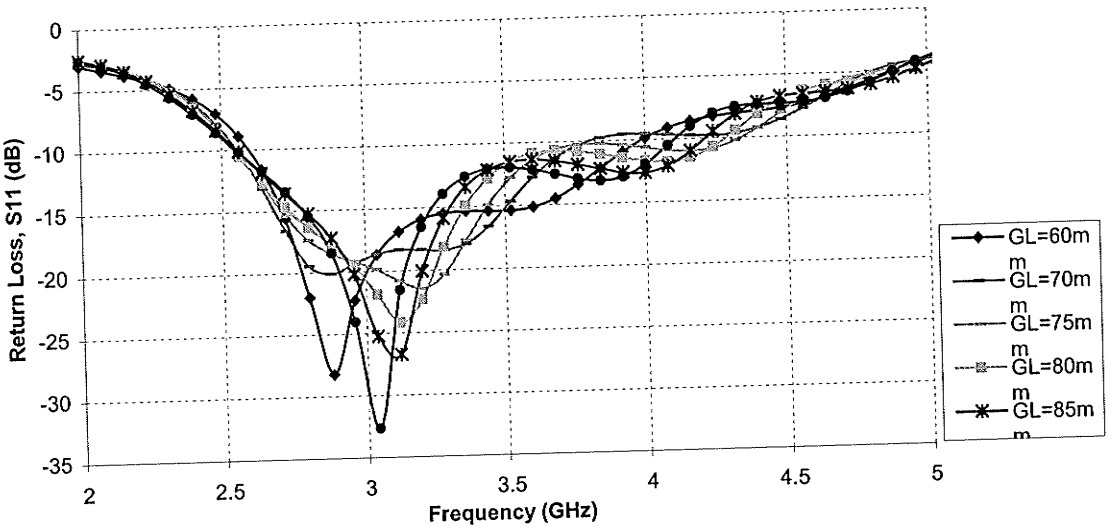

Fig. 3.14: The effect of varying ground plane length (G_L) of the slot antenna in Fig. 3.8 on its return loss. Others parameters are kept the same as in Table 3.1.

Table 3.7: The effect of varying ground plane length (G_L) on the impedance bandwidth and operating frequency of the antenna in Fig. 3.8

G_L (*mm*)	Frequency Limits (*GHz*)	Center Frequency (*GHz*)	Frequency for min. S_{11} (*GHz*)	BW (%)
50	2.67 - 4.1	3.385	2.98	42.2%
55	2.65 - 4.05	3.35	2.92	41.8%
60	2.6 - 3.99	3.295	2.88	42.2%
65	2.57 - 3.89	3.23	2.84	40.9%
70	2.55 - 3.8	3.175	2.84	39.4%
75	2.55 - 4.34	3.445	3.2	52%
80	2.54 - 4.29	3.415	3.12	51.2%
85	2.55 - 4.21	3.38	3.08	49.1%
90	2.55 - 4.1	3.325	3.04	46.6%

From table 3.7, it is found that, with G_L= 75mm, a bandwidth of 52% (2.55 to 4.34 GHz) is achieved. In the range G_L = 75 to 85 mm, more than 49% impedance bandwidth is achieved. The variation in the frequency for the minimum S_{11} is not that much significant.

3.3.1.7 Effects of Dielectric Substrate Permittivity

High permittivity substrate materials are not good for radiation, because they trap the electric fields inside the substrate. They also have the effect on the impedance bandwidth of microstirp antenna. Keeping St = 6, fl = 18.5 mm and rest of the parameters fixed as in table 3.1, the effect of varying only ε_r on the impedance bandwidth of the antenna under consideration is shown in Fig. 3.15. A bandwidth in excess of 49% is achieved with ε_r =2.5 to 4.5. With ε_r = 4.5, 51.2% (2.54 to 4.29 GHz)

bandwidth is found. If ε_r is increased further, the bandwidth goes down. The frequency for the minimum S_{11} goes down from 3.68 GHz to 2.76 GHz when ε_r is increased from 2.5 to 10.2.

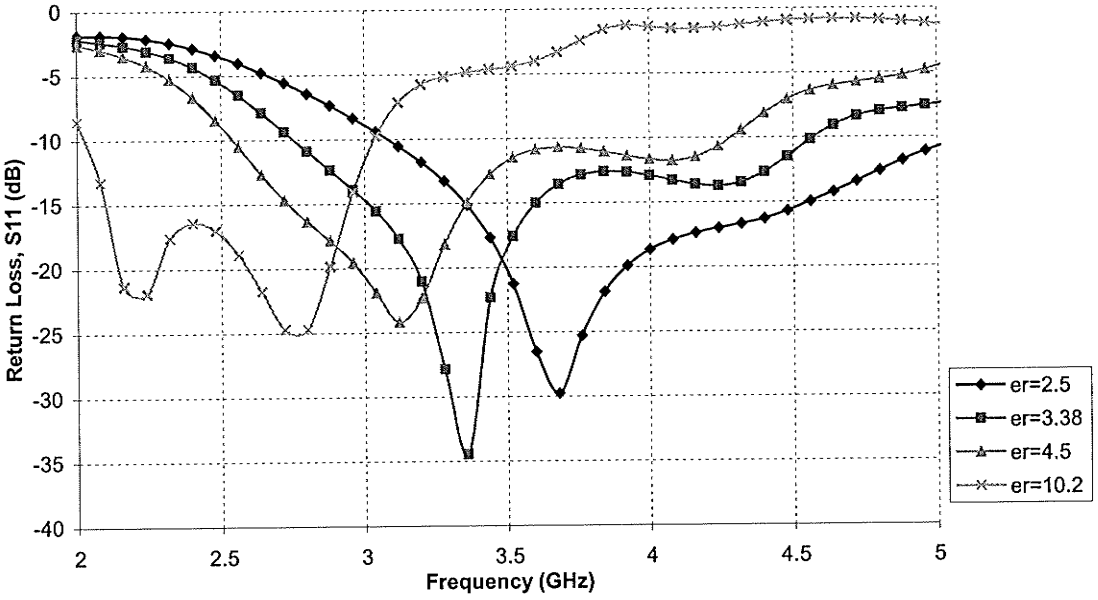

Fig. 3.15: The effect of varying the substrate permittivity (ε_r) of the slot antenna in Fig. 3.8 on its return loss. Other parameters are kept the same as in Table 3.1.

Table 3.8: The effect of varying the substrate permittivity (ε_r) on the impedance bandwidth and operating frequency of the antenna in Fig. 3.8

ε_r (*mm*)	Frequency Limits (*GHz*)	Center Frequency (*GHz*)	Frequency for min. S_{11} (*GHz*)	BW (%)
2.5	3.08 - 5.13	4.105	3.68	50%
3.38	2.75 - 4.57	3.66	3.32	49.7%
4.5	2.54 - 4.29	3.415	3.12	51.2%
10.2	2.03 - 3.04	2.52	2.76	40%

3.3.1.8 Effects of Dielectric Substrate Height

The impedance bandwidth of microstrip antenna is sensitive to the height of the dielectric substrate. In Fig. 3.16, the effect of using dielectric substrate materials of different height (h) is shown. Here also, St = 6 mm and fl = 18.5 mm. When h = 0.8128 mm or higher, the impedance bandwidth is 47.2% (2.67 to 4.32 GHz) or more. But with h = 0.6096 mm, the bandwidth is only 19.9% (2.63 to 3.21 GHz).

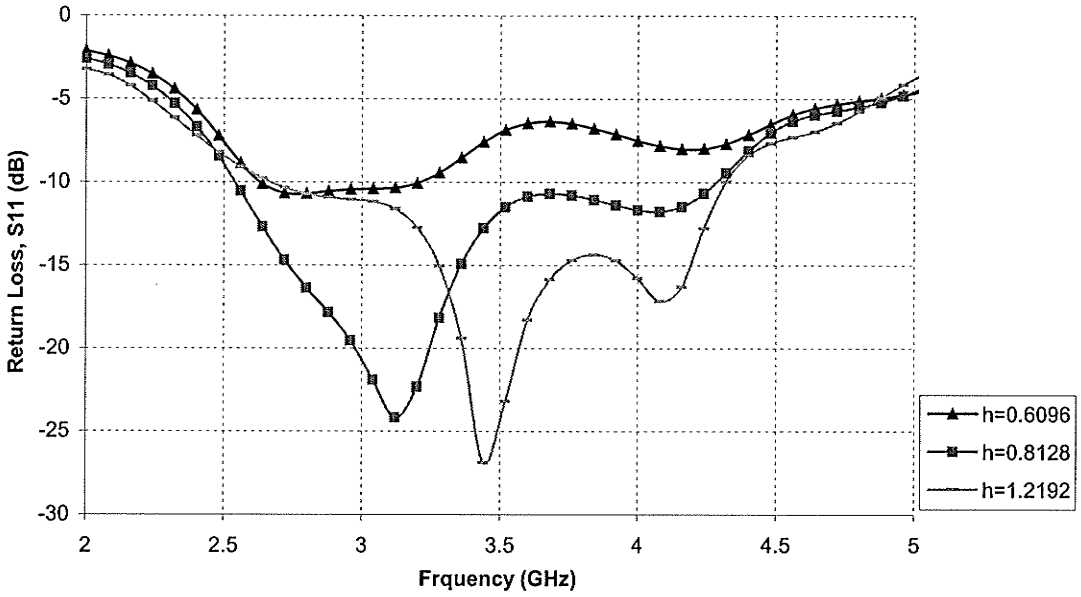

Fig. 3.16: The effect of varying the substrate height (h) of the slot antenna in Fig. 3.8 on its return loss. Other parameters are kept the same as in Table 3.1.

Table 3.9: The effect of varying the substrate height (h) on the impedance bandwidth and operating frequency of the antenna in Fig. 3.8

h (*mm*)	Frequency Limits (*GHz*)	Center Frequency (*GHz*)	Frequency for min. S_{11} (*GHz*)	BW (%)
0.6096	2.63-3.21	2.92	2.76	19.9%
0.8128	2.54-4.29	3.415	3.12	51.2%
1.2192	2.67-4.32	3.495	3.44	47.2%

From the above parametric study, it is apparent that this microstrip-line fed slot antenna is potentially a very wide band antenna. For each of the parameters, -10 dB return loss bandwidth above 50% is achieved. Moreover, any desired bandwidth, ranging from 10% to 53%, can be found only by changing these parameters. Among these, stub length (St), feed line length (fl) and its position (L_f) appear to be the most vital parameters.

In the Smith chart study for all these cases, it was found that the input impedance locus for each case traces one or multiple loops, which is a representation of wide band property of this antenna. These Smith charts are not included here for brevity, but for certain cases, these will be added later. For a given slot size, the loop diameter on the Smith Chart is increased when the feed line position (L_f) is increased. This specifies that, the coupling between the feed line and slot is less when the feed line is close to the shorted end of the slot. The stub length changes the reactance of the slot antenna. Therefore, stub can be used to rotate the loop on the Smith chart.

Since, for each parameter, the peak bandwidth is 50% or larger, as mentioned in the previous discussion, we can expect that if those parameters are chosen, an optimum antenna design can be obtained which will have an impedance bandwidth of 50% or more. For S_W = 3 mm, G_W = 50 mm, G_L = 80 mm, the stub length (St), feed line length (fl) and feed line position (L_f) are varied according to the parametric study to get an optimum design. With St = 8 mm, fl = 18.5 mm and L_f = 15 mm, an impedance bandwidth of 56.17% (2.42 to 4.31 GHz) is achieved, which is larger than that of any of the cases in the parametric study. The simulated return loss for this optimized case is shown in Fig. 3.17(a).

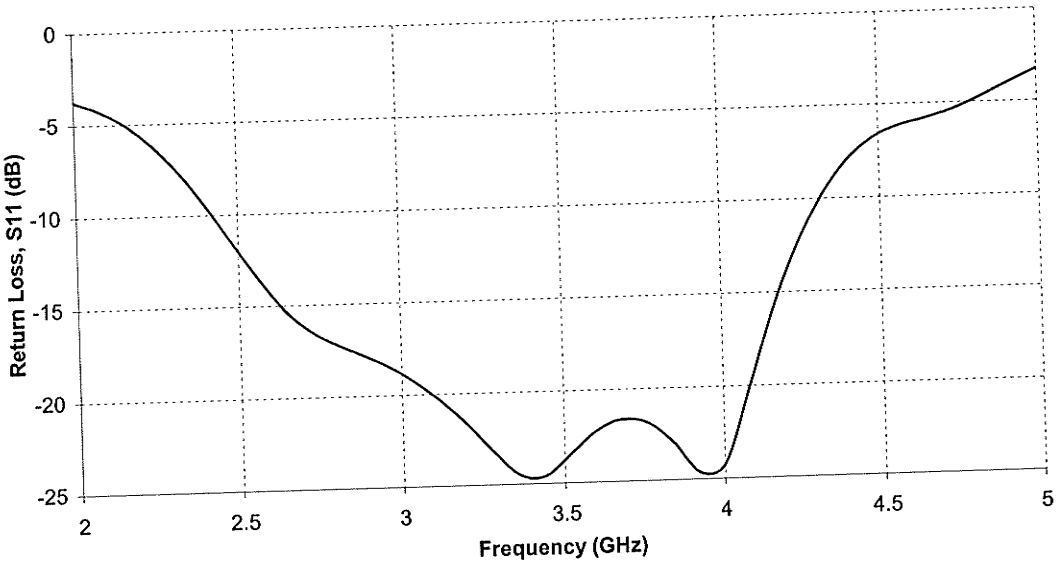

(a)

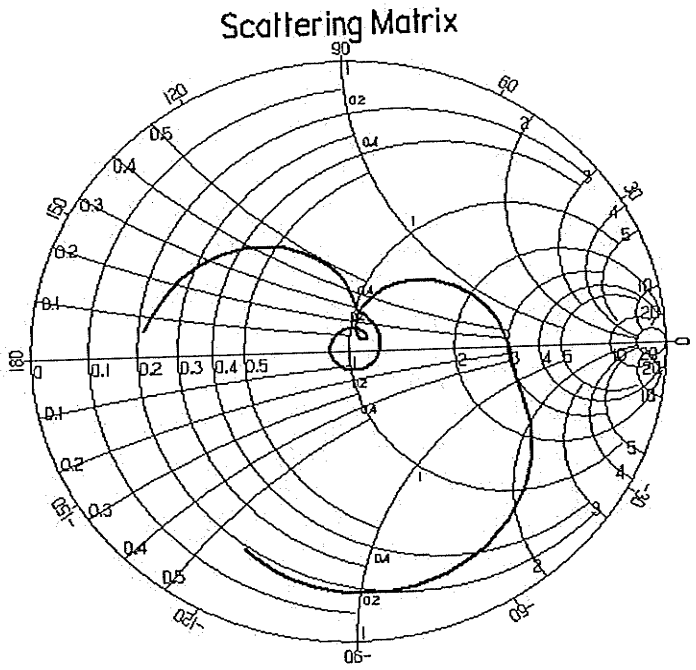

(b)

Fig. 3.17: Simulated (a) return loss and (b) impedance plot of the antenna in Fig. 3.8 with S_W=3mm, L_f=15mm, fl=18.5mm, St=8 mm. Other parameters are the same as in Table 3.1.

In Fig. 3.17(b), the input impedance of this antenna is shown on a Smith chart. The presence of multiple loops, close to the center of the Smith chart, indicates wideband and good impedance matching of this antenna to the 50Ω SMA probe. It should be noted that here $St \cong 0.2\lambda_d$ and $fl \cong 0.4\lambda_d$ where λ_d is the wavelength in the dielectric at center frequency.

The radiation characteristics are important for any antenna. The radiation patterns for the above-mentioned antenna are simulated using HFSS 8.0. The simulated gain patterns at 3.6 GHz for two principal planes are demonstrated in Fig. 3.18. In $\phi = 0^o$ plane, shown in Fig. 3.18(a), E_θ is the co-polarized component and radiates along broadside direction. The radiation is maximum at $\theta = 0^o$ and 180^o, which is a representation of bi-directional radiation as expected for the slot. E_ϕ component is the cross-polarized component in this plane and it has peak radiation is along $\theta = +90^o$ and -90^o. As this is a wide slot, E_ϕ component is also strong due to the surface currents along the width of the slot as shown in the current distribution plot in Fig. 3.19.

Both E_θ and E_ϕ in the $\phi = 0^o$ plane are symmetric as the slot is symmetrically placed in the ground plane. The induced currents in the ground plane are also symmetric. It is known that the surface current density is higher around the slot. These currents are the main source of radiation. In the $\phi = 90^o$ plane in Fig. 3.18(b), E_ϕ is the co-polarized component and this is due to the currents along the slot side. From the figure it is clear that it has omni-directional radiation pattern. Since the slot length is monopole, this radiation pattern is expected. The gain is greater than 0 dBi in the whole θ variation with peak gain of 2.6 dBi along $\theta = 170^0$.

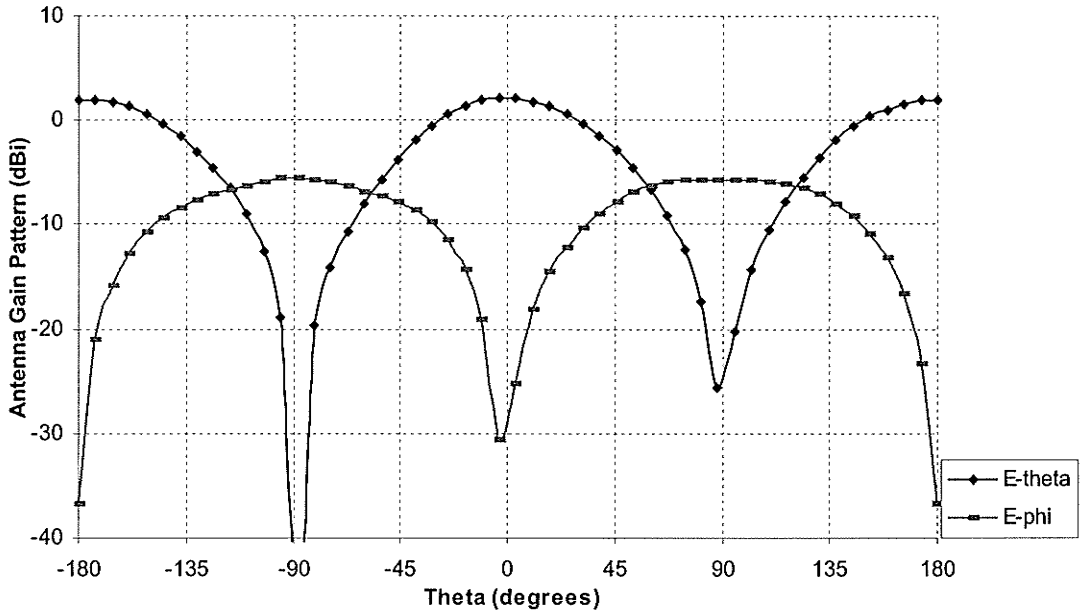

(a)

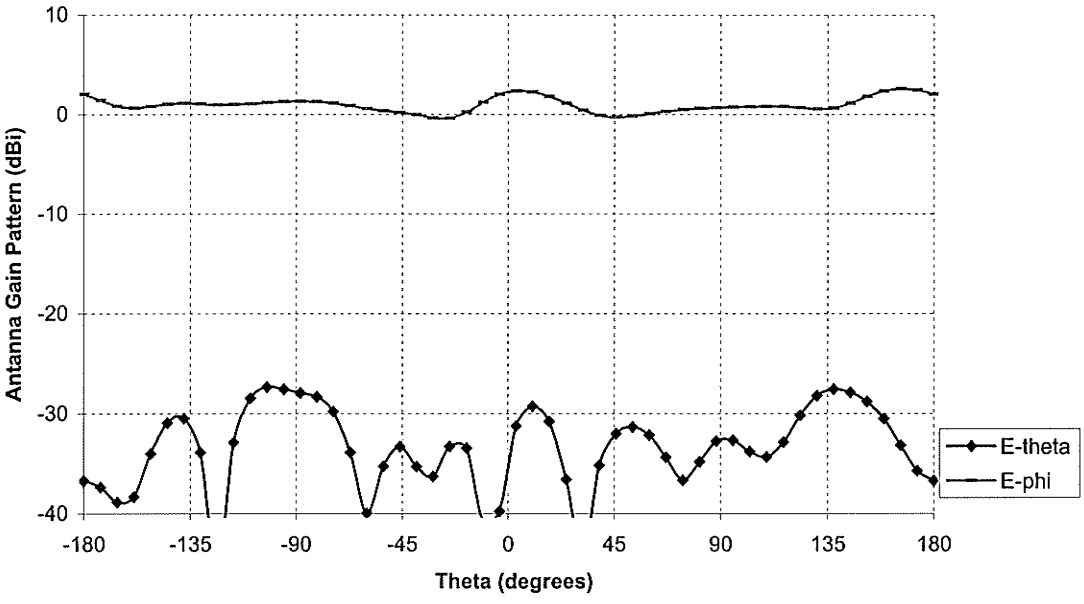

(b)

Fig. 3.18: Simulated gain pattern at 3.6 GHz for the antenna in Fig. 3.8 with S_W = 3mm, L_f = 15mm, fl = 18.5mm, St = 8 mm at (a) $\phi = 0^o$ and (b) $\phi = 90^o$. Other parameters are the same as in Table 3.1.

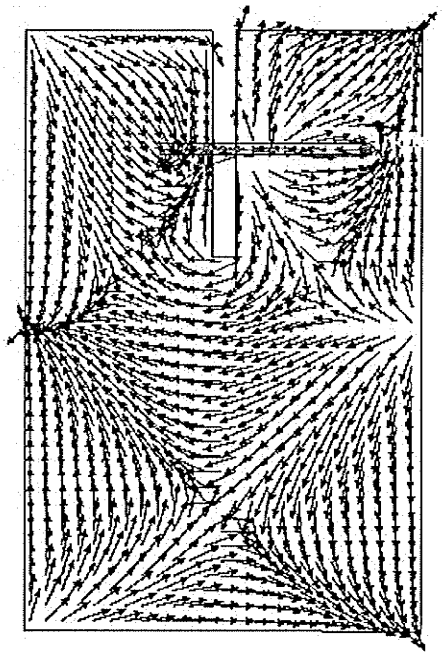

Fig. 3.19: Simulated surface current distribution on the ground plane at 3.6 GHz for the antenna in Fig. 3.8 with S_W = 3mm, L_f = 15mm, fl = 18.5mm, St = 8 mm. Other parameters are the same as in Table 3.1.

If the dielectric substrate permittivity and height are changed, the width of feed line will have to be changed for 50Ω characteristic impedance of the feed line. In the parametric study, the effects of using different substrate material and height were studied with a fixed feed line width. For a given slot size, it was found that the same impedance bandwidth and radiation characteristics can be obtained for different substrate materials, if the same electrical lengths of stub and feed line are used. Earlier it was demonstrated that in FR-4 substrate (ε_r = 4.5, h = 0.8128 mm and $tan\delta$ = 0.02), an impedance bandwidth of 56.17% (2.42 to 4.31 GHz) was achieved with $St \cong 0.2\lambda_d$ and $fl \cong 0.4\lambda_d$, where λ_d is the wavelength in dielectric at center frequency. The width of the microstrip line is chosen such that its characteristic impedance is 50Ω on FR-4

substrate. Now, when the dielectric material is changed (ε_r = 2.5, h = 1.57 mm and $tan\delta$ = 0.02), the electrical length of the feed line and stub is kept same as the previous case, that means $St \cong 0.2\lambda_d$ and $fl \cong 0.4\lambda_d$, where λ_d is the wavelength in new dielectric at center frequency. The width of the microstrip line is also changed such that its characteristic impedance is 50Ω on this substrate. The simulated return loss and input impedance for this antenna are shown in Fig. 3.23(a) and (b) with the parameters of the antenna. The bandwidth for –10 dB return loss of this antenna is 58.8% (2.46 to 4.51 GHz), which is very close to the bandwidth of the antenna on FR-4 substrate. In the input impedance plot, the loop is at the center of the Smith chart. It means that this antenna is matched well to the 50Ω SMA probe in this frequency range.

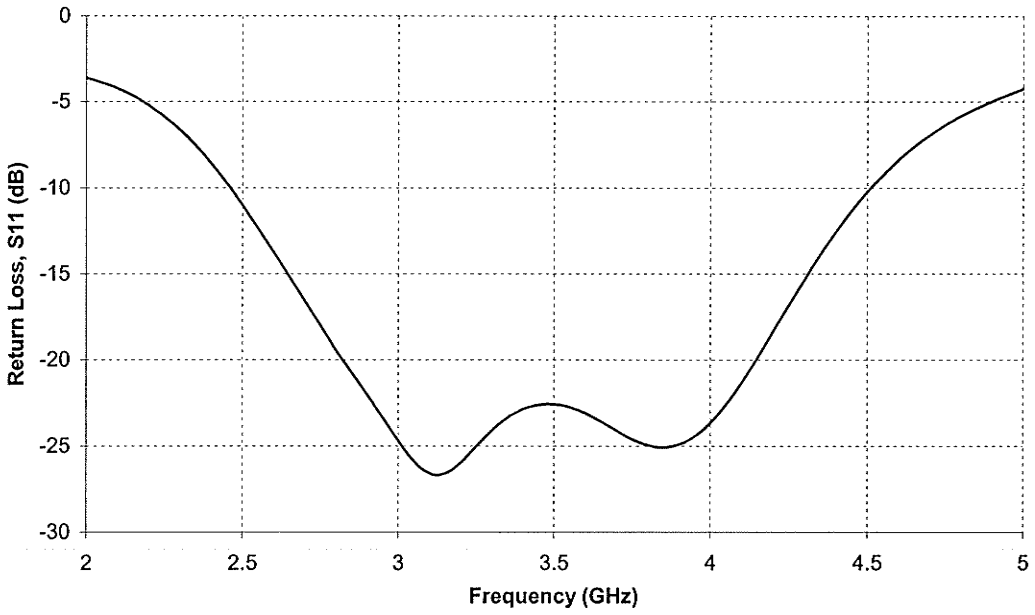

Fig. 3.20(a)

Fig. 3.20 contd.

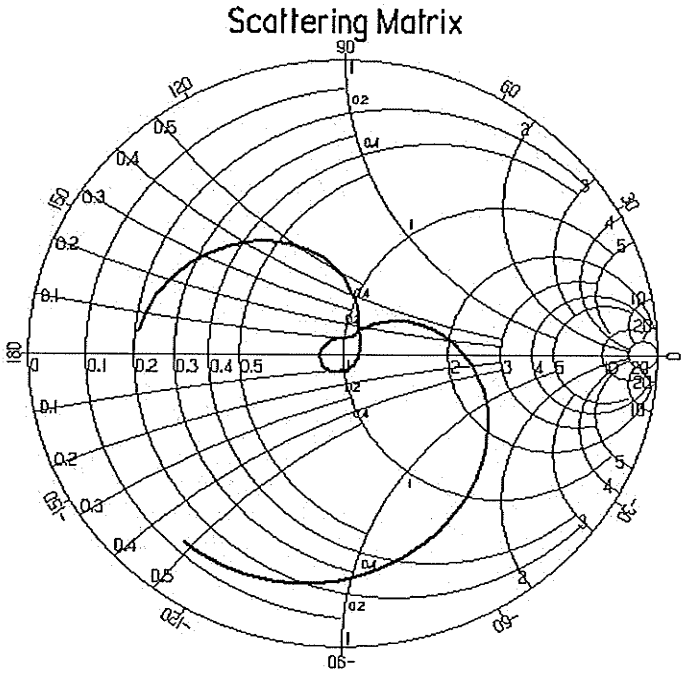

Fig. 3.20(b)

Fig. 3.20: Simulated (a) return loss and (b) input impedance plot of the antenna in Fig. 3.8 with S_W = 3mm, L_f = 15mm, fl = 24mm, St = 11 on a substrate with ε_r = 2.5, h = 1.57 mm and tanδ = 0.001. Microstrip feed line and SMA probe are of 50Ω

The simulated gain pattern at 3.6 GHz, in principal planes, are shown in Fig. 3.21 (a) and (b) for the antenna on a substrate with ε_r = 2.5, h = 1.57 mm and $tan\delta$ = 0.001. Like the antenna on the FR-4 substrate, it shows a bi-directional radiation in the $\phi = 0^o$ plane. In the $\phi = 90^o$ plane, E_ϕ component is the co-polarized component, and here also, it shows an omni-directional radiation pattern. In this plane, the cross-polarized component is E_θ and its level is slightly up compared to that in Fig. 3.18(b) because of the increased substrate height. It can be stated at this point that this study can be applied for the use of any substrate material with different heights. Of course, for good radiation, low-permittivity materials should be used.

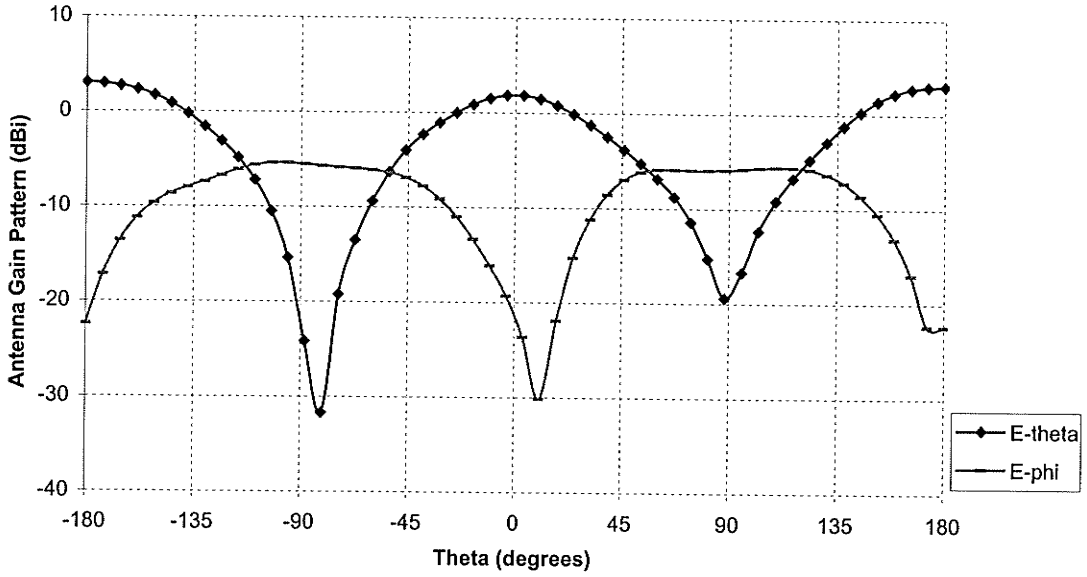

(a)

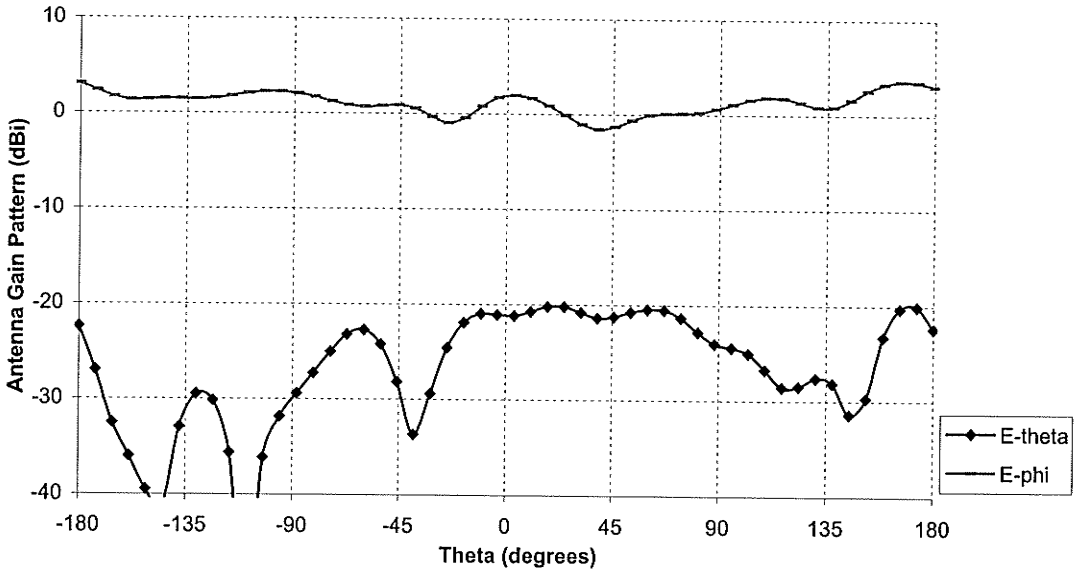

(b)

Fig. 3.21: Simulated gain pattern at 3.6 GHz for the antenna in Fig. 3.8 with S_W = 3mm, L_f = 15mm, fl = 24mm, St = 11 on a substrate with ε_r = 2.5, h = 1.57 mm and tanδ = 0.001 at (a) $\phi = 0^o$ and (b) $\phi = 90^o$. Microstrip feed line and SMA probe are of 50Ω.

3.4 Experimental Verification

In order to confirm the simulation results, the antenna discussed at the end of previous section was chosen for fabrication. The dielectric substrate used has relative permittivity, ε_r = 2.5, height, h = 1.57 mm and loss tangent, $tan\delta$ = 0.001. A monopole slot of length, L_S = 30 mm and width, S_W = 3 mm was cut on the finite ground plane edge. The ground plane size was 50mm×80mm. The slot was fed electromagnetically by a 50Ω microstrip line, which was excited by a 50 Ω SMA probe. Its simulated return loss and input impedance plot, obtained using Ensemble 8.0 [37], were shown earlier in Fig. 3.20(a) and (b). The stub length, feed line length and feed line position were also mentioned in that figure. The antenna was tested in the Antenna Laboratory at the University of Manitoba. The return loss and input impedance were measured by ANRITSU ME7808A Network Analyzer and shown in Fig. 3.22 (a) and (b). Its –10 dB return loss bandwidth from simulation was 58.8% (2.46 to 4.51 GHz), while the measured bandwidth was found to be 59.97% (2.51 to 4.66 GHz).

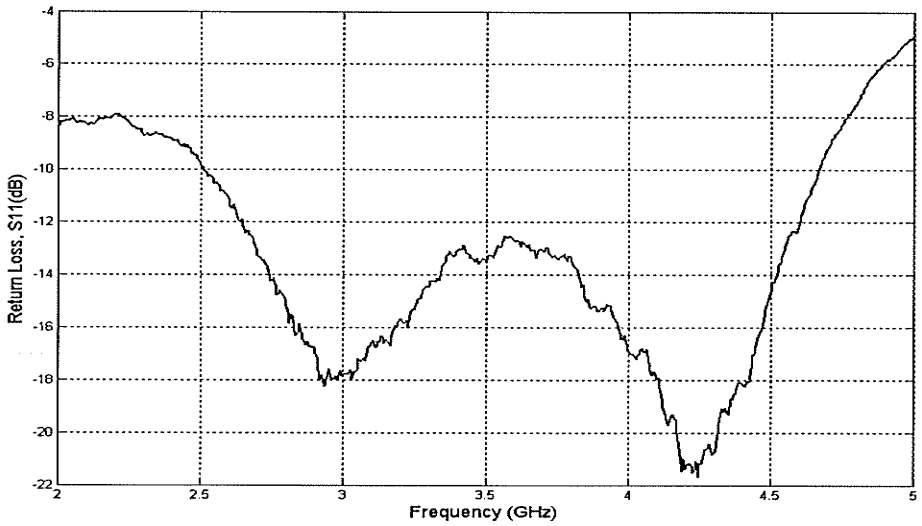

Fig. 3.22(a)

Fig. 3.22 contd.

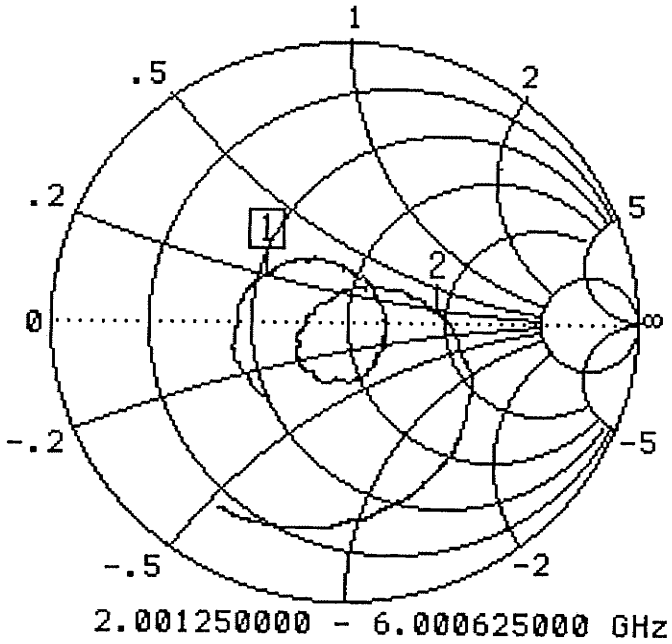

- Marker 1 2.51 GHz
- Marker 2 4.66 GHz

Fig. 3.22(b)

Fig. 3.22: Measured (a) return loss and (b) input impedance plot of the antenna in Fig. 3.8 with S_W = 3mm on a substrate with ε_r = 2.5, h = 0.787mm and tanδ = 0.001 using a tuning stub. Other parameters are mentioned in Fig. 3.20

Since this antenna is an omni-directional antenna, it radiates in all directions. As such, the reflections of the radiated wave occur from the cable, devices and the walls in the lab. In simulation, these practical issues are not taken into account. For this reason, while measuring the antenna, a slight mismatch was found at the input of the antenna, which was compensated for, using a simple tuning stub on the microstrip line. Considering these practical issues, both the simulated and measured results are in good agreement.

The radiation characteristics of the fabricated antenna were also measured in the anechoic chamber in Antenna Laboratory at the university of Manitoba and its gain patterns at three frequencies, within the frequency band, are compared with the simulated results, in two principal planes, in Figs. 3.23-3.25. The simulation results were found using HFSS 8.0. The fabricated antenna was mounted on a dielectric support to keep it away from the tower. Since the antenna is very small in size and it has a bi-directional radiation property, its interaction with the dielectric support is obvious. For this reason, some ripples appeared in the measured gain patterns, as can be seen in Figs. 3.23-3.25. However, in comparison with the simulated gain patterns, it is apparent that the measured gain patterns are close to the simulated ones.

In Fig. 3.23, the comparison of the simulated and measured gain patterns of the antenna at 3.1 GHz is presented. The peak of the E_θ component in both cases was directed along $\theta = 0^0$ and 180^0 in the $\phi = 0^0$ plane, showed in Fig. 3.23(a), which represents bi-directional radiation pattern. Measured peak gain was 3.29 dBi along $\theta = 180^0$ in this plane. The measured cross-polarized component E_ϕ, in this plane, was slightly higher compared to that of simulated one. In the $\phi = 90^0$ plane, in Fig. 3.23(b), E_ϕ is the co-polarization component and shows omni-directional radiation pattern for both simulated and measured cases, though, some ripples were present in the measured results due to the interaction between the antenna and the dielectric support. The measured cross-polarized component E_θ was also higher in this plane compared to that of the simulated one, because of the presence of the dielectric support. Measured peak gain, in this plain, was 4.13 dBi along $\theta = 156^0$.

In Fig. 3.24, the comparison between the simulated and measured gain patterns at mid-frequency (3.6 GHz) is presented. In the $\phi = 0^0$ plane, in Fig. 3.24(a), measured E_θ component was lower compared to the simulated one. In measured cross- polarized component E_θ, the ripples were present. In the $\phi = 90^0$ plane, in Fig. 3.24(b), E_ϕ component represents an omni-directional radiation pattern for both cases. The measured gain was in between –1.56 to +1.6 dBi in the whole θ variation. The measured cross-polarization level was higher, in this plane, compared to the simulated one, again, due to the dielectric support holding the antenna with the measuring system.

At 4.2 GHz, the measured and simulated gain patterns are compared in Fig. 3.25. In the $\phi = 0^0$ plane, in Fig. 3.25(a), the measured E_ϕ component level was also higher at this frequency, compared to the simulated one; therefore, the measured E_θ component was slightly below the simulated component. In the $\phi = 90^0$ plane, in Fig. 3.25(b), both measured and simulated E_ϕ components are representing an omni-directional radiation pattern. Surface currents along the slot length, on the ground plane, were responsible for this radiation. The measured E_θ component was dominant here also due to the interaction between the antenna and the dielectric support. This created ripples in the measured radiation patterns.

Measured and simulated return loss, input impedance and radiation characteristics agree well with some exceptions due to the small size of the antenna, its bi-directional radiation property, less control on reflection from the nearby objects and its dielectric support for mounting. Hence, this experimental verification confirms the accuracy of the simulation results.

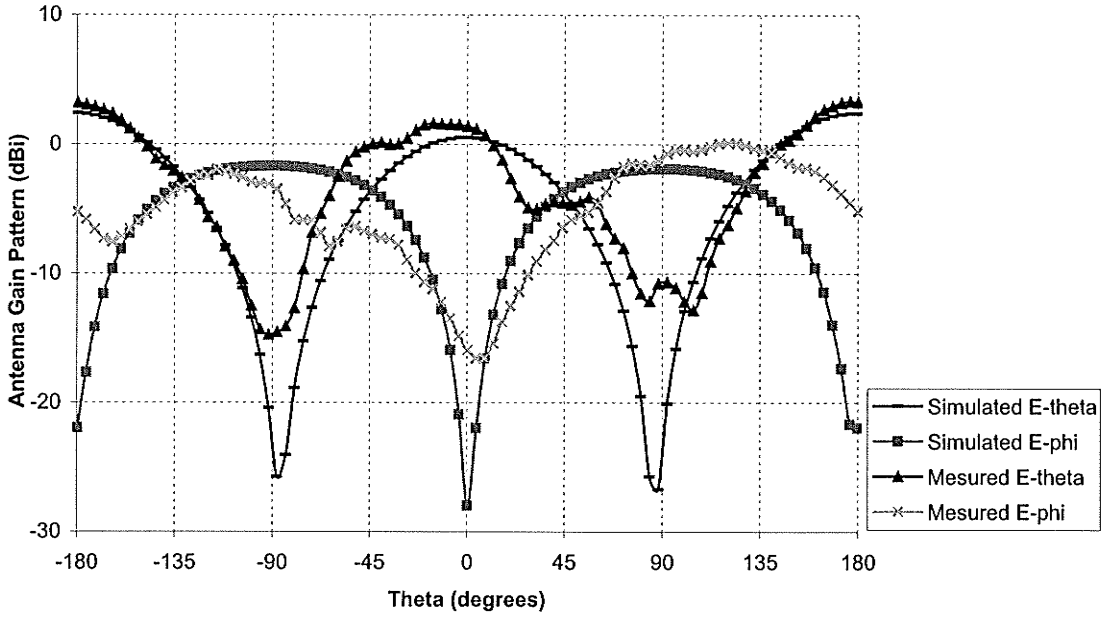

(a)

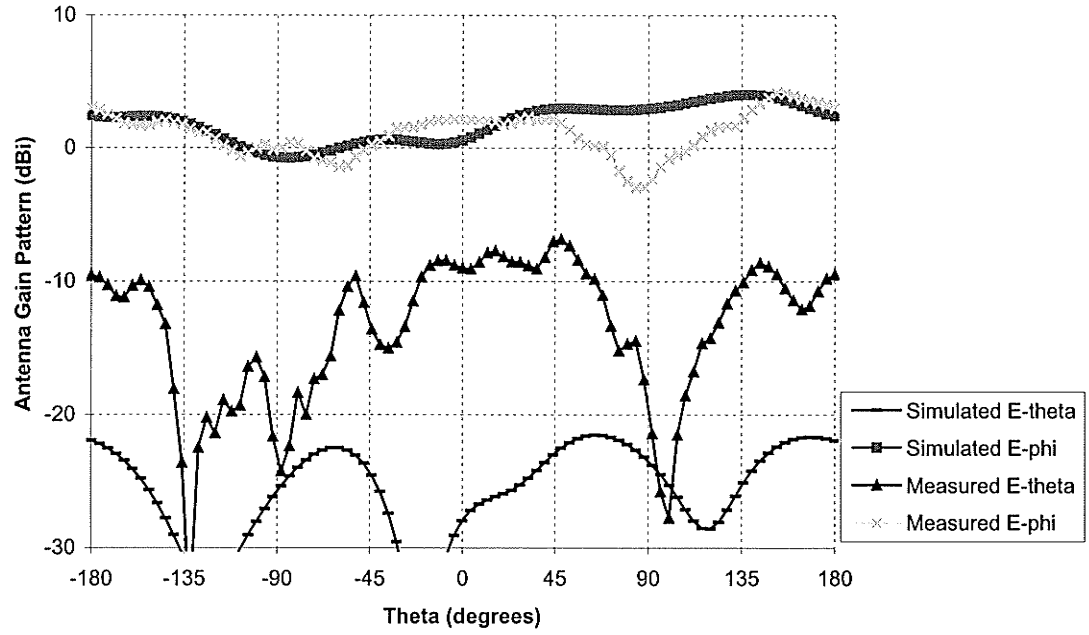

(b)

Fig. 3.23: Measured and simulated gain patterns at 3.1 GHz for the antenna in Fig. 3.8 with S_W = 3mm on a substrate with ε_r = 2.5, h = 0.787 mm and tanδ = 0.001 at (a) ϕ=0° and (b) ϕ=90°. Other parameters are mentioned in Fig. 3.20

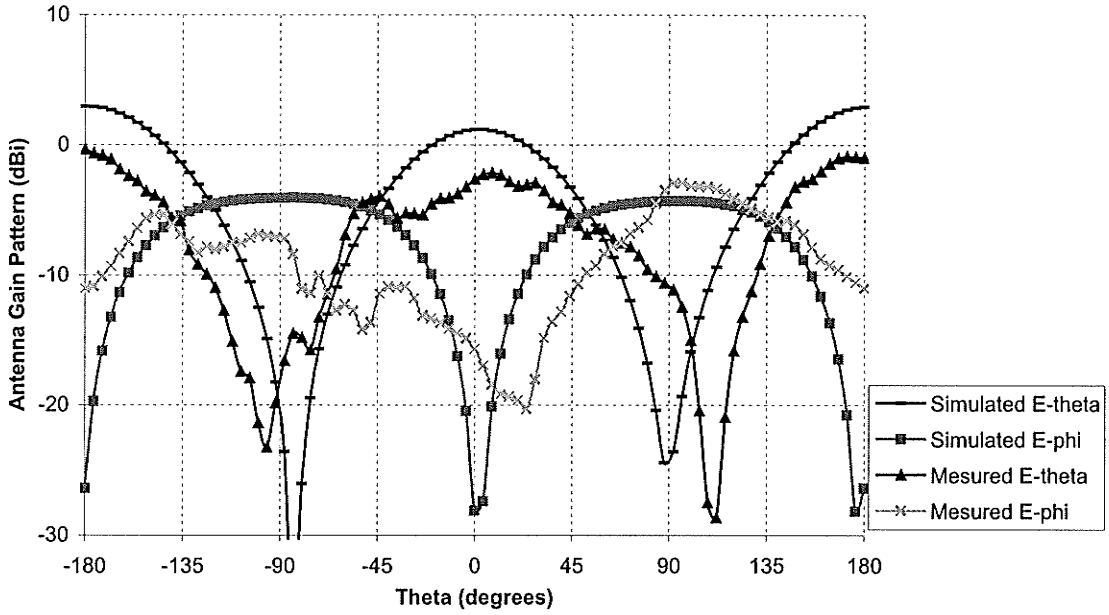

(a)

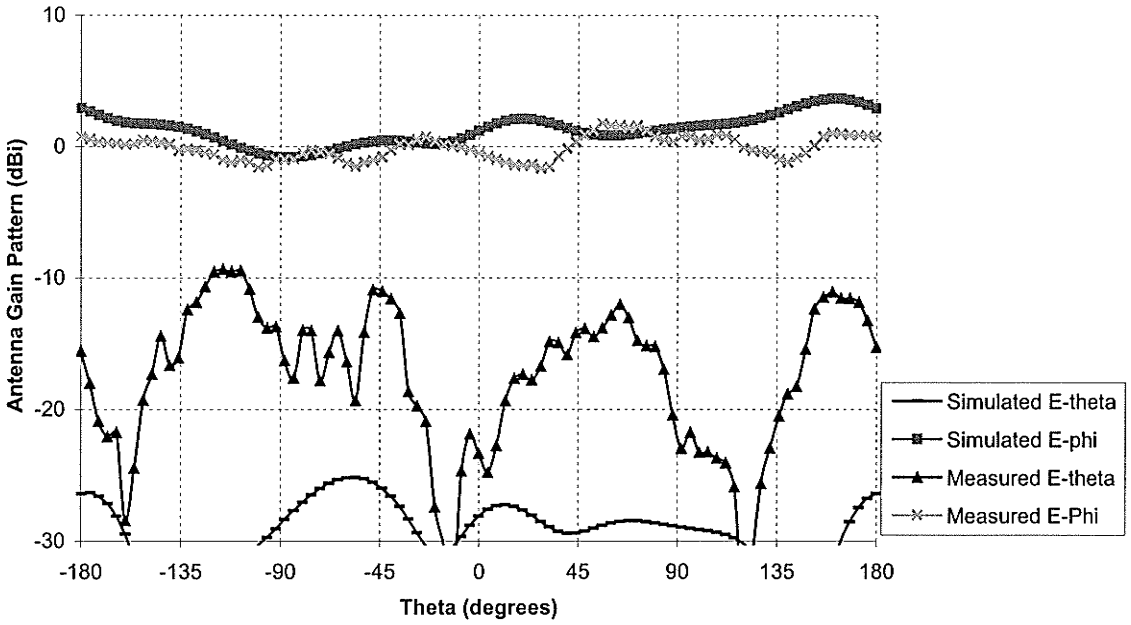

(b)

Fig. 3.24: Measured and simulated gain patterns at 3.6 GHz for the antenna in Fig. 3.8 with S_W=3mm on a substrate with ε_r=2.5, h=0.787 mm and tanδ=0.001 at (a) $\phi=0^o$ (b)$\phi=90^o$. Other parameters are mentioned in Fig. 3.20

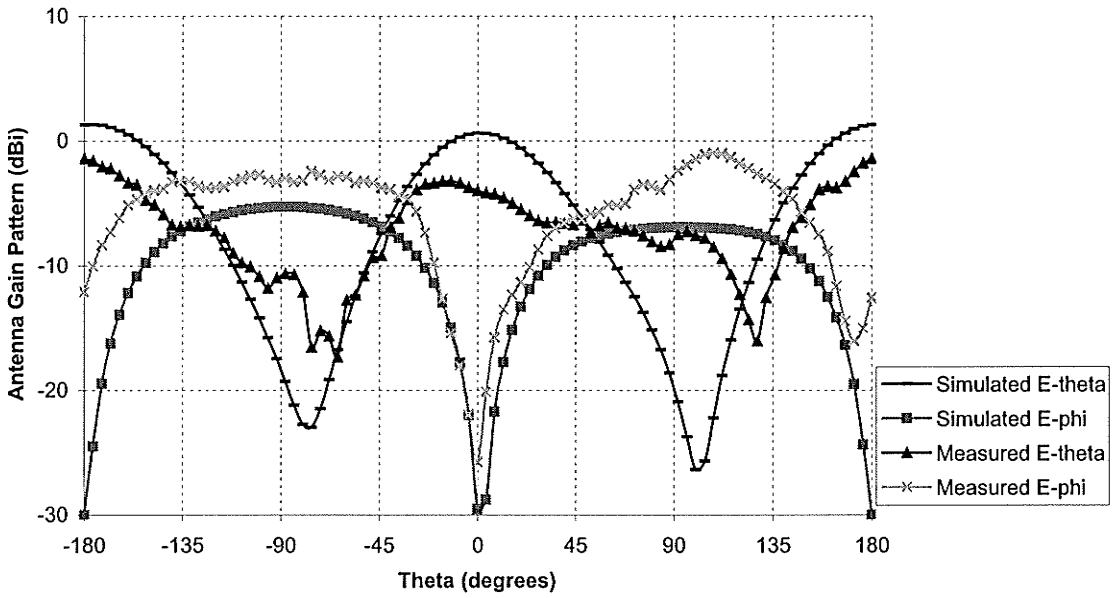

(a)

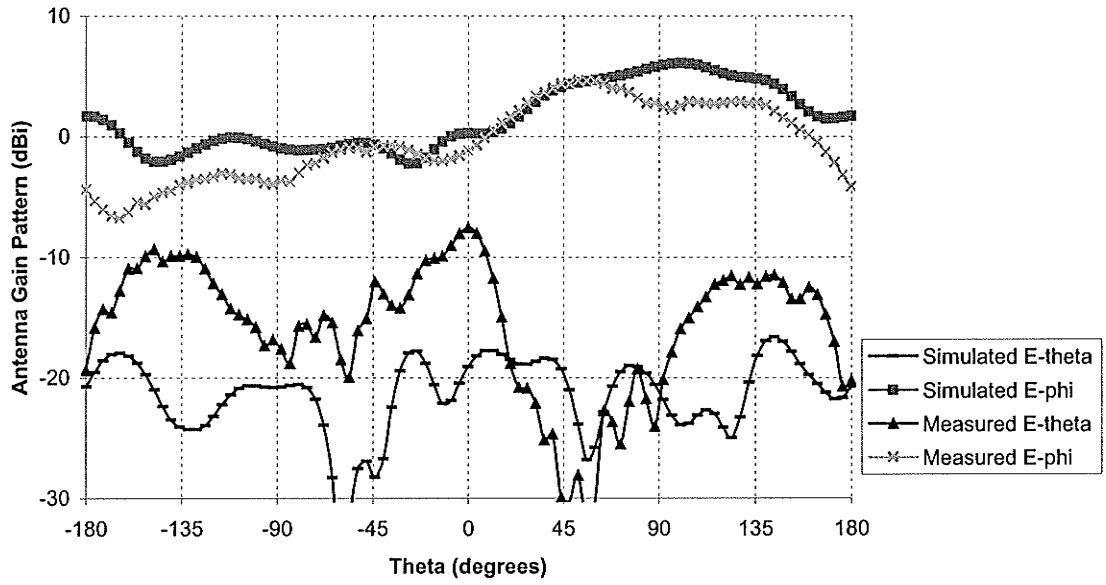

(b)

Fig. 3.25: Measured and simulated gain patterns at 4.2 GHz for the antenna in Fig. 3.8 with S_W = 3mm on a substrate with ε_r = 2.5, h = 0.787 mm and tanδ = 0.001 at (a) ϕ = 0^o (b)ϕ = 90^o. Other parameters are mentioned in Fig. 3.20

3.5 Conclusion

In this chapter, microstrip line-fed slot antenna was studied extensively. The theory of microstrip slot antennas was reviewed briefly. A slot in the ground plane of a microstrip line can be fed centrally. Again, slightly offset feed line or inclined feed line can be used to feed the slot. Each of these feeding techniques has the effect on the radiation resistance of the slot. Stub tuning is also a widely accepted technique in microstrip line-fed slot antenna to match the impedance of the slot to the characteristic impedance of the microstrip feed line. A monopole slot on the center of the ground plane edge was investigated parametrically. The effects of varying individual parameter on its impedance bandwidth were discussed. The radiation patterns of the antenna were also studied. A prototype antenna was fabricated and measured. The simulated and measured results of the antenna for its bandwidth, input impedance and radiation characteristics were compared, which showed good agreements. Measured impedance bandwidth of this antenna was about 60% (2.51 to 4.66 GHz) with an omni-directional radiation pattern.

CHAPTER FOUR

Microstrip L-Slot Antenna for Wideband Operation

4.1 Introduction

This chapter deals with microstrip monopole L-slot antenna. This antenna exhibits a very wide impedance bandwidth. In chapter three, a straight slot cut at the center of the ground plane edge was discussed in detail. If the slot is bent, we will get L-shaped slot. This shape will provide more space in the ground plane to be used by the electronic circuitry when the overall slot length is kept at a quarter-wavelength. Moreover, it provides even a wider impedance bandwidth. The position of the feed line, its length and stub length have immense effects on the impedance bandwidth and operating frequency of the antenna as was in the straight slot case. These effects are investigated along with the radiation pattern for different feed line schemes. Experimental results are also presented at the end of this chapter.

4.2 Microstrip Monopole L-Shaped Slot Antenna

The geometry of the antenna is shown in Fig. 4.1. The L-shaped slot is positioned at one edge of the ground plane and fed by a microstrip line. The slot starts from the center of the ground plane edge and then turns to its right to resemble an English letter "L" form. In fact, the L-slot can be considered as one vertical slot of length L_1 and one horizontal slot of length L_2 connected at their ends. The slot width is uniform along its length except at the bend. The width of the microstrip feed line is

chosen such that the characteristic impedance of the line is 50 Ω, based on the relative permittivity and height of the feed line substrate. The feed line is excited by 50 Ω SMA probe as shown in the figure. For the low-cost FR-4 substrate with $\varepsilon_r = 4.5$, $h = 0.8128$ mm and $tan\delta = 0.02$, the feed line width is calculated to be 1.528 mm.

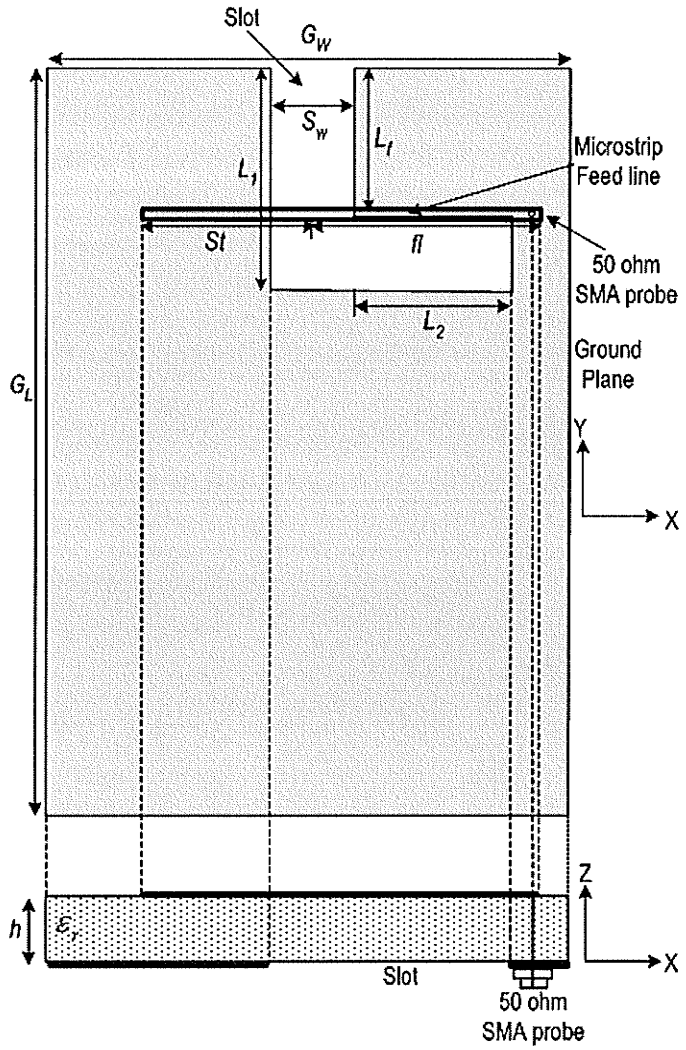

Fig.4.1: The geometry of the L-shaped slot antenna fed by a 50 Ω straight feed line with the co-ordinate system: G_W = 50mm, G_L = 80mm, S_W=7mm (except at the bend), L_1 = 18.5mm, L_2 = 11.5mm, on a substrate with ε_r=4.5, h = 0.8128mm and tanδ = 0.02

4.2.1 Straight Feed Line

At first a straight feed line is used to feed the L-slot as was used to feed the rectangular slot on the ground plane, discussed in chapter three. Both feed line and stub lengths, (*fl*) and (*St*) respectively, are measured from the center of the slot L_1. By selecting proper feed line length (*fl*), feed position (L_f) and stub length (*St*), the operating frequency of the antenna can be changed, and an extremely wide impedance bandwidth can be achieved as well. In fact, by changing these parameters, the impedance of the slot can be matched with the impedance seen by the feed line. This ensures less reflection of power at the slot-microstrip line transition. With *fl* = 18.5 mm, *St* = 9 mm and L_f = 11 mm, an impedance bandwidth of 82.1% (2.24 GHz to 5.36 GHz) is found. The simulated return loss is shown in Fig. 4.2 where the variation of S_{11} with frequency is presented.

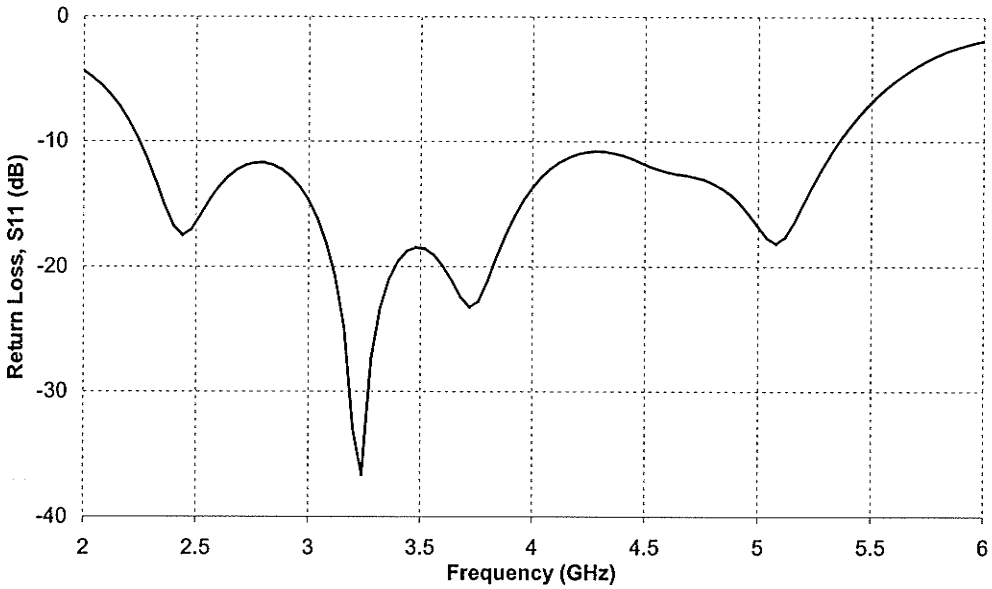

Fig. 4.2(a)

Fig. 4.2 contd.

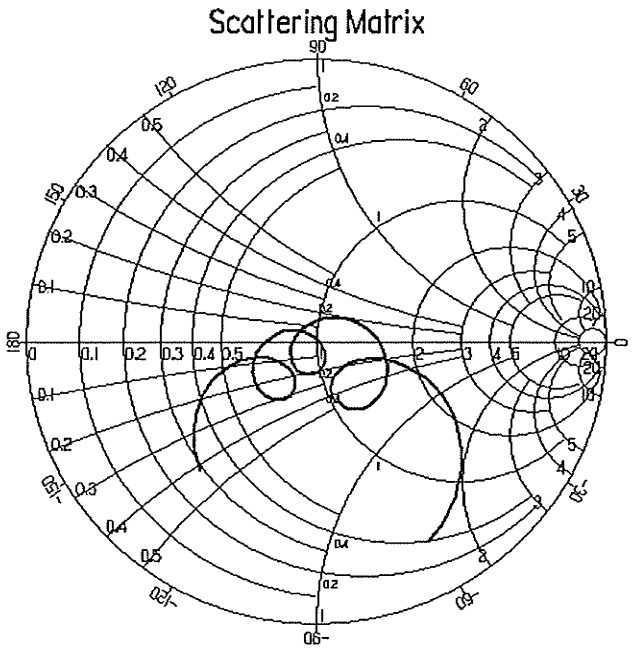

Fig. 4.2(b)

Fig. 4.2: Simulated (a) return loss (S_{11} vs. frequency) and (b) input impedance plot for L-shaped slot antenna in Fig. 4.1. L_f= 11mm, fl = 18.5mm, St = 9mm. Other parameters are the same as in Fig. 4.1

The impedance bandwidth is much greater than that of a rectangular straight monopole slot case, discussed in chapter three. In a straight slot case, the coupling between the feed line and slot excites several modes and two of them are dominant. They are indicated by a single loop on the Smith chart and two nulls on the return loss plots, as shown in Figs. 3.20(a) and (b). Fig. 4.2(a), however, shows four nulls on the return loss plot and three loops in the Smith chart in Fig. 4.2(b). Thus, an L-shaped monopole slot shows four dominant resonances. It appears, therefore, that the two orthogonal arms of the slot act as separate and tightly coupled resonators and their mutual coupling displaces their resonances towards lower and higher frequencies, as shown in Fig. 4.2. This phenomenon enlarges the bandwidth significantly.

The current distribution of the microstrip slot antenna at 4.1 GHz is provided next which will give a good insight for the radiation pattern and polarization. Since slot is present on the ground plane, current distribution is not uniform on the ground plane. Rather, the current is very strong at the slot edges, and its density is higher around the slot than that in other regions of the ground plane. The circulating currents around the slot are the main source of radiation and the rest of the induced ground plane currents will only aid the main radiation from the slot. Hence, the electric field across the slot has both *x*- and *y*- components (refer to Fig. 4.1 for co-ordinate system), which is evident in the radiation pattern plots in Fig. 4.4.

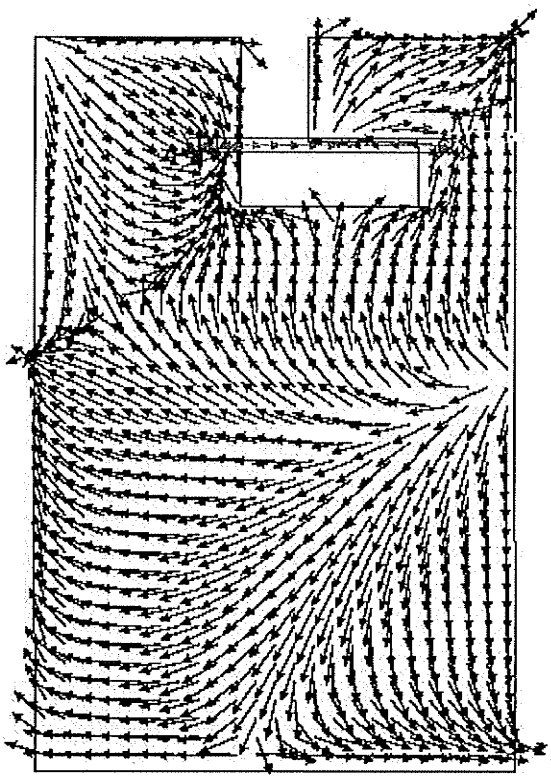

Fig. 4.3: The current distribution at 4.1 GHz of the antenna in Fig. 4.1. L_f= 11mm, fl = 18.5mm, St = 9mm. Other parameters are the same as in Fig. 4.1

From Fig. 4.4(a), it is apparent that the slot antenna has a bi-directional radiation. In the $\phi = 0^{o}$ plane, E_{θ} is the x-polarized component and has the peak radiation at $\theta = 0^{o}$ and 180^{o}. This radiation is from the L_2 slot along the x- axis. Again, for the L_1 slot, the y-component or E_{φ} component is dominant. Since, the geometry of the slot is asymmetric, both E_{θ} and E_{φ} components are asymmetric in this plane. In the $\varphi = 90^{o}$ plane in Fig. 4.4(b), y-directed currents radiate effectively so that almost an omni-directional radiation pattern is found which is represented by E_{φ}. The gain is greater than 2 dBi in the range $\theta = 45^{0}$ to 140^{0}, and greater than 0 dBi along the entire θ variation. Compared to straight slot case [see Fig. 3.21(b)], the x-directed component E_{θ} is higher in this plane. The reason behind this is, once again, the presence of the L_2 slot along the x- axis.

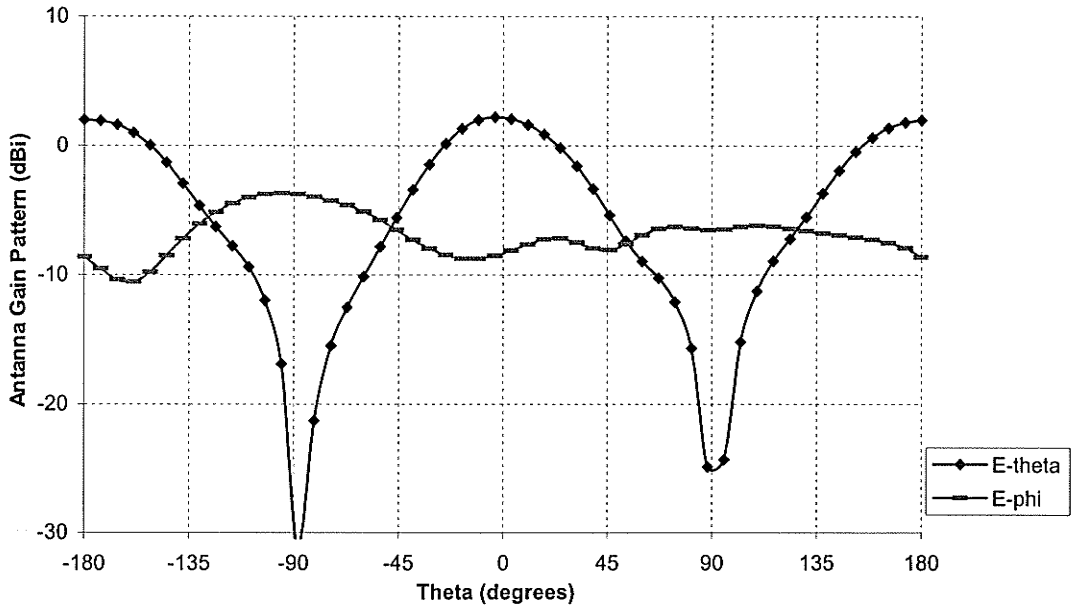

Fig. 4.4(a)

Fig. 4.4 contd.

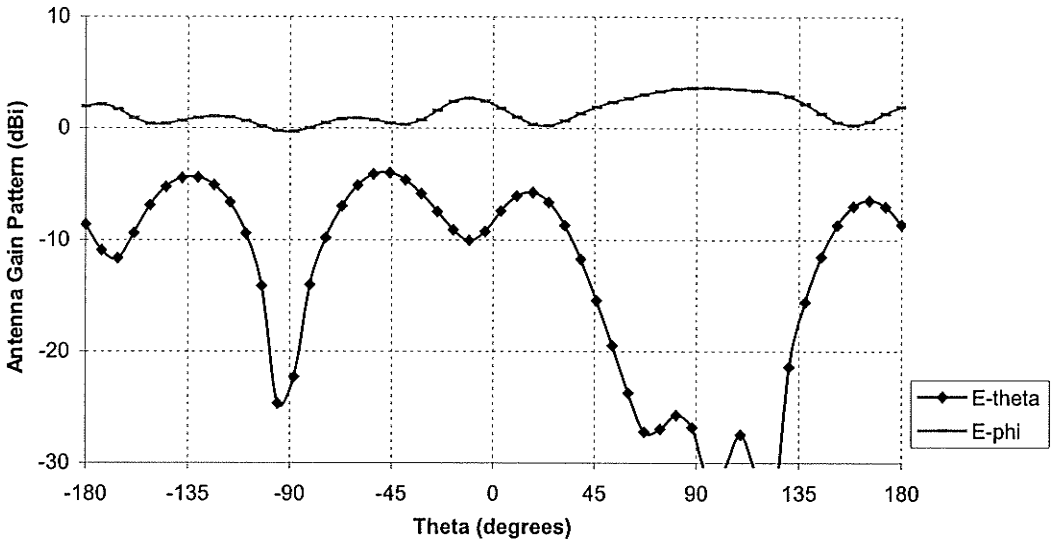

Fig. 4.4(b)

Fig. 4.4: Simulated gain patterns at4.1 GHz for the antenna shown in Fig. 4.1 at (a) $\phi = 0^o$ and (b) $\phi = 90^o$ planes. The parameters are given in Figs. 4.1 and 4.2

4.2.2 Inclined Feed Line

The use of an inclined feed line is common for feeding microstrip slot antennas. An inclined microstrip feed line is introduced here to excite the L-shaped slot in its ground plane. The slot length, shape and width are kept the same as earlier. The stub length (*St*) is measured from the center of the slot at the bend toward the open end of the microstrip feed line, as shown in Fig. 4.5. With *fl* = 16.5 mm, *St* = 7.5 mm, -10 dB return loss bandwidth is 75.7% (2.48 to 5.5 GHz). The variation of S_{11} with frequency is shown in Fig. 4.6, which also shows strong excitation of three resonances in the slot. Hence, a wide impedance bandwidth is found for this antenna with inclined feed line, but slightly less than that (82.1%) of the case, discussed in section 4.2.1.

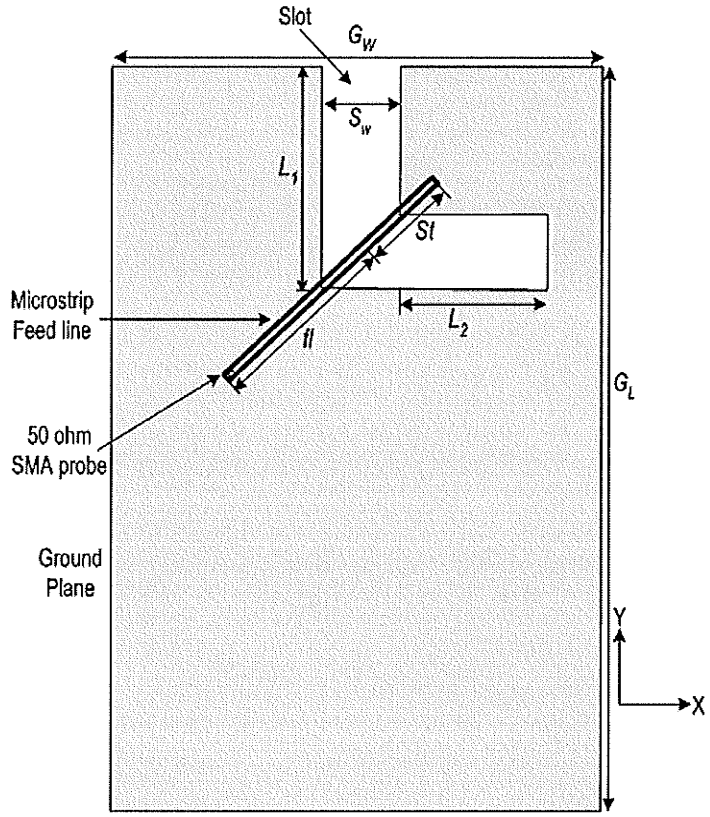

Fig. 4.5: The L-shaped slot antenna fed by an inclined 50 Ω microstrip feed line. fl = 16.5mm, St = 7.5mm. Other parameters are the same as in Fig. 4.1

The impedance bandwidths of the L-shaped slot antenna, fed by two different feed lines, are close. The slight reduction in the bandwidth, of the later case, is due to the inclination of the feed line. The stub length has a similar effect on the operating frequency of the antenna for both cases. However, the inclined feeding system has the advantage from fabrication point of view. It will be easier to excite the inclined feed line by connecting the 50Ω SMA probe than to excite the straight feed line from side on the upper part of the antenna. This is because, the bottom part of the ground plane can be used for the electronic circuitry, therefore, simpler to excite the feed line from this side.

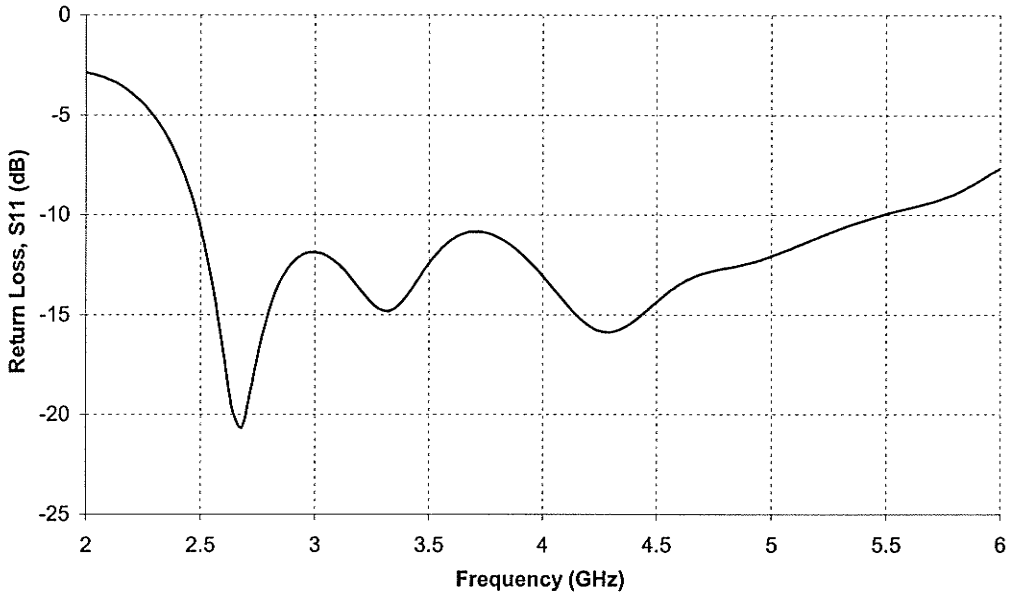

Fig. 4.6: Simulated return loss of the L-shaped slot antenna in Fig. 4.5. fl = 16.5mm, St = 7.5mm. Other parameters are the same as in Fig. 4.1

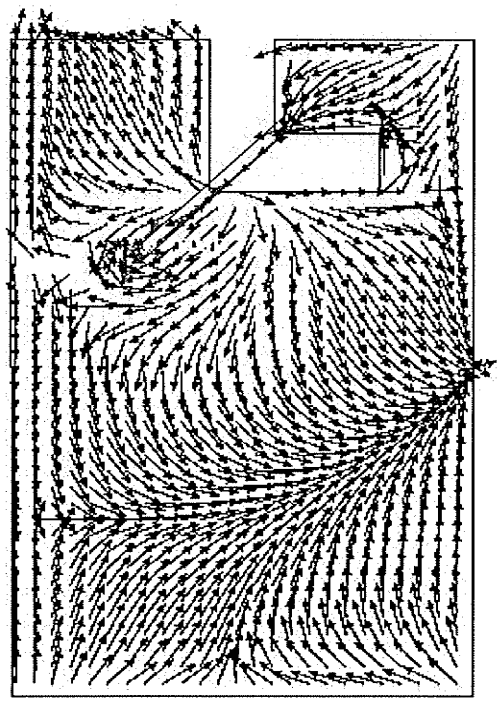

Fig. 4.7: The simulated surface current at 4.1 GHz distribution of the antenna in Fig. 4.5 fl = 16.5mm, St = 7.5mm. Other parameters are the same as in Fig. 4.1

The surface current distribution of the antenna with inclined feed line excitation at 4.1 GHz is shown in Fig. 4.7. This is very similar to the current distribution of the antenna when excited using a straight feed line, except that the origin of the surface currents is changed according to the probe position. There is a strong presence of surface currents along the $\phi = 45^0$ plane.

In Fig. 4.8, the simulated gain patterns of the L-shaped antenna with an inclined feed line is shown. They are very similar to those in Fig. 4.4. Its bi-directional radiation property is apparent in the $\phi = 0^o$ plane shown in Fig. 4.8(a). The peak gain is 2.5 dBi along $\theta = 0^0$. In the $\varphi = 90^o$ plane in Fig. 4.8(b), it is evident that, the E_φ component is omni-directional in nature, due to the magnetic current across the slot aperture. Because of the presence of the L_2 slot along the x-axis, the x-directed component, E_θ level is higher in this plane, as was in Fig. 4.4(b).

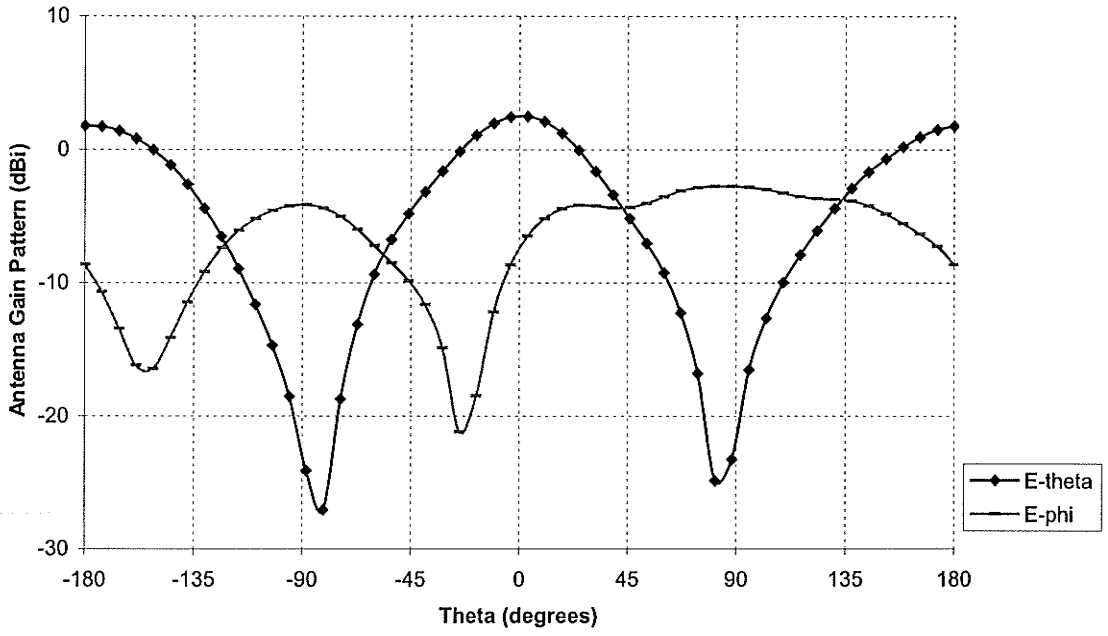

Fig. 4.8(a)

Fig. 4.8 contd.

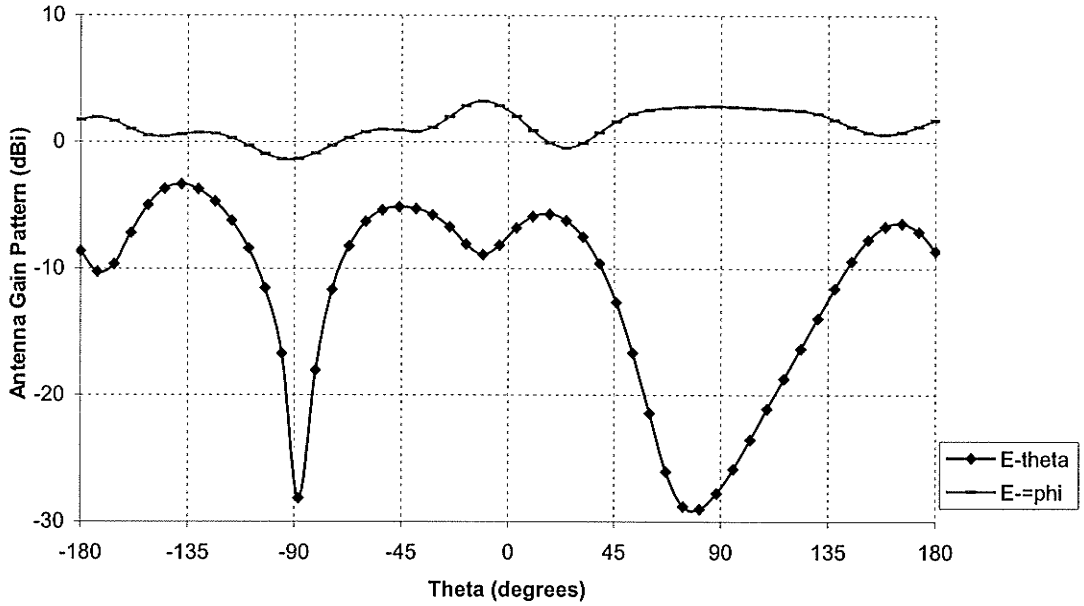

Fig. 4.8(a)

Fig. 4.8: Simulated gain patterns at 4.1 GHz for the antenna shown in Fig. 4.5 at (a) $\phi = 0^o$ and (b) $\phi = 90^o$ planes. The parameters are given in Figs. 4.6 and 4.7

4.2.3 Bent Feed Line

Instead of the inclined straight feed line, a bent feed line is introduced here to investigate its effect on the impedance bandwidth and the radiation characteristics of the antenna. The geometry is shown in Fig. 4.9. The L-slot length is kept the same as the previous two cases; only the inclined feed line used in Fig. 4.5, is bent at the corner of the L-slot, where the slot starts bending. In other words, the feed line is bent at the joining point of slots L_1 and L_2. In this figure, stub length is measured from the L-shaped slot center, at its bending point, toward the open end of the microstrip line. The feed line length is measured from the slot center, at the bend of the L-shaped slot, to the probe position.

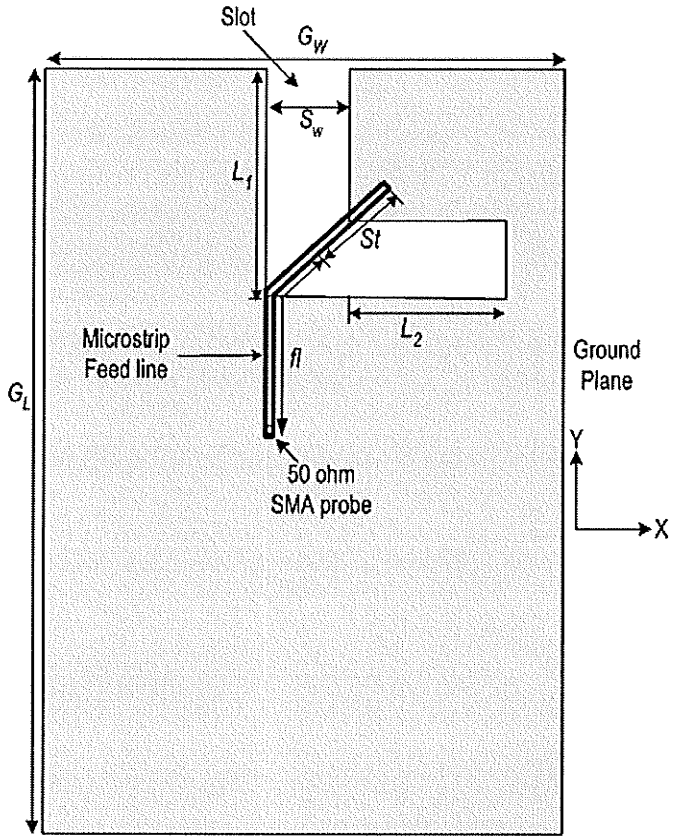

Fig. 4.9: The L-shaped slot antenna fed by a bent 50 Ω microstrip feed line. fl = 17mm, St = 7.5mm. Other parameters are the same as in Fig. 4.1

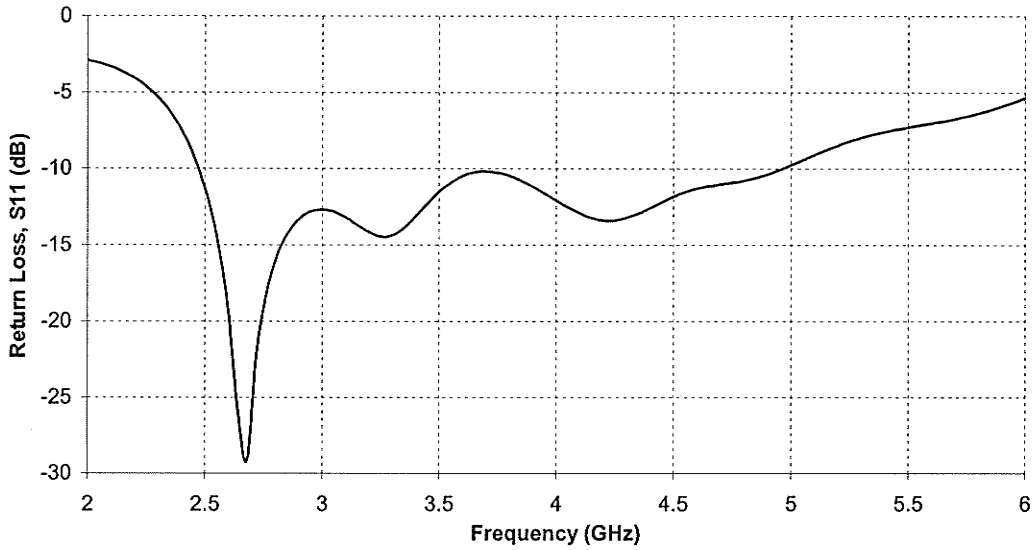

Fig. 4.10: Simulated S_{11} vs. frequency for L-shaped slot antenna of Fig. 4.9 fl = 17mm, St = 7.5mm. Other parameters are the same as in Fig. 4.1

When the stub length (St) is kept the same as it was in the inclined feed case (7.5mm), an impedance bandwidth (S_{11} = -10 dB) of 67.2% (2.47 to 4.97 GHz) is achieved for fl = 17. Due to the bending of the feed line, the coupling between the slot and the feed line reduces resulting in a reduction in the impedance bandwidth.

The current distribution and radiation characteristics are similar to those of the microstrip slot antenna, fed by an inclined feed line. Therefore, these are not included here for brevity.

4.3 Effects of Varying Slot Width

Since the slot width of a micrsotrip slot antenna is an important parameter, for the L-shaped slot antenna also, its effects on the the impedance bandwidth are analyzed. It was shown in the previous section that an L-shaped slot, fed by microstrip line, is a wideband antenna. The variation in the slot width changes the impedance bandwidth, which was also revealed in chapter three for the straight slot case. For the L-shaped slot, changing the slot width also changes the overall slot length. Here, the slot length is always kept the same, i.e. the sum of slots L_1 and L_2 to be 30 mm. The straight feed line is used for this analysis which is excited by a 50Ω SMA probe.

Table 4.1: Impedance bandwidth of the L-shaped antenna for different slot widths

Slot Width	***Slot Length***		***Stub Length***	***Feed Position***	***Frequency Range***	***BW***
(S_W)	L_1 (mm)	L_2 (mm)	(St)	(L_f)	(GHz)	(%)
5	17.5	12.5	11	12	2.15-5.24	83.7
7	18.5	11.5	9	11	2.24-5.36	82.1
9	19.5	10.5	7.5	10	2.37-5.50	79.5

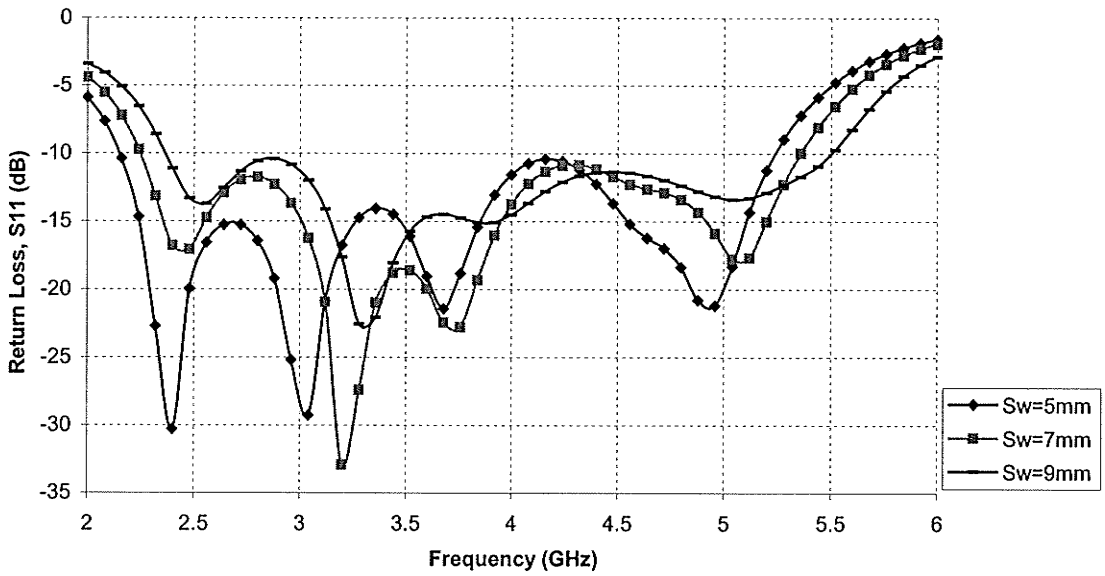

Fig. 4.11: Simulated return loss of the L-shaped antenna in Fig.4.1 for different slot widths. $G_W = 50mm$, $G_L = 80mm$, $\varepsilon_r = 4.5$, $h = 0.8128$ *and* $\tan\delta = 0.02$. *Other parameters are tabulated in Table 4.1*

The influence of varying slot width of the L-shaped slot antenna, fed by a straight feed line is shown in Fig. 4.11. The variation in the slot width changes the impedance bandwidth of the antenna as the radiation resistance of the slot changes. With different slot widths from 5 mm to 9 mm, an impedance bandwidth around 80% can be achieved by selecting appropriate stub lengths. Keeping the feed line length fixed (fl = 18.5 mm) for all the three cases, the feed line position and stub length are changed to get a maximum bandwidth for each slot width. The maximum bandwidth achieved is 83.7% (2.15 to 5.24 GHz) for S_W = 5 mm. As the slot width increases, the maximum impedance bandwidth, by adjusting the stub length properly, decreases. The results are summarized in table 4.1. It is interesting to notice here that these maximum bandwidths are achieved when the feed line is positioned right over the junction of L_1 and L_2 slots comprising the L-shaped slot.

4.4 Experimental Verification

In order to check the accuracy of the simulation results, an L-shaped slot antenna fed by a straight microstrip feed line (Fig. 4.1) was fabricated on a substrate material with a dielectric constant ε_r = 2.5, h = 0.787 mm and $tan\delta$ = 0.001. The microstrip feed line was excited by a 50Ω SMA probe. The monopole L-shaped slot was positioned at one edge of the ground plane. L_1 arm of the slot is at the center of the ground plane width (G_W) and at the end of L_1 slot, to its side, L_2 arm was cut. The remaining dimensions of the antenna are stated in Fig. 4.12, where the simulated return loss and input impedance plot of the L-shaped antenna, obtained using Ensemble 8.0, is depicted. From the simulated return loss plot, -10 dB return loss bandwidth of the antenna is 82% (2.42 to 5.78 GHz).

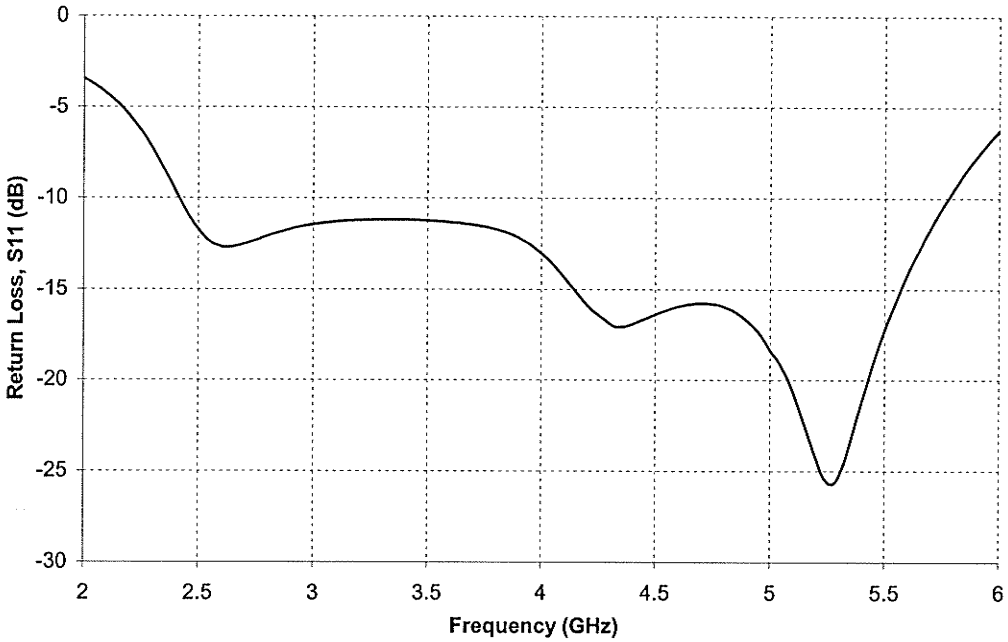

Fig. 4.12 (a)

Fig. 4.12 contd.

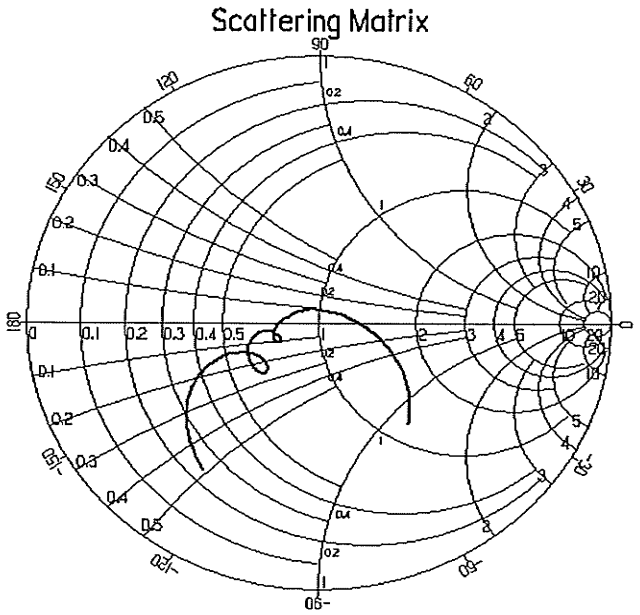

Fig. 4.12 (b)

Fig. 4.12: Simulated (a) return loss (S_{11} vs. frequency) and (b) input impedance plot for the L-shaped slot antenna in Fig. 4.1 with fl = 23mm, St = 11mm on a substrate with ε_r=2.5, h =0.787mm and tanδ =0.001. Other parameters are the same as in Fig. 4.1

The return loss and input impedance plot of the fabricated L-shaped slot antenna was measured by ANRITSU network analyzer, and is shown in Fig. 4.13. Measured –10 dB return loss bandwidth is 83.7% (2.41 to 5.88 GHz) which is very close to the bandwidth obtained from simulation. As discussed in chapter three, due to a lesser control on reflections of electromagnetic wave from the objects, all around this omni-directional antenna during measurement, the measured return loss plot has some differences from that of simulated result, so as the Smith chart. In fact, for a slight change in the position of the antenna, a great difference in the return loss and input impedance plot was found because of the omni-directional nature of this antenna, but the bandwidth did not change. A simple stub was also used here on the microstrip feed

line to compensate for the effects of measuring cables, which was not considered during the simulation. However, considering the bandwidth, the measured result agrees well with the simulated one.

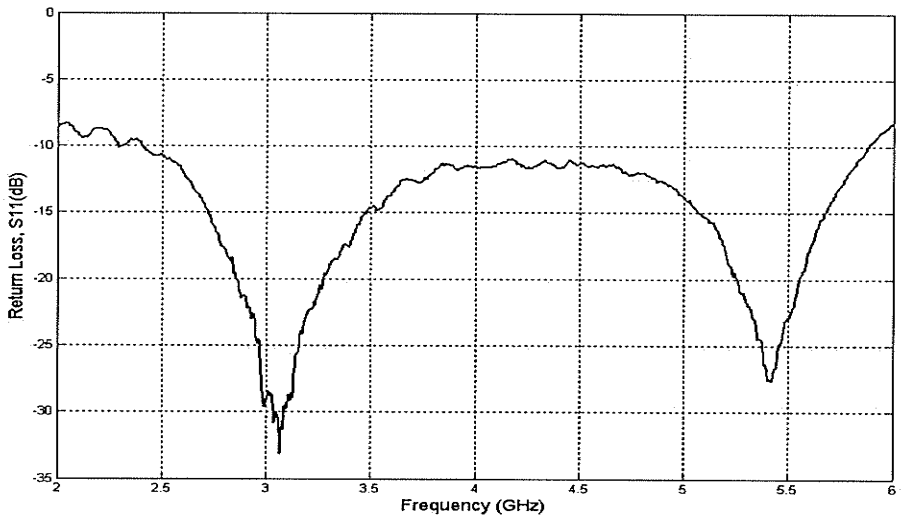

(a)

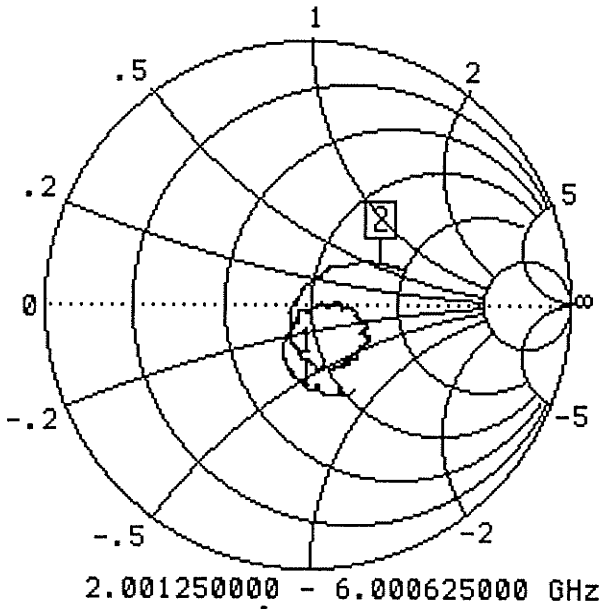

(b)

Fig. 4.13: Measured (a) return loss (S_{11} vs. frequency) (b) input impedance plot for the fabricated L-shaped slot antenna. The geometry is shown in Fig. 4.1 and dimensions are stated in Fig. 4.12

The radiation characteristics of the fabricated wideband L-shaped slot antenna were measured in the anechoic chamber in Antenna Laboratory at the university of Manitoba. Its gain patterns at three frequencies are compared with the simulated results in Fig. 4.14-4.16. The fabricated antenna was mounted on a dielectric support to keep it away from the tower, as was done in the case of straight slot. However, some ripples still are present in the measured radiation patterns, due to the interaction between the dielectric support and the antenna itself.

In Fig. 4.14(a), the comparison of the simulated and measured gain patterns of the antenna at 3.1 GHz is presented. Asymmetric radiation patterns were found for both simulated and measured results in the $\phi = 0^0$ plane, shown in Fig. 4.14(a). The measured peak gain of the E_θ component, in this plane, was 3.56 dBi and was directed along $\theta = 176^0$. The radiation is bi-directional for this L-shaped slot antenna also. The measured cross-polarized component E_ϕ, in this plane, has numerous ripples. In the $\phi = 90^0$ plane, in Fig. 4.14(b), E_ϕ is the co-polarization component and shows omni-directional radiation pattern for both simulated and measured cases. The measured gain was greater than 1.5 dBi along the most θ variation, except from $\theta = -155^0$ to 0^0.

In Fig. 4.15, the comparison between the simulated and measured gain patterns at 4.1 GHz is shown. In the $\phi = 0^0$ plane, in Fig. 4.15(a), the measured E_θ component was lower compared to the simulated one, but peak of both were directed along $\theta = 180^0$. This is due to the increase in the cross-polarized component in this plane. In the $\phi = 90^0$ plane, in Fig. 4.15(b), E_ϕ is the co-polarized component, for both simulated and measured cases, and represents an omni-directional radiation pattern. The measured

peak gain was 3.2 dBi along $\theta = 90^0$. The measured cross-polarization level was higher, possibly due to the dielectric support holding the antenna with the measuring system and the long cable, connected to the probe. The probe, in the L-slot antenna case, is very close to the slot edge and the SMA connector, connected to the probe, obstructs the radiation from the slot, when measurement was done. Consequently, there were some differences in the co- and cross-polarization components, when compared with the simulated ones. Some dips were also found in the measured E_ϕ pattern.

At 5.4 GHz, the measured and simulated gain patterns are compared in Fig. 4.16. At this higher frequency, the E_ϕ component is strong in both planes, and was found in both measured and simulation results. In the $\phi = 90^0$ plane, in Fig. 4.16(b), both measured and simulated E_ϕ components are omni-directional in nature. Ripples were also present in all the measured gain patterns.

Comparing the measured radiation characteristics, conducted in the Antenna Laboratory at the University of Manitoba, with the simulated results, presented in Figs. 4.14-4.16, good conformity was found. Since, this L-shaped slot antenna is very small and possesses bi-directional radiation pattern, a dielectric support was used to mount the antenna on the measuring tower. Again, due to the close proximity of the probe to the slot edge, the long cable connected to the probe was responsible for the scattering of the radiated energy. Therefore, the cross polarization levels were found to be higher in both $\phi = 0^o$ and $\phi = 90^o$ planes compared to those in simulation results, especially at higher frequencies. The interaction between the dielectric support and the antenna resulted in some ripples appearing in the radiation patterns. Neglecting these effects, the measured

radiation patterns were in good agreement with those obtained by simulation. Thus, the accuracy of simulation results is verified for the L-shaped slot antenna.

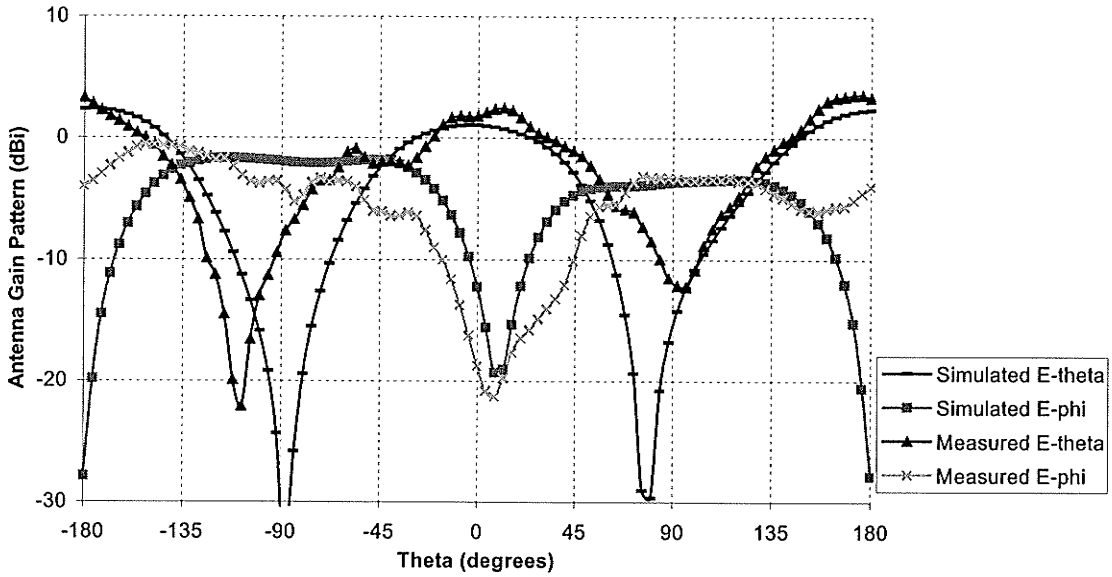

(a)

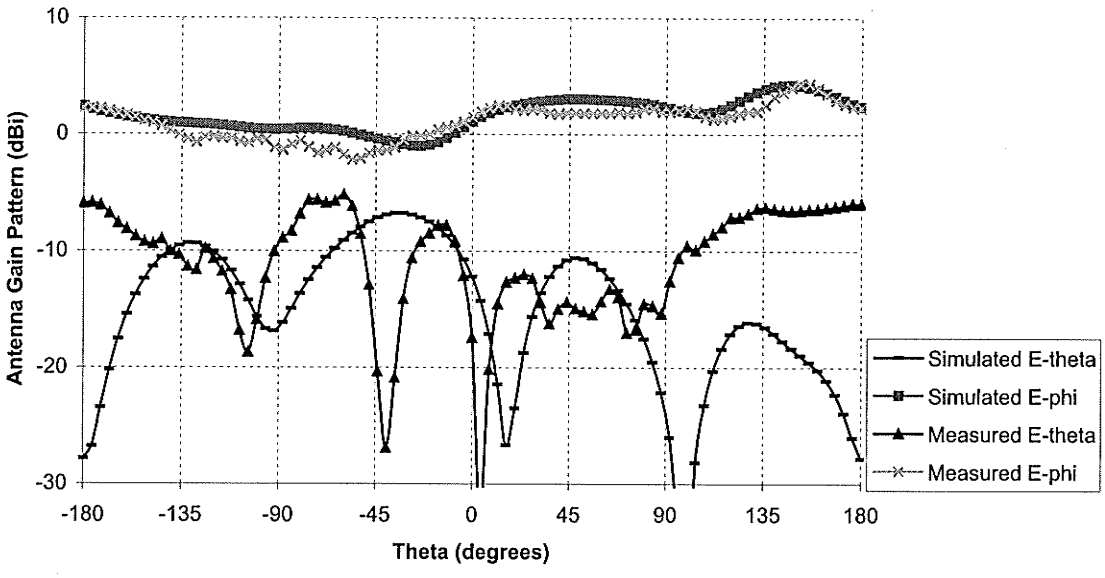

(b)

Fig. 4.14: Measured gain patterns at 3.1 GHz for the L-shaped antenna shown in Fig. 4.1 at (a) $\phi = 0^o$ and (b) $\phi = 90^o$ planes on a substrate with $\varepsilon_r = 2.5$, $h = 0.787mm$ and $\tan\delta = 0.001$. Other parameters are given in Fig. 4.12

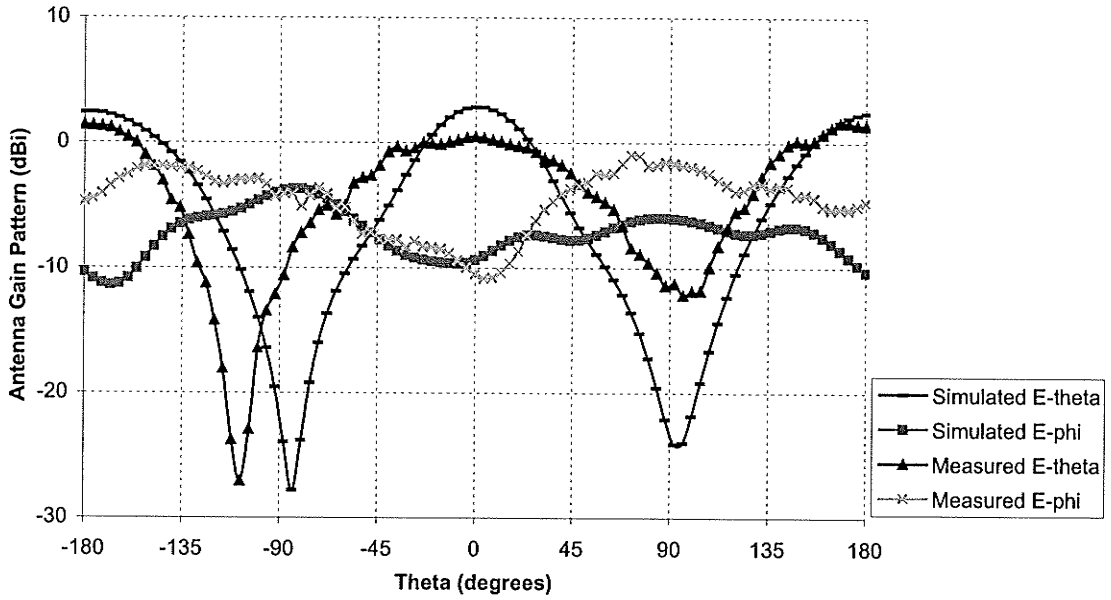

(a)

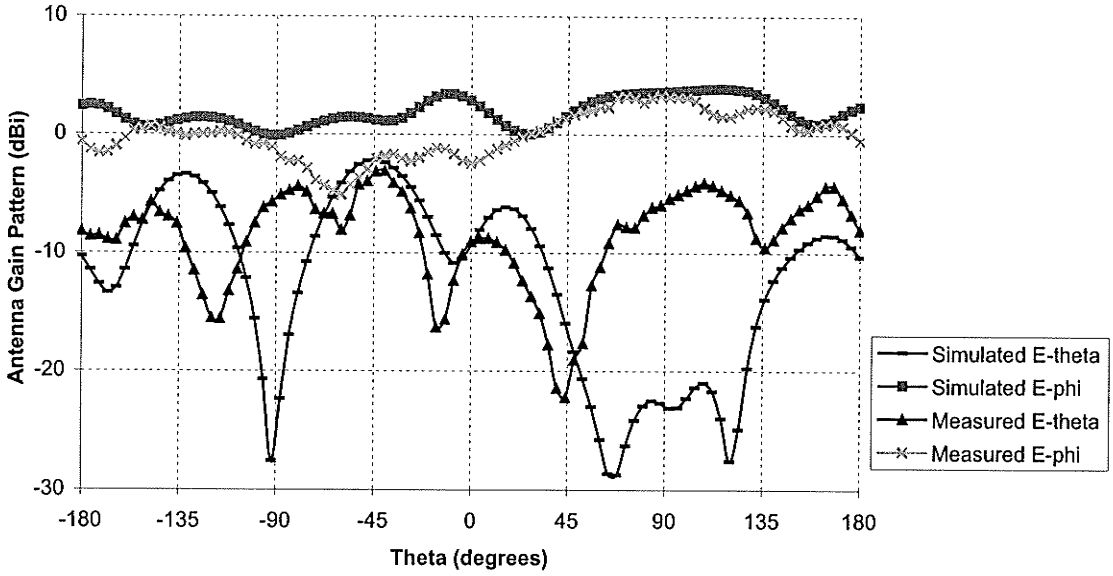

(b)

Fig. 4.15: Measured gain patterns at 4.1 GHz for the L-shaped antenna shown in Fig. 4.1 at (a) $\phi = 0^o$ and (b) $\phi = 90^o$ planes on a substrate with $\varepsilon_r = 2.5$, $h = 0.787mm$ and $\tan\delta = 0.001$. Other parameters are given in Fig. 4.12

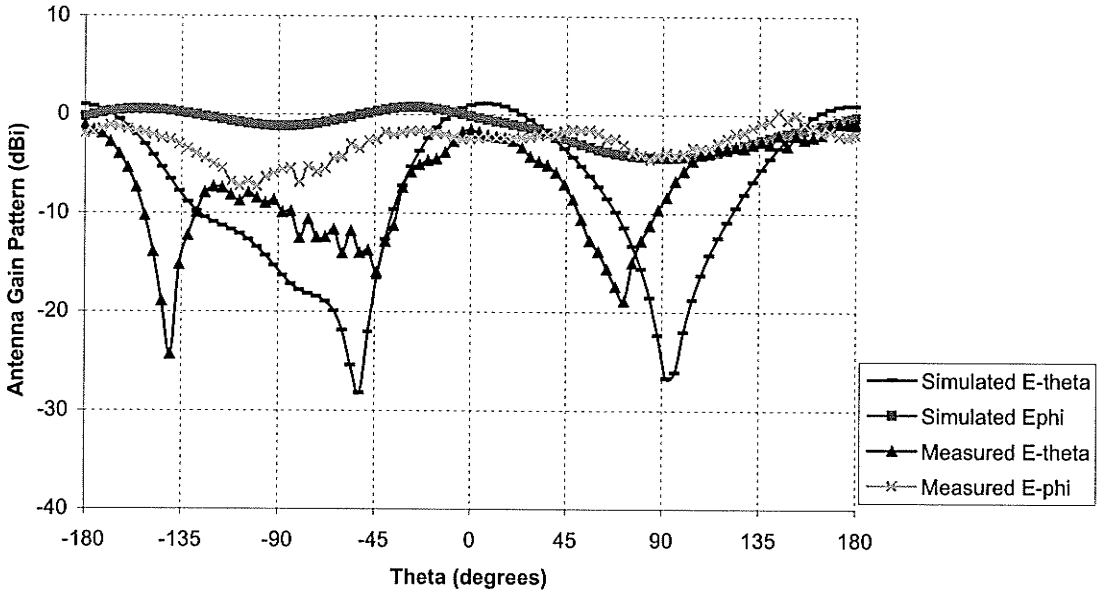

(a)

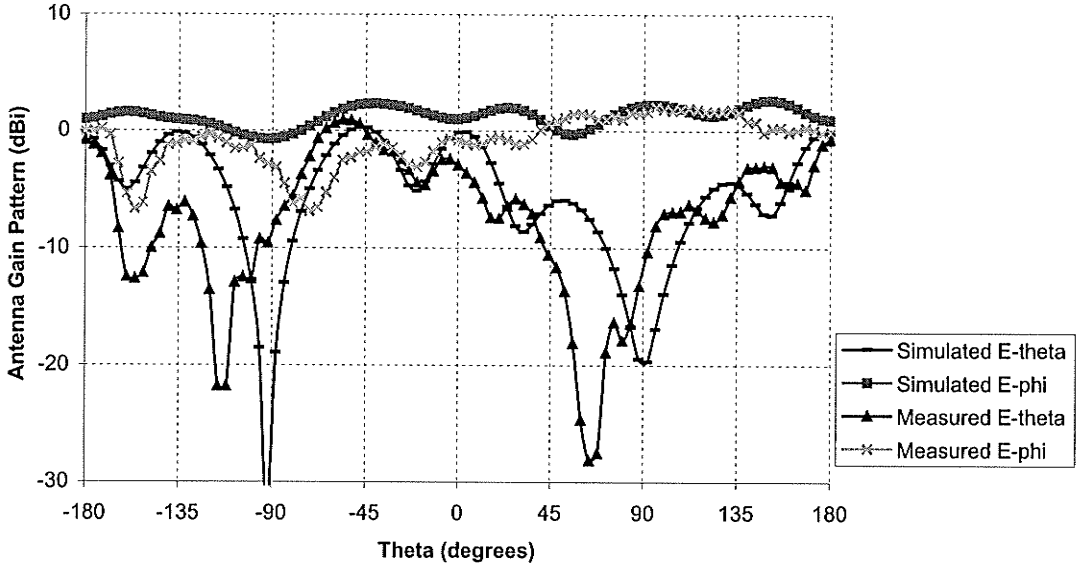

(b)

Fig. 4.16: Measured gain patterns at 5.4 GHz for the L-shaped antenna shown in Fig. 4.1 at (a) $\phi = 0^o$ (b) $\phi = 90^o$ planes on a substrate with $\varepsilon_r = 2.5$, $h = 0.787mm$ and $\tan\delta = 0.001$. Other parameters are given in Fig. 4.12

4.5 Conclusion

Using L-shaped slots cut on the ground plane and excited by a microstrip feed line, higher impedance bandwidths could be achieved, compared to those of straight slots of the same length and width. This was because of the excitation of resonant modes in the slot. The bandwidth was also dependent on the proper selection of the feed line length, stub length and the feed line position. These issues were discussed carefully in this chapter. For achieving a wide impedance bandwidth, the feed line should be placed over the junction of the two arms of the L-shaped slot. It was important to notice that, the feed line shape had a significant effect on the impedance bandwidth of the L-shaped slot antenna. But, the current distribution on the ground plane was mainly dependent on the slot shape, cut on the ground plane. Therefore, the radiation characteristics changed much less, due to the change in the feed line shape. Rather, radiation patterns were dependent on the shape of the slot. Moreover, additional space was available in the ground plane, to be used by the electronic circuitry, which can be fabricated on the substrate, when an L-slot was used instead of a straight slot.

The effects of varying the L-shaped slot width, quarter-wavelength in length, were also presented. Due to the increase in the radiation resistance with the increase in slot width, the impedance bandwidth decreases. The simulation result was confirmed by comparing those with the measured one, obtained testing a fabricated L-shaped slot antenna, fed by a 50Ω microstrip feed line, on a dielectric substrate with ε_r = 2.5, h = 0.787 mm and $tan\delta$ = 0.001. Its measured impedance bandwidth was found to be 83.7%, in good agreement with the simulated results. The measured radiation characteristics also showed good agreement with the simulated results.

CHAPTER FIVE

Microstrip Inverted T-Slot Antenna and Polarization Diversity

5.1 Introduction

The geometry of the slot in microstrip slot antenna plays a significant role on the performance of the antenna. Starting with a straight slot, discussed in chapter three, an L-shaped slot antenna was presented in chapter four, which exhibited very wide impedance bandwidth. The idea is extended in this chapter and an inverted T-shaped slot antenna is studied. In some applications, for example, in mobile communications, polarization purity is not a major issue; where the T-shaped slot antenna will find application, which will be clear when the radiation characteristics of this antenna is discussed. The T-shaped slot is then divided into two parts and separately excited by two bent feed lines. The radiation patterns of this antenna are investigated to achieve polarization diversity.

5.2 Microstrip Inverted T-Shaped Slot Antenna

The geometry of the antenna is shown in Fig. 5.1. The slot has two parts: the vertical slot L_1 is added to the center of the horizontal L_2 slot. These two slots form the inverted T-shape slot. The feed line is placed over the junction of the vertical and horizontal slots and excited by a 50Ω SMA probe. Hence, this is almost like the L-slot except that here the configuration is symmetric. The sum of slots L_1 and L_2 is 30 mm, i.e. it is monopole in length in free space wavelength. Using FR-4 substrate (ε_r = 4.5, h = 0.8128 mm and $tan\delta$ = 0.02), the slot is cut at the center of ground plane at its upper edge. The size of the ground plane is 50mm × 80 mm.

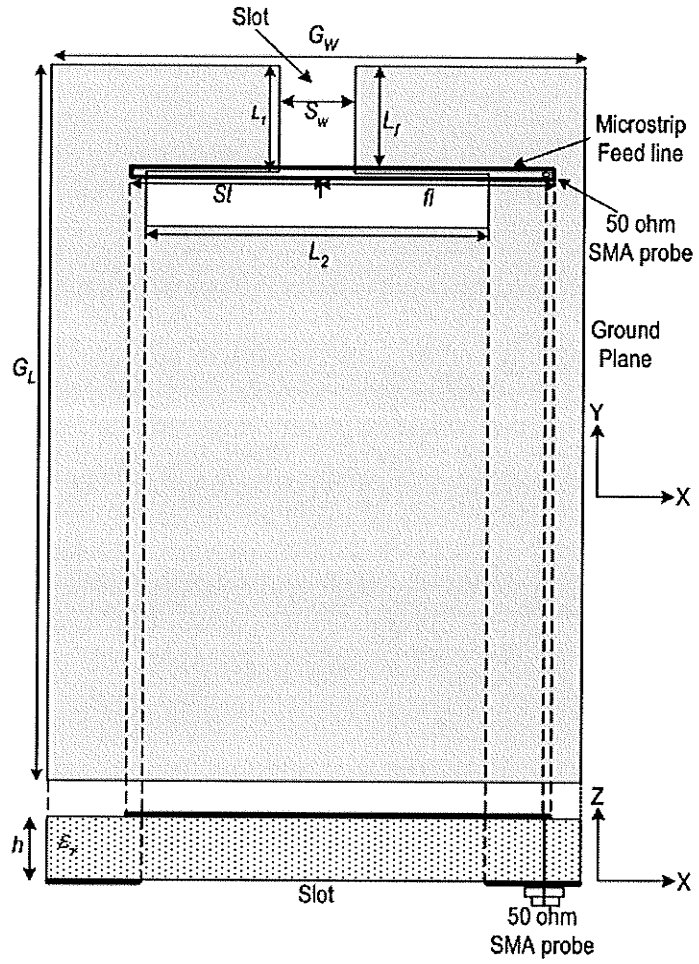

Fig. 5.1: The geometry of the inverted T-shaped slot antenna fed by a microstrip feed line with the co-ordinate system: G_W = 50mm, G_L = 80mm, S_W =7mm, L_1=7, L_2=23mm, on a substrate with ε_r =4.5, h=0.8128mm and tanδ= 0.02

The simulation result for the return loss and impedance plot are shown in Fig. 5.2 with *fl* = 22.5 mm, *St* = 10 mm. The antenna shows an impedance bandwidth of 78% (2.56 to 5.8 GHz). It is evident in the plot that three resonances are excited here, two of them are dominant, appeared in the Smith chart as loops, and these are combined by properly selecting stub length and feed line length. The stub length (*St*) has important effect on the lower end frequency limit while the feed line length (*fl*) has influence on the upper end frequency limit.

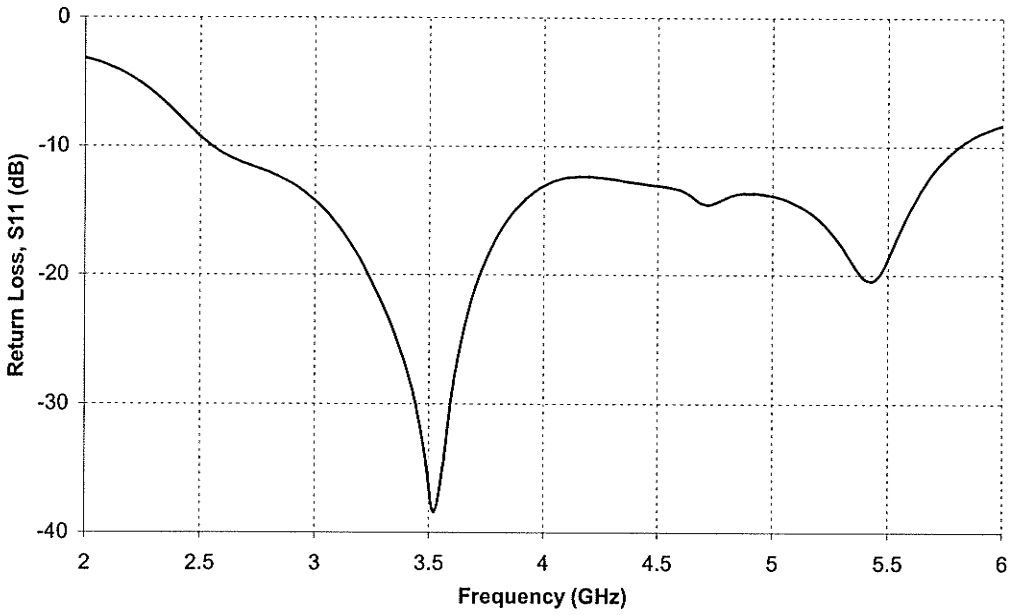

(a)

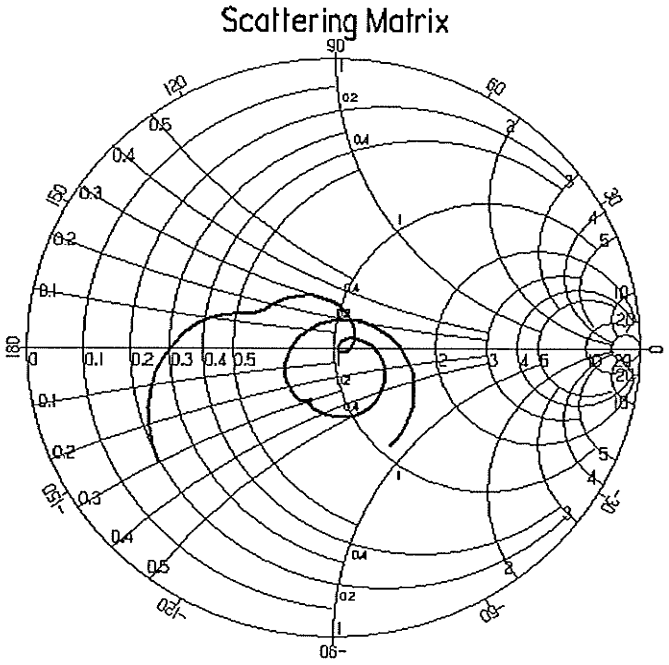

(b)

Fig. 5.2: Simulated (a) return loss (S_{11} vs. frequency) and (b) impedance plot for the inverted T-shaped slot antenna in Fig. 5.1. L_f = 7mm, fl = 22.5mm, St = 10mm. Other parameters are mentioned in Fig. 5.1

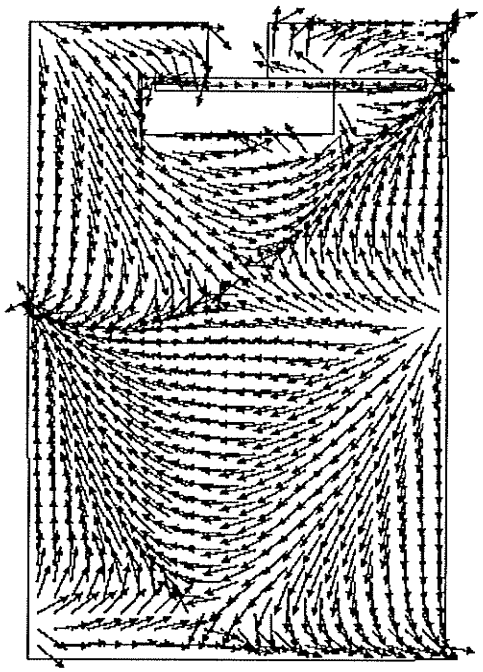

Fig. 5.3: The current distribution at 4.1 GHz of the antenna in Fig. 5.1

The simulated antenna gain pattern at 4.1 GHz is shown in Fig. 5.4. The radiation characteristics are very similar to those of the L-shaped slot antenna, presented in chapter four. From Fig. 5.4(a), it is evident that the T-shaped slot antenna is radiating bi-directionally, as the main peak of the E_θ component is along $\theta = 0^0$ and 180^0, in the $\phi = 0^0$ plane, with peak gain of 3.53 dBi along $\theta = 0^0$. Due to the symmetric configuration of the T-shaped slot antenna, the radiation pattern is also symmetric, which is evident in the surface current distribution in the ground plane, as mentioned in Fig. 5.3. The density of surface current is higher at the edges. In this plane, the gain patterns were not symmetric in the L-shaped slot antenna case. The E_ϕ component level is higher in this plane, compared to that of the L-slot antenna, which can be found in Fig. 4.4(b). This is because the length L_2 of slot, along the x-axis is longer for the inverted T-slot than for the L-shaped slot antenna. In the $\phi = 90^0$ plane,

in Fig. 5.4(b), the E_ϕ component is the main polarization component and the cause of radiation. This shows an omni-directional radiation pattern having a gain greater than 0 dBi through the entire θ variation in the space.

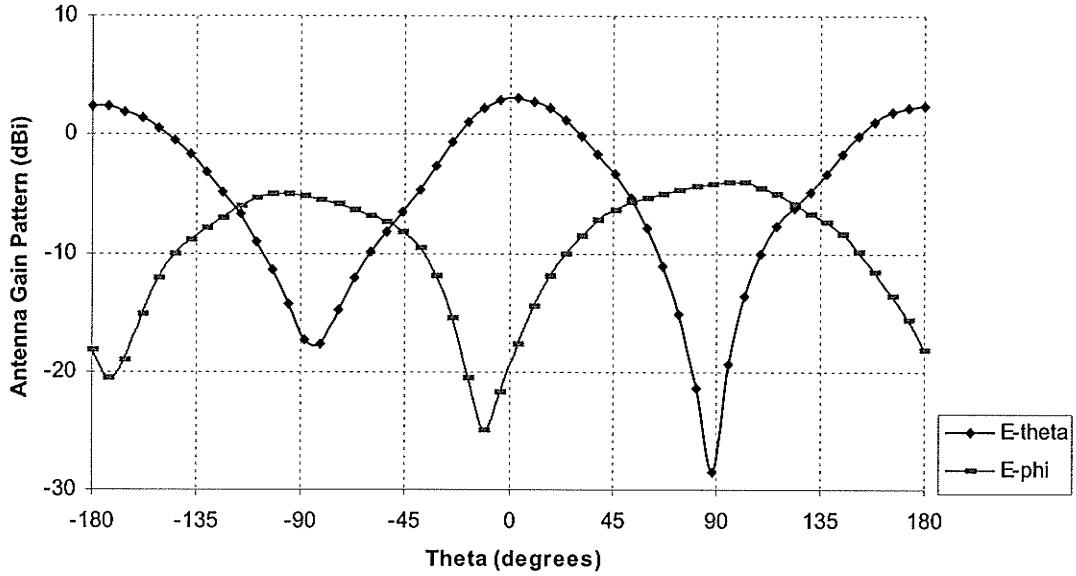

(*a*)

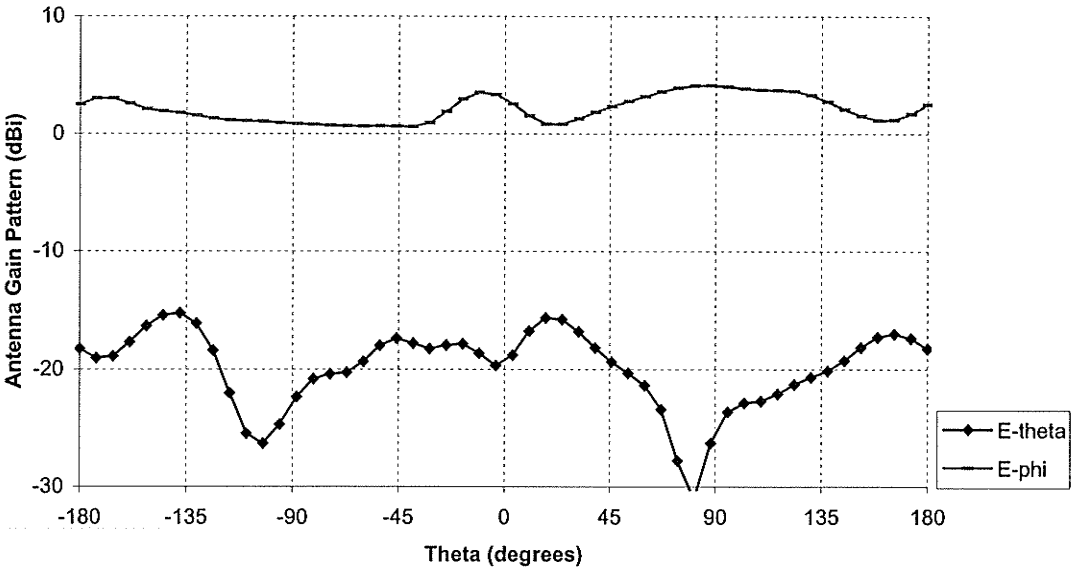

(*b*)

Fig. 5.4: Simulated gain patterns at 4.1 GHz for the antenna shown in Fig. 5.1 at (a) $\phi = 0^o$ and (b) $\phi = 90^o$ planes. The parameters are given in Figs. 5.1 and 5.2

In terms of space availability on the ground plane to be used by the electronic circuitry as electrical ground, which may be fabricated on the substrate, the inverted T-shaped slot antenna is advantageous. For slot width S_W = 7 mm, in the straight slot case, discussed in chapter three, the slot is occupying 37.5% of the ground plane length, G_L; the L-shaped slot, presented in chapter four, is occupying 23%, while the T-shaped slot is occupying only 17.5% of the ground plane length. Thus, more space is available for this case to be used by the electronics, which is very important in present trend of compactness.

5.3 Two-L-Slot Array for Polarization Diversity

Electromagnetic waves are composed of oscillating electric and magnetic fields, which are perpendicular to each other. Both of them are also at right angle to the direction of propagation of the wave. The polarization of an antenna in a given direction is usually the polarization of the wave [1], and is defined by the direction of the electric field only. It describes the behavior of the electric field with time [38]. A linearly polarized wave has an electric field vector tracing a straight line with time. Linear polarization may be vertically or horizontally oriented, depending on the line traced by the electric field. The polarization can also be circular or elliptical.

Signal fading in mobile communication systems causes severe reception problems. Therefore, antenna diversity techniques are employed to reduce the fading effects. The antenna diversity can be of any forms: space diversity, polarization diversity and directivity diversity. In polarization diversity schemes, two orthogonal polarizations are needed, which increases the overall average received signal power,

hence, reducing the overall fading effect. This scheme also allows the use of low transmit power.

To explain the principle of polarization diversity, a mobile communication system is considered comprising of a base station and a mobile unit. In this system, two different polarizations, vertical and horizontal, from the two antennas carry two signals on one radio frequency. In wireless radio environment, strong mutual coupling is present. This means that, after signal propagation through the mobile radio medium, the signal energy in the vertically polarized wave can be cross-coupled into the horizontally polarized wave and vice-versa. In Fig. 5.5, a schematic of a mobile communication system is depicted. It has two collocated vertical and horizontal antennas in its base station. In the mobile unit also, there are two antennas, vertical and horizontal, collocated at the same spot. For this system, the following terms are defined [39]:

Γ_{11} = Transmit vertical, receive vertical

Γ_{12} = Coupling vertical into horizontal (from base to mobile)

Γ_{21} = Coupling horizontal into vertical (from base to mobile)

Γ_{22} = Transmit horizontal, receive horizontal

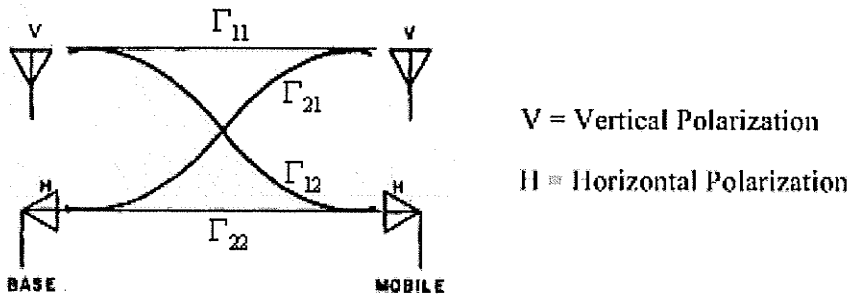

Fig. 5.5: Vertical and horizontal polarization signals in a mobile communication system

The two differently polarized waves (E_V and E_H) received by dual polarization antennas, at the mobile unit, can be expressed as [39]

$$\begin{aligned} E_V &= \Gamma_{11} + \Gamma_{21} \\ E_H &= \Gamma_{22} + \Gamma_{12} \end{aligned} \tag{5.1}$$

Since the principle of reciprocity is applied to polarization components, the two differently polarized waves, E_V' and E_H', arriving at the base station, can be expressed as:

$$\begin{aligned} E_V' &= \Gamma_{11} + \Gamma_{12} \\ E_H' &= \Gamma_{22} + \Gamma_{21} \end{aligned} \tag{5.2}$$

Cross-coupled energy is very small compared to the main stream; i.e. $\Gamma_{11} > \Gamma_{12}$ and $\Gamma_{22} > \Gamma_{21}$. Therefore, from equations (5.1) and (5.2), it can be found that $E_V \approx E_V'$ and $E_H \approx E_H'$. By measurement, also it was found that $E_V \approx E_H$ [39].

In polarization diversity, it is evident that two orthogonal polarizations are present. To receive both polarizations, in present compact mobile units, two separate antennas with different polarizations must be used [40]. But this will cause an overall increase in the antenna volume. It will be very useful, if one antenna can generate different polarizations.

In L- and T-shaped slot antennas discussed earlier, two slots, one vertical and another horizontal, are present which can generate both horizontal and vertical polarizations. In order to get an effective radiation, to be used in polarization diversity scheme, the two L-shaped slots are cut, opposite to each other, on the ground plane separated by a distance, S_p, as shown in Fig. 5.6. In other words, the T-shaped slot is divided into two parts and separated from each other by a distance, S_p. This distance

should be fairly large to reduce the coupling between the two slots. Again, both ends of each slot are kept open, in this case, to achieve an effective radiation and reduce coupling. Both slots are excited using two identical bent feed lines shown in the Fig. 5.6. The reason behind using this type of feed line is that, it will be easy to excite them by 50Ω SMA probes, from this portion of the ground plane. The width of the feed line is chosen such that its characteristic impedance is 50Ω on a substrate having a dielectric constant, ε_r = 4.5, height, h = 0.8128 mm and $tan\delta$ = 0.02. Other parameters are mentioned in Fig. 5.6.

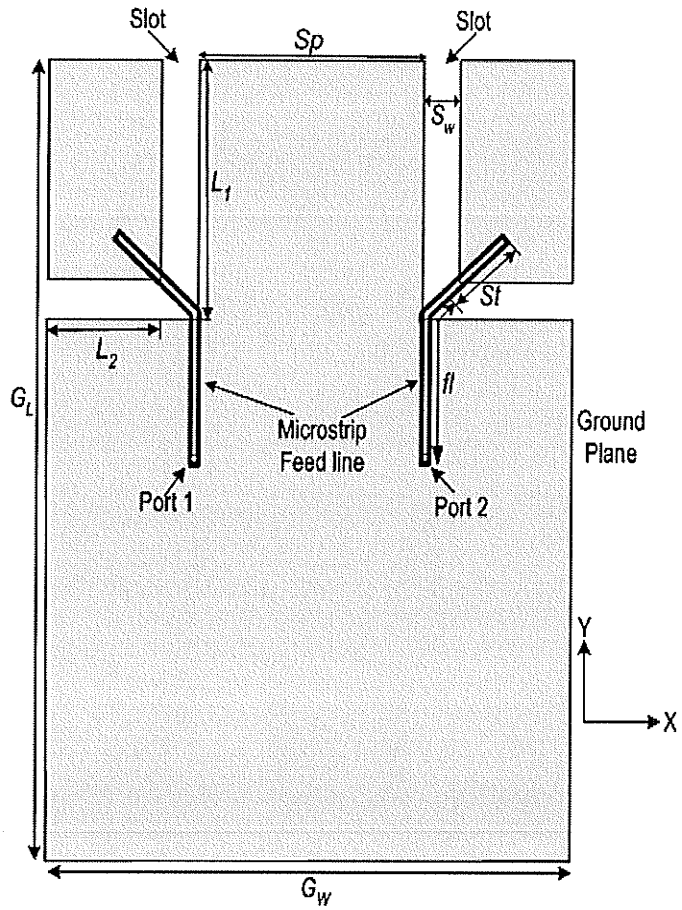

Fig. 5.6: The antenna geometry with two L-shaped slots on the ground plane fed by microstrip feed lines, with the co-ordinate system: G_W=50mm, G_L=80mm, S_p =24mm, S_W=3mm, L_1=24mm, L_2=10mm, on a substrate with ε_r=4.5, h=0.8128mm & $tan\delta$=0.02

The simulation results were obtained by exciting one of the slots, while terminating the other feed line with a short circuit. The simulated return losses are shown in Fig. 5.7(a), S_{11} when port 1 is excited, S_{22} when port 2 is excited and isolation S_{12} between the two ports, when both are energized. When port 1 is excited, its -10 dB return loss bandwidth is 87% (2.52 to 6.4 GHz), while in the case of port 2, it is 86.2% (2.52 to 6.34 GHz) with good impedance match, depicted in Fig. 5.7(b). The coupling between the two ports, which is also called isolation, is below –15 dB in almost the entire frequency range, except from 2.52 to 2.8 GHz. Therefore, this antenna exhibits a very wide impedance bandwidth, with good isolation between the ports necessary for applications in polarization diversity.

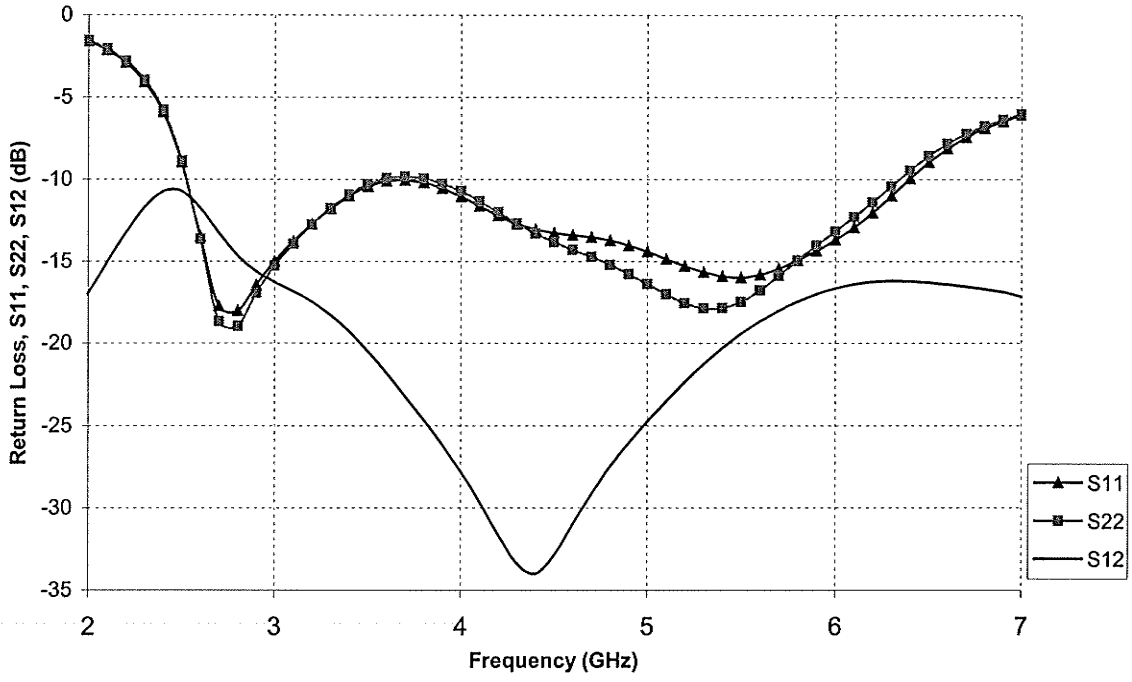

Fig. 5.7(a)

Fig. 5.7 contd.

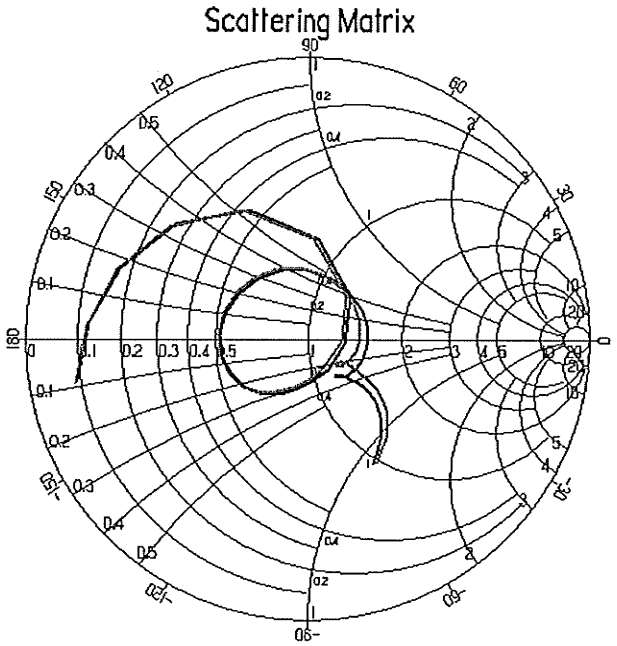

Fig. 5.7(b)

Fig. 5.7: Simulated (a) return loss for each of the slots, while terminating the other, and isolation between them (S_{11}, S_{22}, S_{12} vs. frequency) and (b) impedance plots for the slot antenna in Fig. 5.6. fl =14mm, St =9mm. Other parameters are the same as in Fig. 5.6

The polarization diversity property of the antenna can be visualized by examining its radiation characteristics. In Fig. 5.8, its gain patterns at 4.5 GHz are presented at four different planes, when port 1 is excited. Since, the left slot is excited, in the $\phi = 0^0$ plane, in Fig. 5.8(a), a partial omni-directional radiation pattern is found for the E_ϕ component. From $\theta = -180^0$ to 0^0, the gain is between –0.5 to 1.77 dBi. Again, from Fig. 5.9(a), it can be seen that, due to the excitation of the right slot by energizing port 2, using a 50Ω SMA probe, E_ϕ component shows a partial omni-direction pattern in the $\phi = 0^0$ plane for $\theta = 0^0$ to 180^0 variation. Thus, in the $\phi = 0^0$ plane, a complete omni-directional radiation pattern is found with the E_ϕ as the main

radiating component, when both ports are excited alternatively. When the left slot is fed by exciting port 1, in the $\phi = 90^0$ plane, in Fig. 5.8(c), the gain is greater than 0 dBi in the ranges $\theta = -180^0$ to -120^0, $\theta = -50^0$ to 35^0 and $\theta = 140^0$ to 180^0, with the E_θ as the co-polarized component. Similarly, when right slot is fed by exciting port 2, the same range of θ variation, in the $\phi = 90^0$ plane, has reasonable gain for the E_θ component, as it can be seen in Fig. 5.9(c), due to the symmetrical positioning of the two slots.

Since, both slots are L-shaped, or one vertical slot is connected to a horizontal slot, the radiation along $\phi = 45^0$ and $\phi = 135^0$ planes is significant. Hence, the computed gain patterns are included in Figs. 5.8 and 5.9, when port 1 or port 2 is excited, respectively. From Figs. 5.8(b) and 5.9(b), it is clear that in the $\phi = 45^0$ plane, the E_ϕ is the co-polarization component showing partial omni-directional radiation pattern from $\theta = -180^0$ to 0^0 variation, when port 1 is excited and from $\theta = 0^0$ to 180^0 variation, when port 2 is excited. Therefore, in the $\phi = 45^0$ plane, the E_ϕ component shows an omni-directional radiation pattern with gain level between –0.5 to 2.9 dBi.

Again, in the $\phi = 135^0$ plane, partial omni-directional radiation pattern is found from $\theta = 0^0$ to 180^0 variation when port 1 is excited [Fig. 5.8(d)] and from $\theta = -180^0$ to 0^0 when port 2 is excited [Fig. 5.9(d)], with the E_ϕ as the co-polarization component. Thus, the E_ϕ component shows an omni-directional radiation pattern in the $\phi = 135^0$ plane also by alternately exciting two ports. The gain level is in between –0.5 to 2.9 dBi, from $\theta = 0^0$ to 360^0 in this plane. It can be concluded at this point that, by exciting the two L-shaped slots alternately, omni-directional radiation patterns can be found with the E_ϕ as the co-polarized component in the two orthogonal planes. The E_θ

components, in these planes, are filling the nulls created by the E_ϕ component. As a result, there will be less signal-fading problem. The above discussion suggests that, the two-L-slot array antenna can be used as a polarization diversity antenna.

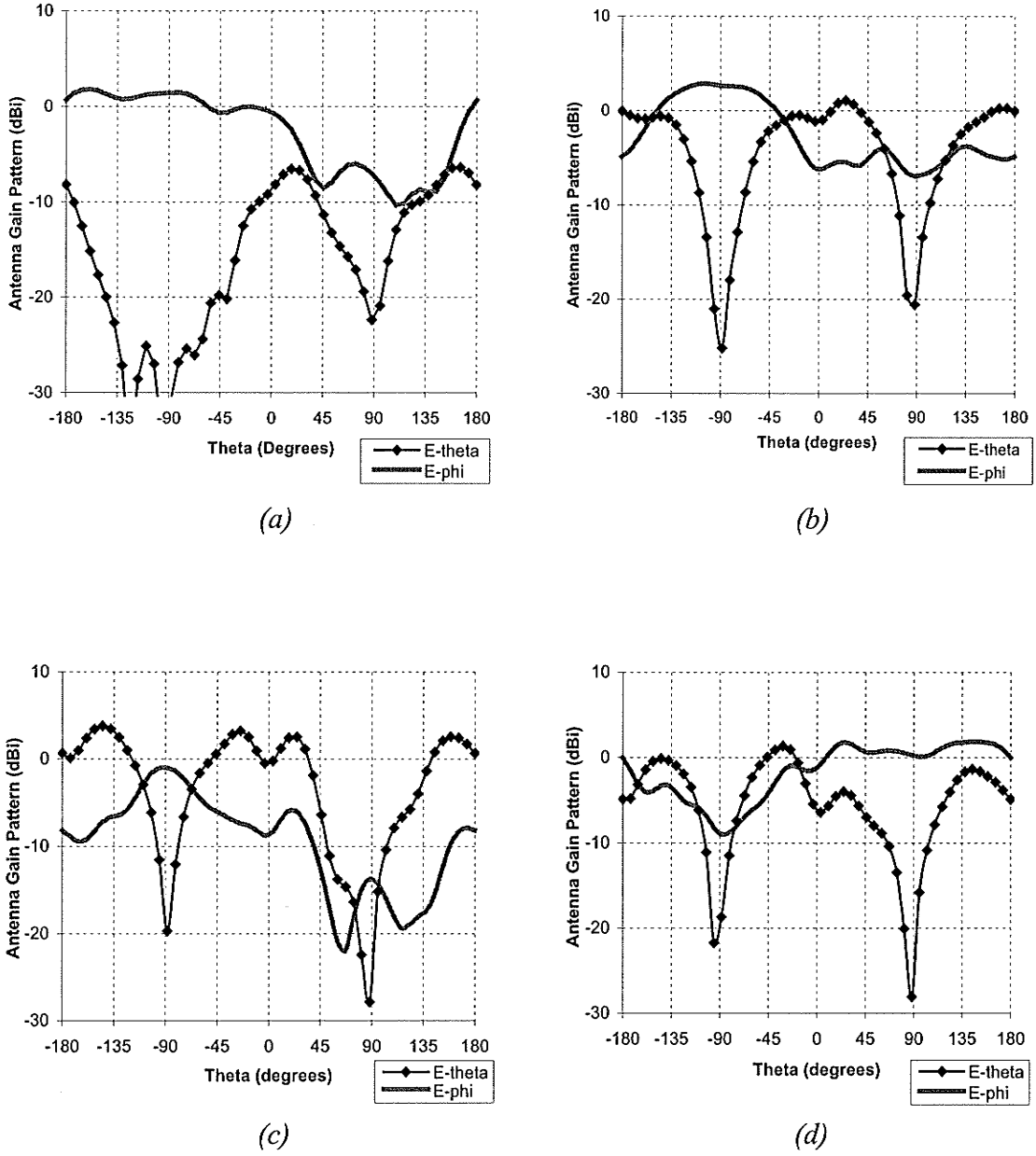

Fig. 5.8: Simulated gain patterns at 4.5 GHz for the antenna in Fig. 5.6 at (a) $\phi = 0^o$, (b) $\phi = 45^o$, (c) $\phi = 90^o$ and (d) $\phi = 135^o$ planes, when port 1 is excited and port 2 is terminated with a short circuit. The parameters are given in Figs. 5.6 and 5.7

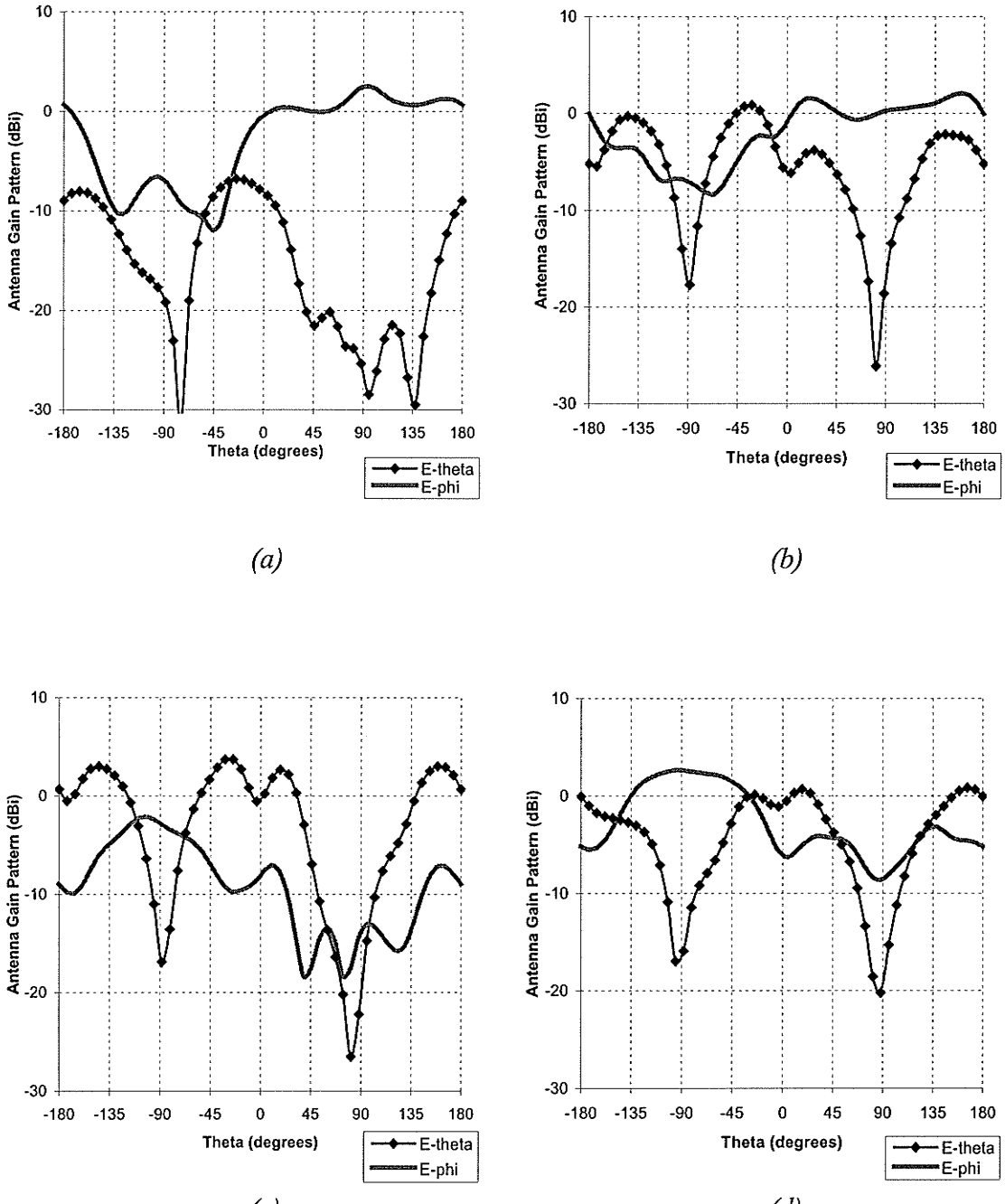

Fig. 5.9: Simulated gain patterns at 4.5 GHz for the antenna shown in Fig. 5.6 at (a) $\phi=0^{o}$, (b) $\phi=45^{o}$, (c) $\phi=90^{o}$ and (d) $\phi=135^{o}$ planes, when port 2 is excited and port 1 is terminated with a short circuit. The parameters are given in Figs. 5.6 and 5.7

5.4 Experimental Verification

An inverted T-shaped slot, cut on the ground plane of a micrsotrip line, was fabricated on a substrate with a dielectric constant ε_r = 2.5, h = 0.787 mm and $tan\delta$ = 0.001. The measured results were compared with the simulation results in order to verify the accuracy of the computation results. The ground plane size was, once again, 50 mm × 80 mm. The T-slot was placed at the center of the ground plane width, at its upper edge. The slot comprises of the vertical slot L_1 and horizontal slot L_2, as shown in Fig. 5.1. The slot was electromagnetically fed by a microstrip feed line, excited by a 50Ω SMA probe. Remaining dimensions of the antenna are stated in Fig. 5.10.

The simulated return loss and input impedance plot of the inverted T-shaped slot antenna, obtained using Ensemble 8.0, are shown in Fig. 5.10. From this plot, its -10 dB return loss bandwidth was found to be 80% (2.74 o 6.4 GHz). The measured bandwidth was 80.5% (2.74 to 6.43 GHz), as can be found in Fig. 5.11(a). The measurement was done using an ANRITSU Network Analyzer in the Antenna Laboratory at the University of Manitoba. In order to compensate for the cable effect and reflection from objects, all around this omni-directional antenna, a simple tuning stub was used on the microstrip feed line to achieve a good impedance match. The measured input impedance of the antenna is shown in the Smith chart in Fig. 5.11(b). It is clear that the reflections were found in the return loss and input impedance plot, and can be seen in the figure. Otherwise, the measured return loss was in very good agreement with the simulated one.

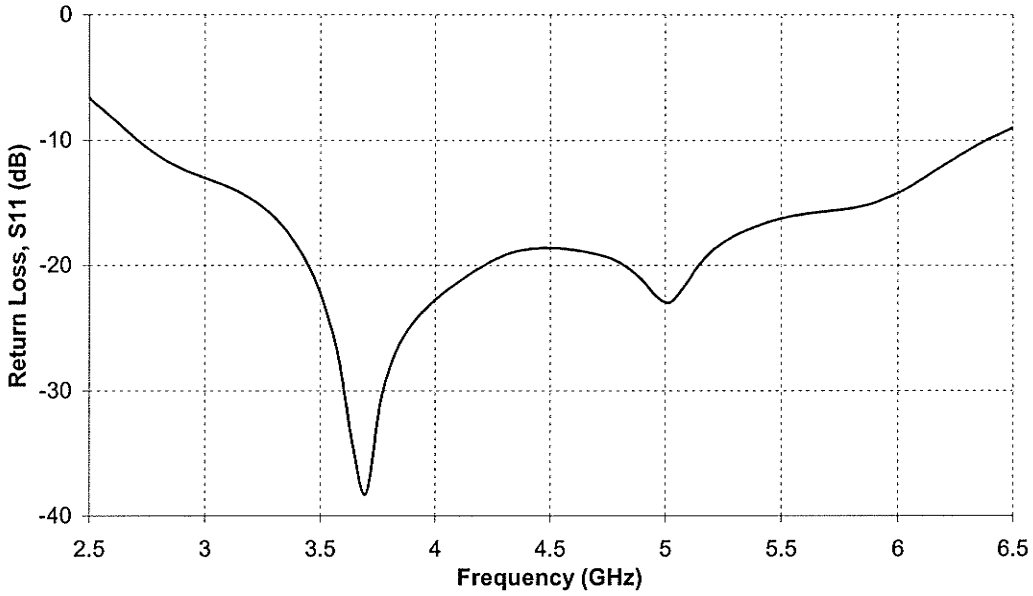

(a)

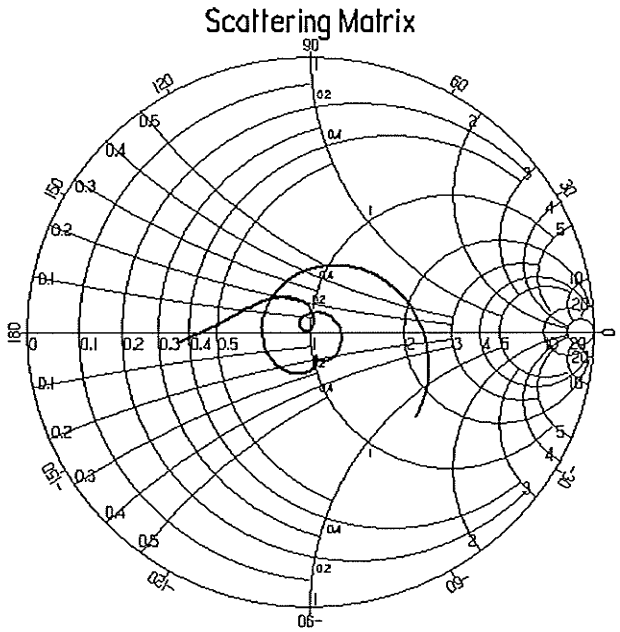

(b)

Fig. 5.10: Simulated (a) return loss (S_{11} vs. frequency) and (b) input impedance plot for the inverted T-shaped slot antenna in Fig. 5.1. G_W = 50mm, G_L = 80mm, S_W = 7mm, L_1 = 7, L_2 = 23mm, L_f = 7mm, fl = 23.5mm, St = 10mm on a substrate with ε_r = 2.5, h = 0.787mm and tanδ = 0.001

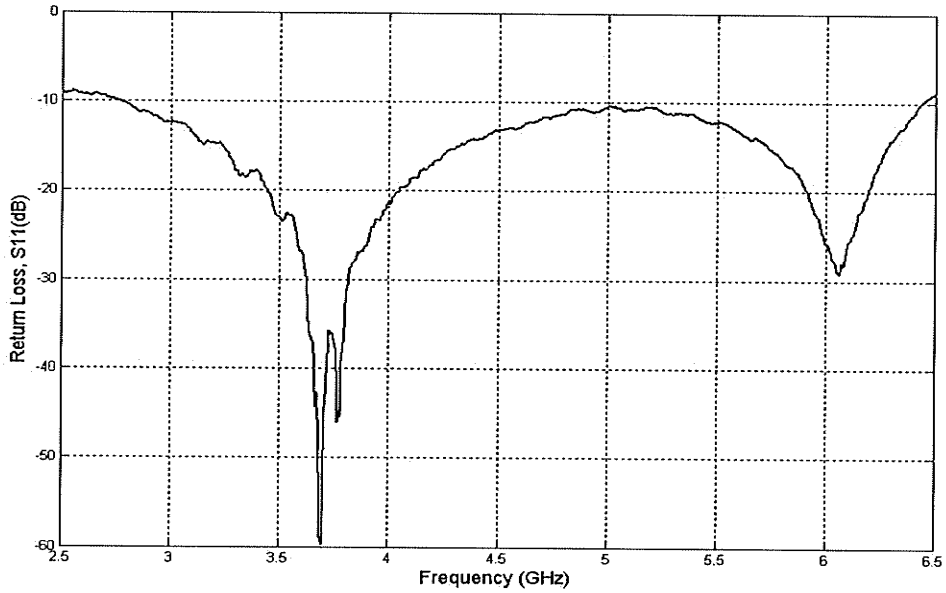

(a)

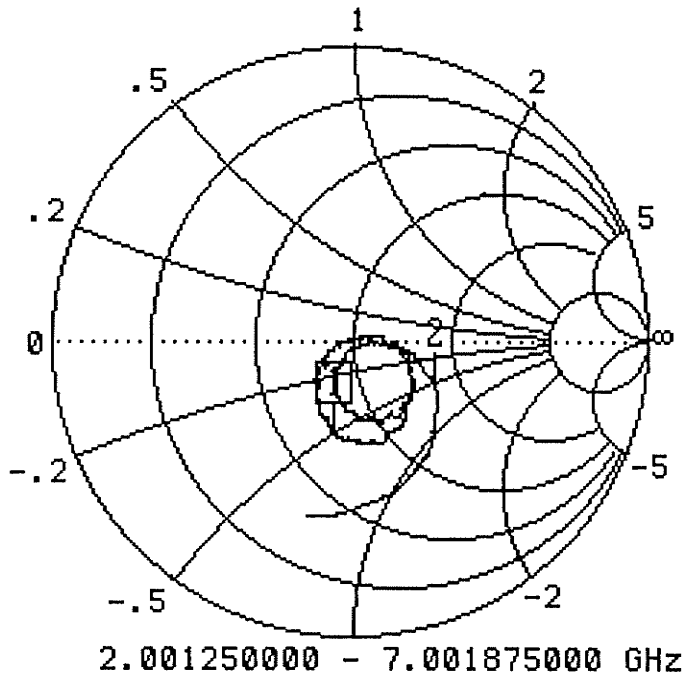

(b)

Fig. 5.11: Measured (a) return loss (S_{11} vs. frequency) and (b) input impedance plot for the fabricated inverted T-shaped slot antenna. The geometry is shown in Fig. 5.1 and dimensions are stated in Fig. 5.10

The simulated and measured gain patterns of the fabricated inverted T-shaped slot antenna are compared in Figs. 5.12-5.14 at three frequencies. The simulation results were found using HFSS 8.0 and measurement was done in the anechoic chamber in the Antenna Lab. Like the straight and L-shaped slot antennas, here also a dielectric support was used to mount the compact-sized antenna on the measuring system. The interaction of the antenna with the dielectric support appears in the measured radiation patterns in the form of ripples, as can be seen in the figures. Since, the slot edge is very close to the SMA probe, like the L-shaped slot antenna, the long cable, connected to the probe, was also in the close proximity of the slot while measuring, causing obstruction to the radiation from the slot. In Fig. 5.12, the comparison of the simulated and measured gain patterns of the antenna at 3.1 GHz is presented in the two principle planes. The peak of the E_θ component, in both cases, is directed along $\theta = 0^0$ and 180^0 in the $\phi = 0^0$ plane, shown in Fig. 5.12(a), which represents a bi-directional radiation pattern. The measured peak gain is 3.8 dBi, along $\theta = 180^0$ in this plane. In the $\phi = 90^0$ plane, in Fig. 5.12(b), the E_ϕ is the co-polarization component and shows an omni-directional radiation pattern for both simulated and measured cases. The measured E_θ component level is slightly higher in this plane, compared to the simulated one. The gain is greater than 2 dBi from $\theta = 0^0$ to 180^0 in this plane.

In Fig. 5.13, the comparison between the simulated and measured gain patterns, at 4.5 GHz, is presented. At this higher frequency, the presence of the long cable, connected to receive signal from the antenna under test, causes severe scattering of the radiated wave, resulting in higher cross-polarization. The measured E_ϕ component is higher, compared to the simulated case, in the $\phi = 0^0$ plane, in Fig. 5.13(a).

Consequently, the measured E_θ component level is lower, compared to the simulated one. In the ϕ = 90^0 plane, in Fig. 5.13(b), the E_ϕ component represents an omni-directional radiation pattern for both cases, but their level is different, due to the higher cross-polarization.

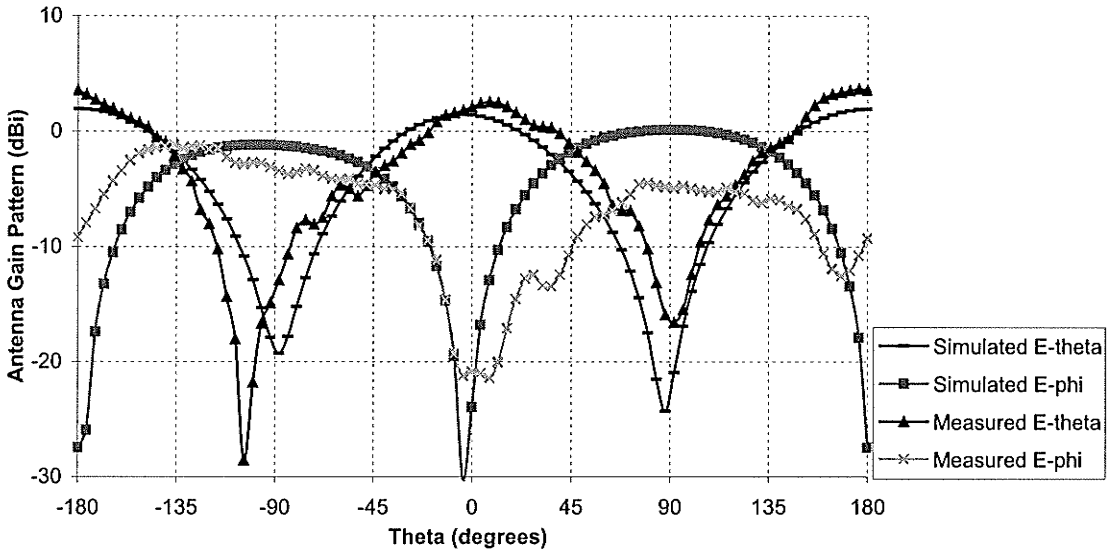

(a)

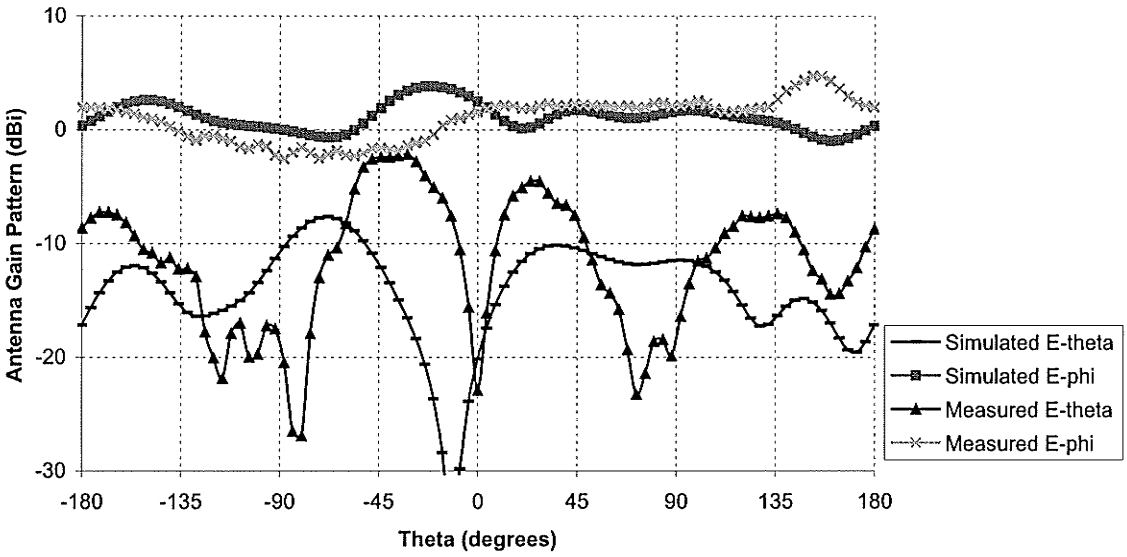

(b)

Fig. 5.12: Measured and simulated gain patterns at 3.1 GHz for the inverted T-shaped antenna shown in Fig. 5.1 at (a) $\phi = 0^o$ & (b) $\phi = 90^o$ planes on a substrate with ε_r=2.5, h=0.787mm & tanδ=0.001. Other parameters are given in Figs. 5.10 and 5.11

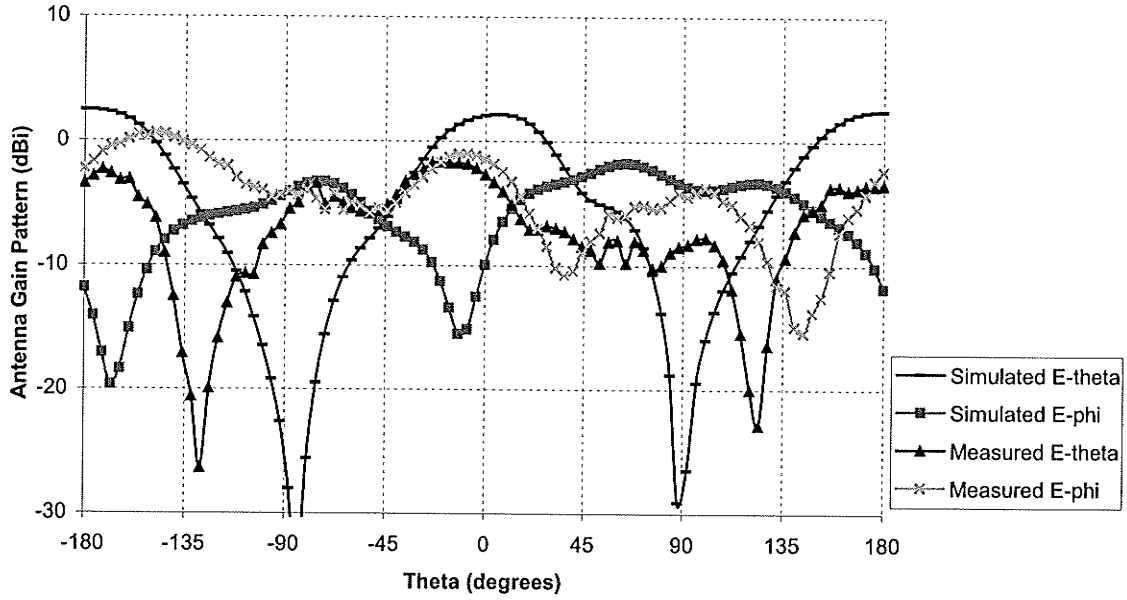

(a)

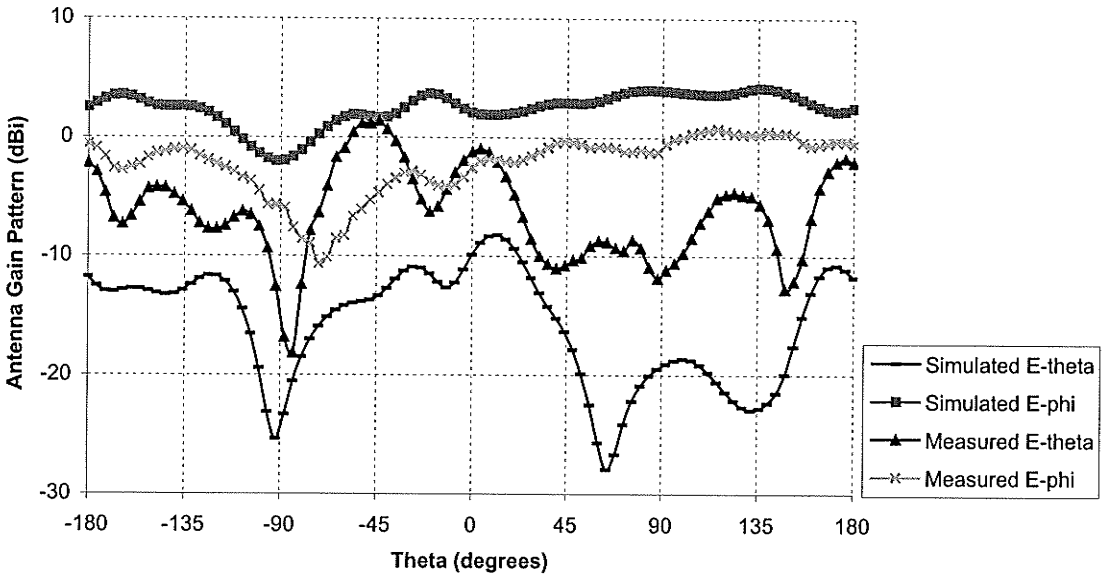

(b)

Fig. 5.13: Measured and simulated gain patterns at 4.5 GHz for the inverted T-shaped antenna shown in Fig. 5.1 at (a) $\phi = 0^o$ & (b) $\phi = 90^o$ planes on a substrate with ε_r=2.5, h=0.787mm & tanδ=0.001. Other parameters are given in Figs. 5.10 and 5.11

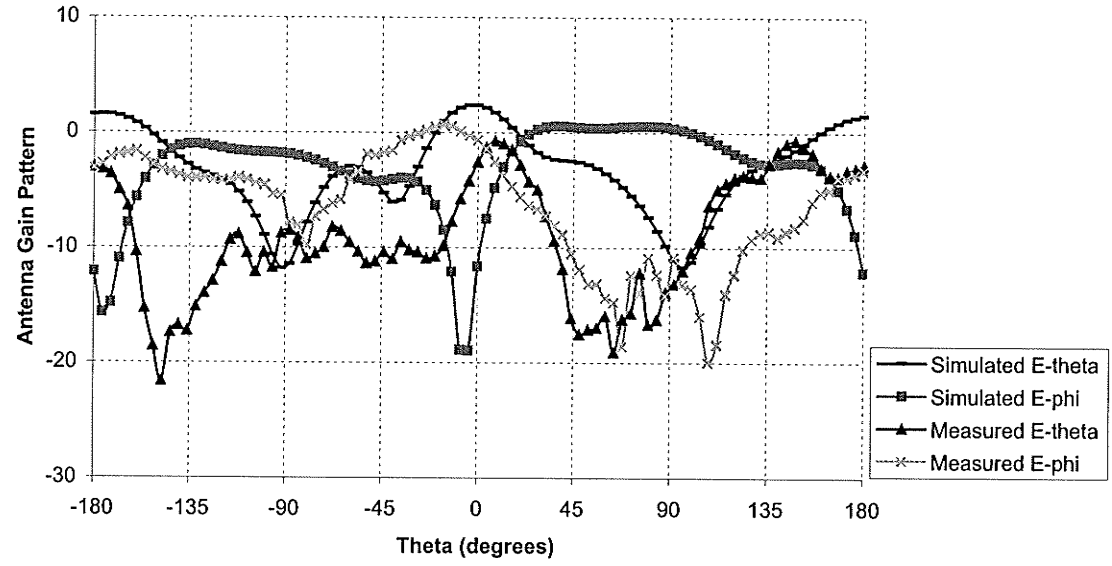

(a)

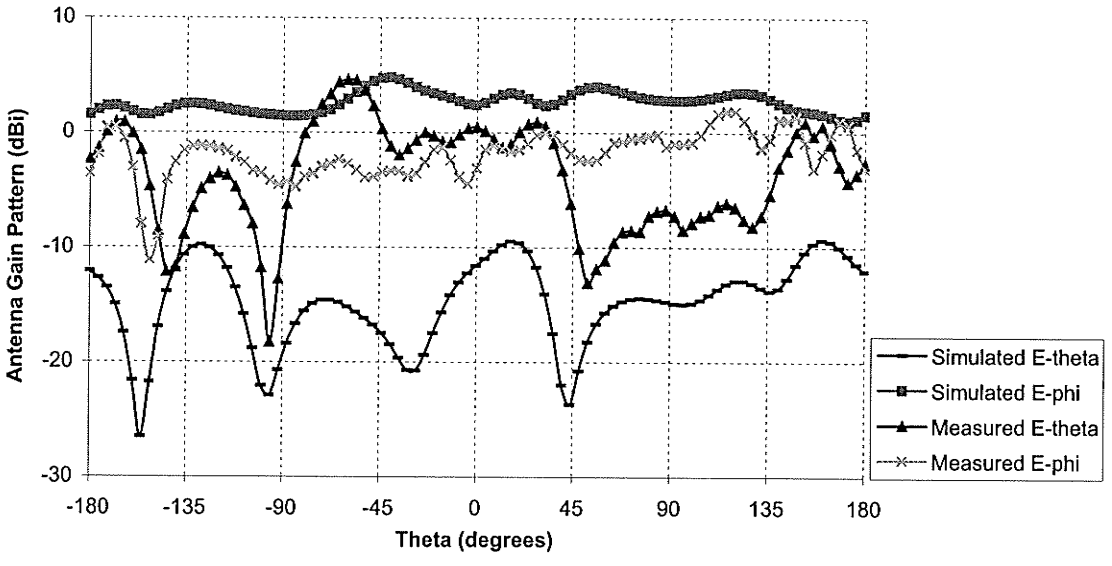

(b)

Fig. 5.14: Simulated and measured gain patterns at 6 GHz for the inverted T-shaped antenna shown in Fig. 5.1 at (a) $\phi = 0^o$ & (b) $\phi = 90^o$ planes on a substrate with ε_r=2.5, h=0.787mm & tanδ=0.001. Other parameters are given in Figs. 5.10 and 5.11

At 6 GHz, the measured and simulated gain patterns are compared in Fig. 5.14. The effects of the presence of the dielectric support and the long SMA cable, close to the slot edge, are detrimental at this higher frequency. Therefore, in the $\phi = 0^0$ plane, the measured E_ϕ component level is higher compared to the simulated one, and the measured E_θ component is slightly below the simulated component. In the $\phi = 90^0$ plane, in Fig. 5.14(b), measured E_ϕ component level is lower than the simulated one. The measured E_θ component is dominant here also, due to the reason mentioned above. This also created ripples in the measured radiation patterns.

5.5 Conclusion

In this chapter, a monopole inverted T-shaped slot, cut on the ground plane of a microstrip line, was studied. It showed a wide impedance bandwidth and good radiation characteristics. When the feed line was placed over the junction of the vertical and horizontal arms of the inverted T-shaped slot, a wide impedance bandwidth was achieved. An inverted T-shaped slot was fabricated and tested in the antenna Laboratory. An impedance bandwidth of 80% was measured for the T-shaped slot antenna. The measured radiation characteristics were quite similar to the simulated ones. Here, 17.5% of the ground plane length is occupied by the slot at the upper portion of the ground plane. Thus, the space available is the ground plane, after the slot is cut, is more than that in the case of straight and L-shaped slot. This available space can be used by the ground plane for electronic circuitry.

For the microstrip inverted T-slot antenna, it was found that both E_θ and E_ϕ components of the electric field are dominant. So the T-shaped slot was divided into two parts and placed back to back, separated by a distance and excited individually by two 50Ω bent feed lines, to achieve a polarization diversity reception. This polarization diversity antenna showed a bandwidth of 87% for each of its slots. Investigation of the radiation characteristics of the antenna, in different planes, suggested that, this antenna could be used for polarization diversity applications with wide impedance bandwidth.

CHAPTER SIX

Conclusion

6.1 Summary

In this thesis, microstrip slot antennas were studied. A monopole slot was cut on the ground plane edge, and fed by a microstrip feed line, and is excited by a 50Ω SMA probe. Due to the coupling between the slot and its feed line, several modes were excited in the slot. By varying different parameters of the antenna, such as, the slot width, feed line length, its position over the slot, the stub length, these modes could be combined to achieve a wide impedance bandwidth. The effects of these parameters on the impedance bandwidth were investigated. Moreover, the influence of varying the dielectric substrate permittivity and height was studied. While analyzing the radiation characteristics, it was found that monopole slot antenna had an omni-directional radiation pattern. In order to confirm the analysis, a monopole slot antenna was fabricated and tested in the Antenna Laboratory at the University of Manitoba. The measured impedance bandwidth of the antenna was 60%. The radiation characteristics were in good agreement with the simulated results.

The size of the ground plane was only 50 mm × 80 mm, and as the slot was cut on the ground plane, there would be a reduction in the overall antenna weight. Thus, this monopole slot antenna is lightweight and compact in size, with a significantly wide impedance bandwidth.

It was found that different slot geometries give rise to the impedance bandwidth, with similar radiation characteristics. In addition, more space could be available in the

ground plane to be used by the electronics, which may be fabricated on substrate, separating the ground plane and the microstrip line. Therefore, two other shapes of the slot were studied, keeping the slot length fixed, to save space on the ground plane. The L-shaped slot antenna exhibited an impedance bandwidth of 83.7%, and the inverted T-shaped slot antenna shows an 80.5%, when measured using a network analyzer. The radiation characteristics were also investigated and a good agreement was found, between the simulated and measured results. In the inverted T-shaped slot antenna, 82.5% of the ground plane length was free, to be used by the electronics.

Polarization diversity reception is very important in present mobile communication systems. The inverted T-shaped slot antenna was splitted into two parts and placed with some spacing between them and fed separately using two 50Ω bent feed lines. The simulated result showed an impedance bandwidth of about 87% for both the ports. The isolation between the ports was also satisfactory. The polarization diversity was achieved by alternately exciting the slots. The gain achieved by this antenna was suitable for mobile communication systems.

Miniaturized, lightweight, as well as wide impedance bandwidth, are the antenna requirements, to be used in the mobile communication systems. The microstrip slot antennas, investigated in this thesis, have all these properties with acceptable radiation characteristics.

6.2 Future Research

This work still has several scopes for future research. They can be summarized as follows:

- More detailed study of both L-shaped slot and inverted T-shaped slot microstrip antennas.
- Study of other geometries to achieve even wider impedance bandwidths with good radiation characteristics.
- Detailed study of the effect of increasing or decreasing ground plane size, keeping the slot locations and dimensions fixed.
- Improving the gain of the microstrip slot antenna.
- More experimental verification to confirm the accuracy of the simulated results.

APPENDIX

Theoretical design method of quarter wavelength patch (short-circuit patch):

A quarter wavelength shorted patch has a very high impedance at its radiating edge. So, regardless of the feeding method, either probe or microstrip line, the feed point should be slightly inside of the radiating edge. In the figure below, an inset fed quarter wave patch, shorted on one of its sides, is shown with its equivalent circuit [13]:

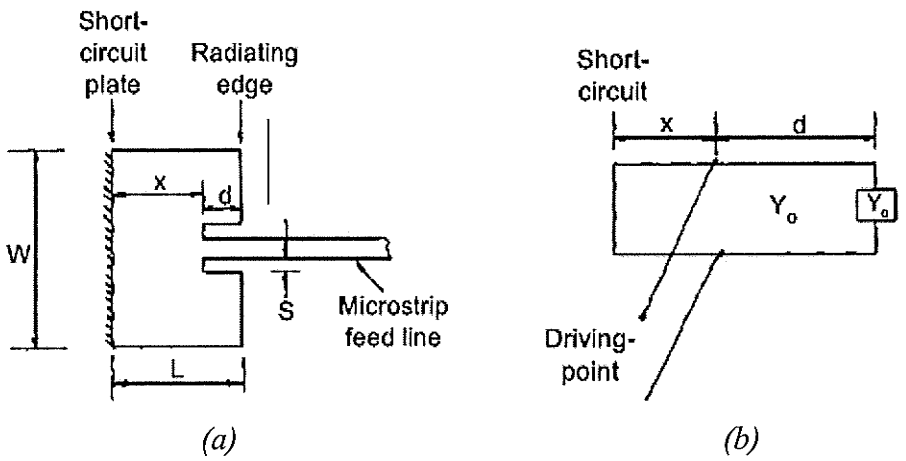

Fig A.1: (a) Microstrip quarter-wavelength patch, (b) Equivalent transmission line model

Here, it is considered that the patch is a short-circuited length of transmission line. Y_o is the characteristic admittance of the microstrip (patch) transmission line. The feed point is located a distance x from the short-circuit plane and d from the radiating edge. The patch resonant length $x+d$ is somewhat less than a quarter-wavelength in the transmission line due to the fringing field extension beyond the physical edge of the patch. Looking into the right-hand side of the transmission line from the feed point, the admittance, assuming a loss less line, is given by,

$$\frac{G_{in}}{Y_0} = \frac{G_a\left(Y_a - B_a \tan \beta d\right) + G_a\left(B_a + Y_0 \tan \beta d\right)\tan \beta d}{\left(Y_0 - B_a \tan \beta d\right)^2 + {G_a}^2 \tan^2 \beta d} \tag{A.1}$$

$$\frac{B_{in}}{Y_0} = \frac{B_a Y_0 + \left({Y_0}^2 - {G_a}^2 - {B_a}^2\right)\tan \beta d - B_a Y_0 \tan \beta d}{\left(Y_0 - B_a \tan \beta d\right)^2 + {G_a}^2 \tan^2 \beta d} \tag{A.2}$$

Here, Y_a is the aperture admittance of the radiating edge, which is made up of the radiation conductance G_a and the susceptance B_a. β is the propagation constant at the operating frequency.

The short circuit to the left of the feed point simply presents a shunt susceptance of value $-jY_0 \cot bx$. To proceed further, G_{in} is set equal to the desired driving point admittance G_{dp} at the center frequency ($\beta=\beta_o$), and equation A.1 is then solved for d.

$$d = \frac{1}{\beta_0}\tan^{-1}\left[-\frac{B}{2} \pm \frac{1}{2}\sqrt{B^2 - 4C}\right] \tag{A.3}$$

$$\text{Here } B = \frac{-2G_{dp}B_a Y_0}{G_{dp}\left|Y_a\right|^2 - G_a {Y_0}^2} \tag{A.4}$$

$$C = \frac{{Y_0}^2\left(G_{dp} - G_a\right)}{G_{dp}\left|Y_a\right|^2 - G_a {Y_0}^2} \tag{A.5}$$

On evaluation, $\beta_o d$ is then inserted into eq. A.2 to obtain B_{in}. Resonance occurs, when the shunt susceptance to the left of the feed point cancels that to the right; i.e. when

$$-jY_0 \cot \beta_0 x = -jB_{in}$$

$$\text{or, } x = \frac{1}{\beta_0}\cot^{-1}\frac{B_{in}}{Y_0}$$

The patch resonant length $x+d$ is thus obtained, together with the feed position relative to the short circuit plane. An expression for characteristic impedance $Z_0 = 1/Y_0$ of the microstrip (patch) transmission line is [13]:

$$Z_0 = \frac{120\pi}{\sqrt{\varepsilon_{eff}}}\left[\frac{W'}{h} + 1.393 + 0.667\ln\left(\frac{W'}{h} + 1.444\right)\right]^{-1}$$

where $\frac{W'}{h} = \frac{W}{h} + \frac{1.25}{\pi}\frac{t}{h}\left(1 + \ln\frac{2h}{t}\right) \qquad for\ W \geq \frac{1}{2}\pi h$

and $\varepsilon_{eff} = \frac{\varepsilon_r + 1}{2} + \frac{\varepsilon_r - 1}{2}\left(1 + \frac{12h}{W}\right)^{-1/2}$

Here, W is patch width, h is the substrate thickness, t is the conductor thickness and ε_r is the substrate dielectric constant. An expression for aperture conductance is given by:

$$G_a \approx \left(1 + \frac{k_0 h}{24}\right)\frac{W}{120\lambda_0}, \quad k_0 = \frac{2\pi}{\lambda_0}, \quad \lambda_0 = \text{free space wavelength}$$

REFERENCES

[1] C. A. Balanis, "Antenna Theory and Design", 2nd Edition, Willy press, 1997.

[2] A. K. Skrivervik, J. F. Zurcher, O. Staub and J. R. Mosig, "PCS Antenna Design: The Challenge of Miniaturization", *IEEE Antenn. and Propagat. Magazine*, Vol. 43, No. 4, Aug 2001, p. 12.

[3] S. B. Cohn, "Slot Line on a Dielectric Substrate", *IEEE Trans. on Microwave Theory and Techniques*, Vol. 17, No. 10, October 1969, pp. 768-778.

[4] S. K. Sharma, N. Jacob and L. Shafai, "Low Profile Wide Band Slot Antenna for Wireless Communications", *Proc. IEEE AP-S Int. Symp. Dig.*, Vol. 1, San Antonio, USA, June 2002, pp. 390-393.

[5] S. K. Sharma, L. Shafai and N. Jacob, "Investigation on Wide Band Microstrip Slot Antenna", *IEEE Trans. on Antenn. and Propagat.*, in press.

[6] R. Garg, I. J. Bhal, P. Bhatia, P. Ittipibon, "Microstrip Antenna Design Handbook", Artech House, Boston, MA, USA, 2001.

[7] D. M. Pozar and D. H. Schaubert, "Microstrip Antennas – The Analysis and Design of Microstrip Antennas and Arrays", IEEE Press, NY, 1995.

[8] L. Shafai, "24.427 Antennas", *Course Notes*, The University of Manitoba, Winnipeg, Canada, 2002.

[9] K. Hirasawa and M. Haneishi, "Analysis, Design and Measurement of Small and Low-Profile Antennas", Artech House, Boston, MA, USA, 1992.

[10] Y. Hwang, Y. P. Zhang, G. X. Zheng and T. K. C. Lo, "Planar Interveted F Antenna Loaded with High Permittivity Material", *Electron. Lett.*, Vol. 31, No. 20, September 1995, pp. 1710-1712.

[11] Y. Hwang, Y. P. Zhang, T. K. C. Lo, K. M. Luk and E. K. N. Yung, "Miniaturization of Planar Antennas with Very High Permittivity Materials", *1997 Asia-Pacific Microwave Conference Proceedings, APMC'97*, Vol. 1, 2-5 December, 1997, pp. 217-220.

[12] M. Sanad, "A Small Size Microstrip Antenna Having a Partial Short Circuit", *9th Intl. Conf. on Antenn. and Propagat. (Conf. Publ. No. 407), ICAP'95*, Vol. 1, 4-7 April, 1995, pp. 282-285.

[13] P.S. Hall, J. R. James, "Handbook of Microstrip Antennas" Peter Peregrinus, London, 1989.

[14] M. Sanad, "Effects of Shorting Posts on Short Circuit Microstrip Antennas", *Proc. IEEE Antenn. and Propagat. Symp.,* 1994, Vol. 2, pp. 794-797.

[15] R. B. Waterhouse, "Small Microstrip Patch Antenna", *Electron. Lett.*, Vol. 31, No. 8, 1995, pp. 604-605.

[16] R. B. Waterhouse, S. D. Targonski and D. M. Kokotoff, "Design and Performance of Small Printed Antennas", *IEEE Trans. on Antenn. and Propagat.* Vol. 46, No. 11, Nov 1998, pp. 1629-1633.

[17] H. –D. Chen, "Compact Circularly Polarized Microstrip Antenna with Slotted Ground Plane", *Electron. Lett.*, Vol. 38, No. 13, June 2002, pp. 616-617.

[18] K. L. Wong, "Compact and Broadand Microstrip Antennas", John Willey and Sons Inc., NY, USA, 2001.

[19] G. Kumar and K. P. Ray, "Broadband Microstrip Antennas", Artech House, Boston, MA, USA, 2003.

[20] S. B. Cohn, "Slot Line - an Alternative Transmission Medium for Integrated Circuits" *Intl. Microwave Symp. Digest*, G-MTT, Vol. 68, No. 1, May 1968, pp. 104–109.

[21] E. Mariani, C. Heinzman, J. Agrios and S. B. Cohn, "Slot Line Characteristics", *IEEE Trans. on Microwave Theory and Techniques*, Vol. 17, No. 12, December 1969, pp. 1091 –1096.

[22] R. C. Hansen, "Antenna Engineering Handbook", 3rd Edition, McGraw-Hill, USA, 1994.

[23] H.G. Akhavan and D. Mirshekar-Syahkal, "Characteristics of Fundamental and First Higher-Order Modes of Microstrip-Fed Slot Antennas", *10th Intl. Conf. on Antenn. and Propagat.*, 14-17 Apr 1997, (Conf. Publ. No. 436), Vol. 1, pp. 74-77.

[24] K. C. Gupta, R. Garg, I. J. Bahl, "Microstrip Lines and Slotlines", Artech House, Dedham, MA, USA, 1979.

[25] Y. Yoshimura, "A Microstrip Slot Antenna", *IEEE Trans. on Microwave Theory and Techniques*, Vol. 20, No. 11, November, 1972, pp. 760-762.

[26] J. P. Kim and W. S. Park, "Network Modeling of an Inclined and Off-Center Microstrip-Fed Slot Antenna", *IEEE Trans. on Antenn. and Propagat.*, Vol. 46, No. 8, August 1998, pp. 1182-1188.

[27] R. W. Breithaupt, "Conductance Data for Offset Series Slots in Stripline", *IEEE Trans. on Microwave Theory and Techniques*, Vol. 16, No. 11, November 1968, pp. 969-970.

[28] J. S. Rao and B. N. Das, "Impedance of Off-Centered Stripline Fed Series Sot", *IEEE Trans. on Antenn. and Propagat.*, Vol. 26, No. 6, November 1978, pp. 893-895.

[29] B. N. Das and K. K. Joshi, "Impedance of a Radiating Slot in The Ground Plane of a Micrsotrip Line", *IEEE Trans. on Antenn. and Propagat.*, Vol. 30, No. 5, September 1982, pp. 922-926.

[30] D. M. Pozar, "A Reciprocity Method of Analysis for Printed Slot and Slot-Coupled Micrsotrip Antennas", *IEEE Trans. on Antenn. and Propagat.*, Vol-34, No. 12, December 1986, pp. 1439-1446.

[31] A. K. Bhattcharyya, Y. M. M. Antar and A. Ittipiboon, "Full Wave Analysis for the Equivalent Circuit of an Inlcined Slot on a Microstrip Ground Plane", *IEE Proceedings – H,* Vol. 139, No. 3, June 1992, pp. 245-250.

[32] J. F. Knorr, "Slot-Line Transitions", *IEEE Trans. on Microwave and Theory Techniques*, May 1974, Vol. 22, No. 5, pp. 548-554.

[33] M. Kahrizi, T. K. Sarker and Z. A Maricevic, "Analysis of a Wide Radiating Slot in the Ground Plane of a Microstrip Line", *IEEE Trans. on Microwave Theory and Techniques*, Vol. 41, No. 1, January 1993, pp. 29-37.

[34] M. K. Kim, K. Kim, Y. H. Suh and I. Park, "A T-Shaped Microstrip-Line-Fed Wide Slot Antenna", *IEEE Intl. Symp. Antenn. and Propagat. Society*, 2000, Vol. 3, July 2000, pp. 1500 –1503.

[35] J. –Y. Sze and K. -L. Wong, "Bandwidth Enhancement of a Microstrip-Line-Fed Printed Wide-Slot Antenna", *IEEE Trans. on Antenn. and Propagat.*, Vol. 49, No. 7, July 2001, pp. 1020-1024.

[36] Ansoft Corporation, USA, Ensemble 8.0.

[37] Ansoft Corporation, USA, HFSS 8.0.

[38] W. L. Stutzman, "Polarization in Electromagnetic Systems", Artech House, Boston, USA, 1992.

[39] K. Fujimoto and J. R. James, Eds., "Mobile Antenna System Handbook", 2nd Edition, Artech House, Boston, USA, 2001.

[40] S. C. C. Ko and R. D. Murch, "A Diversity Antenna for External Mounting on Wireless Handsets", *IEEE Trans. on Antenn. and Propagat.,* Vol-49, no. 5, May 2001, pp. 840-842.